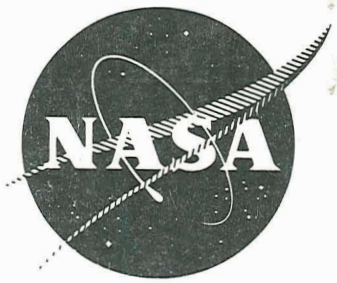

NASA CR-72760

THERMAL DESIGN OF THE SNAP-8 TANTALUM-STAINLESS STEEL BOILER

by

A. J. Sellers

AEROJET-GENERAL CORPORATION
Azusa, California

Prepared for

NATIONAL AERONAUTICS AND SPACE ADMINISTRATION

NASA Lewis Research Center
Contract NAS 3-13458
Martin J. Saari, Program Manager

NOTICE

This report was prepared as an account of Government-sponsored work. Neither the United States, nor the National Aeronautics and Space Administration (NASA), nor any person acting on behalf of NASA:

A.) Makes any warranty or representation, expressed or implied, with respect to the accuracy, completeness, or usefulness of the information contained in this report, or that the use of any information, apparatus, method, or process disclosed in this report may not infringe privately-owned rights; or

B.) Assumes any liabilities with respect to the use of, or for damages resulting from the use of, any information, apparatus, method or process disclosed in this report.

As used above, "person acting on behalf of NASA" includes any employee or contractor of NASA, or employee of such contractor, to the extent that such employee or contractor of NASA or employee of such contractor prepares, disseminates, or provides access to any information pursuant to his employment or contract with NASA, or his employment with such contractor.

Requests for copies of this report should be referred to:

National Aeronautics and Space Administration
Scientific and Technical Information Facility
Post Office Box 33
College Park, Maryland 20740

NASA CR-72760

TOPICAL REPORT

THERMAL DESIGN OF THE SNAP-8 TANTALUM-STAINLESS STEEL BOILER

by

A. J. Sellers

AEROJET-GENERAL CORPORATION

Azusa, California

Prepared for

NATIONAL AERONAUTICS AND SPACE ADMINISTRATION

June 1971

Contract NAS 3-13458

NASA-Lewis Research Center

Cleveland, Ohio

Martin J. Saari, Program Manager

SNAP-8 Program Office

FOREWORD

The design and development effort described in this report was performed by the Aerojet Nuclear Systems Company of the Aerojet-General Corporation, Azusa, California, as part of the SNAP-8 Electrical Systems Contract being conducted within the Power Systems Operations. The work was performed under NASA Contract NAS 3-13458 with Mr. Martin J. Saari as NASA Program Manager and Dr. W. F. Banks as Aerojet-General Corporation Program Manager. Acknowledgement is given Messrs. E. R. Furman and G. M. Thur of NASA-Lewis Research Center for their guidance and assistance.

CONTENTS

CONTENTS (continued)

CONTENTS (continued)

ABSTRACT

This report presents the design analysis of a "once through" type, forced convection mercury boiler. Heat and momentum transfer parameters are established as well as the internal geometry of the working fluid flow passage and overall boiler design configuration. The boiler design was based on heat and momentum transfer correlations derived from idealized wetting and non-wetting two-phase flow models. Predicted performance characteristics as defined by NaK and mercury-side temperature and pressure profiles were in relatively good agreement with test results of experimental and full scale boilers. Considerable care must be exercised in maintaining the cleanliness of the mercury side heat transfer surface. If foreign materials such as oil or air enter the system, undesirable changes in heat transfer can result.

SUMMARY

This report deals with the thermal design of tantalum-stainless steel mercury boilers. The design is based on fluid wetting and non-wetting two-phase flow models postulated for the boiler vapor quality region. Heat and momentum transfer correlations were devised from three models and used to determine both design and off-design performance. Analytical predictions were evaluated with development test results to justify their application.

Two major problem areas were encountered in the early stages of SNAP-8 boiler development. First, the originally selected 9% Chromium-1% Molybdenum (9M) steel alloy tube material exhibited excessive mercury side corrosion and NaK side embrittlement. After considerable testing, it was apparent that this tube material was not sufficiently resistant to mercury corrosion at SNAP-8 operating temperatures (1100-1300^{o}F) to provide the required minimum 10,000-hour life. Secondly, there was a relatively wide deviation between the original predictions and actual heat transfer characteristics. These results led to the conclusion that forced convection dropwise dry wall mercury boiling heat and momentum transfer correlations were not satisfactory for the prediction of optimum boiler performance. Test results indicated that these correlations were not applicable to mercury two-phase flow when the fluid wet the heat transfer surface.

Refractory metals were investigated to eliminate the corrosion problems and produce an optimum boiler design. Tantalum was selected for the following reasons: the solubility of tantalum in mercury at elevated temperature is just barely detectable; tantalum exhibits good mercury wettability properties; and it has a proven history of producibility and fabricability in the chemical industry. To safeguard tantalum against the corrosive effect of flowing NaK, experimental configurations of double containment and bimetal tube concepts were developed and tested. Concentric 316 stainless steel tubes were bonded over tantalum tubes by coextrusion and by explosive bonding. Although both processes produced satisfactory tubes, the coextrusion process exhibited no debonding and was preferred for the bonded bimetal tubes. To meet the safety

requirements of a man-rated Space Nuclear Electric Power system, the double containment concept was adopted. The radioactive primary loop fluid, NaK, is separated from the power loop fluid, mercury, by a non-flowing buffer fluid, also NaK. This static NaK region is contained between an oval stainless steel tube and a round tantalum tube. The purpose of the oval/round tube geometry is to accommodate differential radial thermal expansion of the two different materials. A seven (7) tube boiler was designed for the original system state point conditions and was successfully tested in conjunction with an integrated SNAP-8 breadboard system. A tweleve (12) tube boiler was designed for a revised system state point. A fixed orifice is placed at the entrance of each of the tantalum tubes to provide equal mercury flow distribution and to insure a positive overall boiler pressure drop gradient when the mercury flow is increased from zero to maximum. A tantalum rod with sixteen (16) helical passages is inserted in each tantalum tube. This plug insert induces vortex flow, downstream of the liquid-vapor interface. A swirl wire turbulator is used in the mercury flow passage downstream of the plug insert to sustain the vortex flow throughout the remaining boiler length. A vortex flow is mandatory for effective mercury vaporization and also makes the boiler operation independent of external gravity environments.

Heat transfer characteristics of both the bimetal tube and double containment tube assemblies were experimentally investigated in a tube-in-tube boiler configuration with a single full scale boiler mercury flow passage geometry. The annular NaK flow passage was sized to simulate the full scale boiler NaK side film conductance. Test results of both tube geometries were in relatively good agreement with theoretical predictions. These predictions were based on idealized wetting and non-wetting two-phase flow heat and momentum transfer models. Thus, these models and the associated correlations were considered qualified for the SNAP-8 boiler design and off-design performance.

The basic method of analysis was to subdivide the boiler length into a series of small increments and to write the coupling heat transfer and pressure drop correlations for each increment. The boiler preheat and superheat

sections were subdivided by taking equal increments of the mercury temperature rise. Similarly, the vapor quality region was subdivided by taking equal increments of vapor quality. The solution of the coupling equations at each node provided the local thermal and dynamic operating parameters, increment length, and nodal boundary state conditions. The heat and momentum transfer correlations and their applicability criteria in different mercury flow passage regions are discussed herein. Sequential solution of the nodal equations using standard mathematical and computer techniques resulted in the determination of the predicted optimum overall boiler performance.

One very important result derived from the test experience was the fact that successful operation of a mercury boiler requires considerable care in maintaining cleanliness and vacuum integrity of the working fluid system. To prevent boiler performance degradation, care must be taken not to allow foreign substances such as organic fluids or air to enter the system. Otherwise, a thermal barrier on the mercury exposed surface of the tantalum tube is formed causing degradation. Using chemical cleaning to remove the inadvertent contamination effectively eliminated the thermal barrier surface films from the tantalum and restored the full heat transfer capability of the boiler.

1.0 INTRODUCTION

This report describes the development of the last of a series of boilers used for the SNAP-8 power system. SNAP-8 is a Rankine cycle nuclear-electric power conversion system providing 35 to 90 kWe usable power for space missions for 10,000 to 40,000 hours of operation. The power conversion system was being developed by Aerojet Nuclear Systems Company for the National Aeronautics and Space Administration. The nuclear reactor was being developed for the Atomic Energy Commission by Atomics International. The basic SNAP-8 35 kWe system is shown in Figure 1. Thermal energy is transferred from the reactor to the power conversion system by a primary eutectic NaK loop. Mercury is the working fluid in the Rankine cycle loop. The thermal energy exchange takes place in a counterflow NaK-to-Hg heat exchanger where the Hg is preheated, vaporized and superheated in a "once through" boiler configuration. Superheated Hg vapor drives the turbine-alternator assembly to produce electrical power. Leaving the turbine, the Hg vapor is condensed and pumped back to the boiler. Heat given up by the Hg as it condenses is carried by a secondary NaK heat transfer loop to a radiator where it is radiated to space. Organic fluid in a fourth loop is circulated to the pump-motor and the turbine-alternator assembly for lubrication, and to the electrical components for cooling.

The "once through" boiler concept was selected because of its simplicity and suitability for operation in zero and adverse gravity environments. Only limited experimental and theoretical mercury boiling data for the "once through" boiler concept were available prior to the SNAP-8 program. These data were the dropwise dry wall boiling heat and momentum transfer correlations developed for the design of mercury boilers in the preceding SNAP-2 program. SNAP-2 also was a Rankine cycle power conversion system employing a reactor heated Nak loop in the mercury boiler and was capable of providing 4.5 kWe usable power for space missions (see References 1, 2, and 3).

The initial SNAP-8 boiler design was closely related to SNAP-2 boiler development experience. The semi-empirical correlations originally applied to the relatively small tube size (0.325 inch I.D.) were modified and applied to larger mercury flow passage sizes of 0.902 inch and 0.652 inch inside diameter

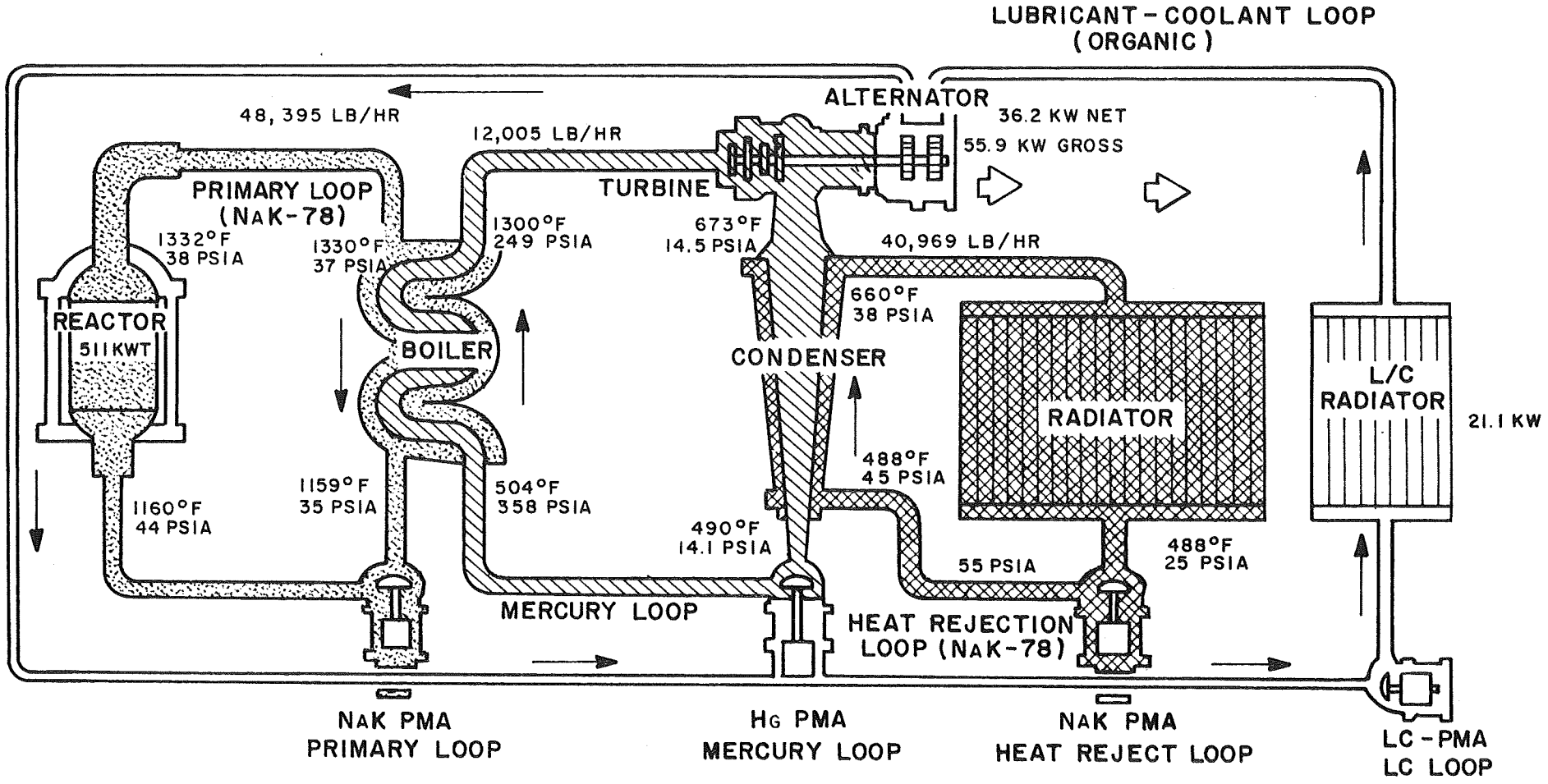

Figure 1.- SNAP-8 System Schematic

used in the first SNAP-8 boilers that were made of 9% chromium-1% molybdenum (9Cr-1Mo) steel alloy for mercury containment.

The major problem in the initial phase of SNAP-8 boiler development was mercury and NaK incompatibility with the low alloy steel tube material (9Cr-1Mo). Excessive mercury side corrosion, NaK side corrosion and embrittlement posed a serious limitation on the life of the SNAP-8 boiler. Also, these early low-alloy steel boilers gave wide variations in thermal performance which was attributed to cleanliness conditions of the mercury flow passage heat transfer surfaces. The relatively wide deviation between predicted and actual heat transfer characteristics, as demonstrated by fully conditioned 9Cr-1Mo alloy boilers, led to the conclusion that dropwise dry wall boiling heat and momentum transfer correlations are not satisfactory for boiler performance predictions. For this reason, the dropwise dry wall boiling correlations were modified and supplemented with the results of Geoscience's theoretical and experimental studies on liquid metal "once-through" boiling (see References 4, 5, 6, 7, 8, and 9).

This report describes the development of the thermal design of the tantalum-stainless steel boilers, the last of a series of boilers used on the SNAP-8 program. Two mercury containment concepts, namely the bimetal stainless steel-tantalum tube and the bare refractory double containment (BRDC) stainless steel-tantalum tube assembly, as shown in Fugure 2D and 2F respectively were visualized as potential solutions of the boiler corrosion problem.

The boiler design is based on two-phase flow, wetting and non-wetting, models. The validity of the models is established with tests of experimental and full-scale boilers. Boiler performance degradation, its causes, and the controlling heat transfer mechanisms involved are discussed, and the results are presented in a separate Geoscience Ltd. report (see Reference 10). This referenced report also provides the basic definitions of various two-phase flow models which are used in boiler design correlations.

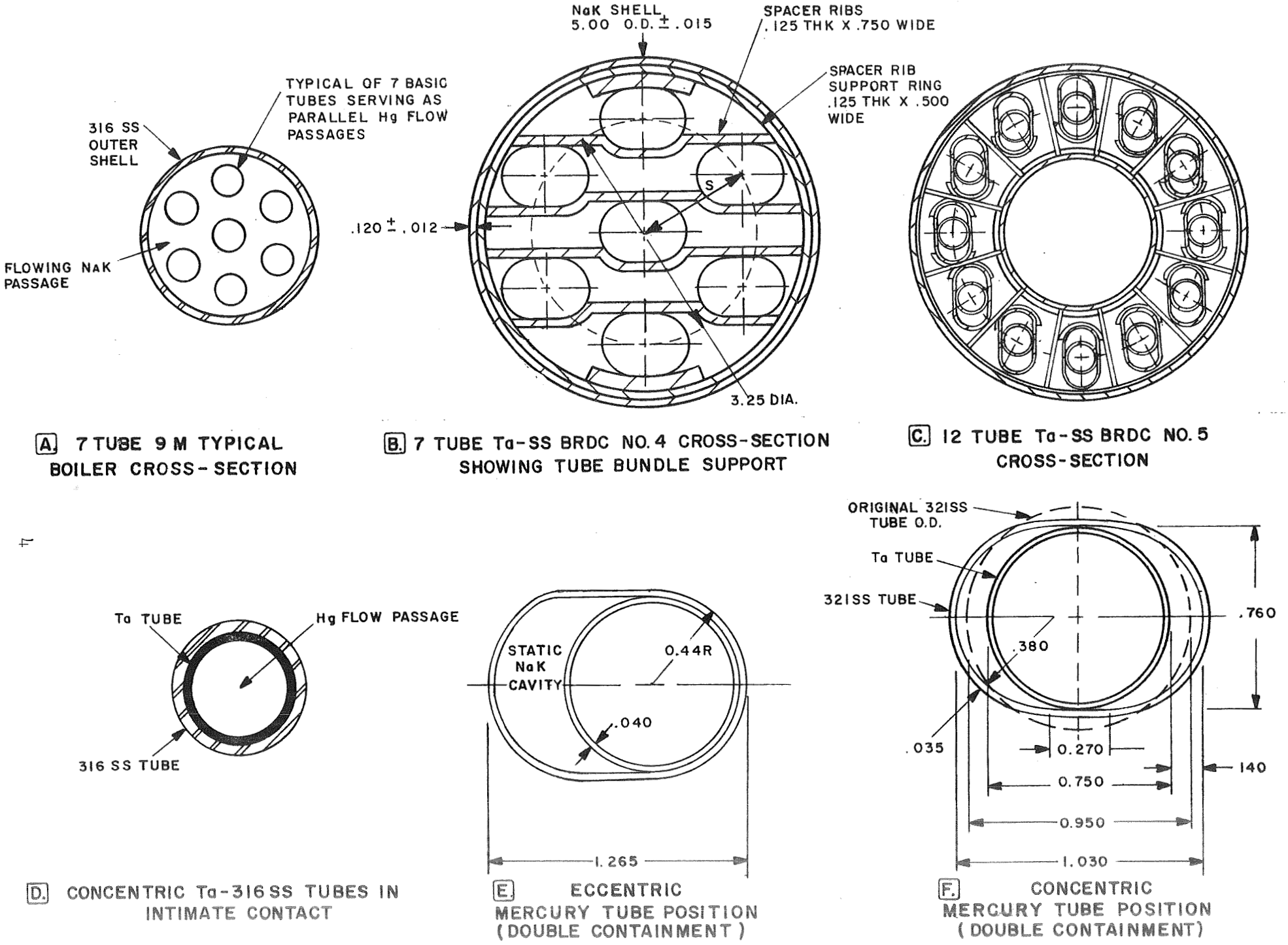

Figure 2.- Typical SNAP-8 Boiler Cross-Section Configurations

2.0 REFERENCE BOILER DESIGN CONFIGURATION

To proceed with a thermal design analysis, the designer must establish a basic boiler configuration suitable for placement in a prescribed system envelope and capable of being instrumented for monitoring boiler performance. The latter requirement suggested the adoption of a tube-in-tube design configuration with a pure counterflow NaK-to-Hg heat transfer arrangement as shown in Figure 3. The most plausible way of determining boiler design and off-design performance is by measurements of the NaK temperature (T_N) as a function of boiler length (l). Heat transfer to the mercury results in a decrease in NaK temperature. Hence, the slope of a NaK temperature profile corrected for heat loss is directly proportional to the local heat flux. Boiler performance degradation due to contaminants in the mercury loop results in a measured NaK temperature profile (T_{N-1}) which is significantly different from the design prediction (T_{N-2}) as shown in Figure 4A. A decrease in the slope of the temperature profile in the boiling section is a typical indication of boiler performance degradation. Therefore, one can see that NaK shell surface temperature measurements are most desirable to confirm analytical predictions and diagnose boiler performance at all system operating conditions.

The mercury tube internal diameter (0.652 inch) and the tube count (7) in the tantalum-stainless steel boiler was identical to that used in the earlier 9Cr-1Mo steel alloy boilers. State point conditions were established based on system studies. A boiler NaK inlet temperature of from 1285° to 1330°F, a mercury flow of 11,800 lb/hr, and an exit pressure of 255 psia were established.

Several limitations in the use of tantalum existed which required special consideration in designing the material into the SNAP-8 system (Reference 11). Air contamination of tantalum exposed at temperatures above 400°F results in the formation of a non-adherent surface oxide. The reaction rate increases with increased exposure temperature. Also, it was postulated that tantalum in a flowing SNAP-8 multimetal NaK system would accumulate interstitial elements, carbon and oxygen, from the NaK resulting in embrittlement and accelerated metal mass transfer. Two basic boiler designs were developed to avoid the above uncertainties. In both designs, the tantalum was protected

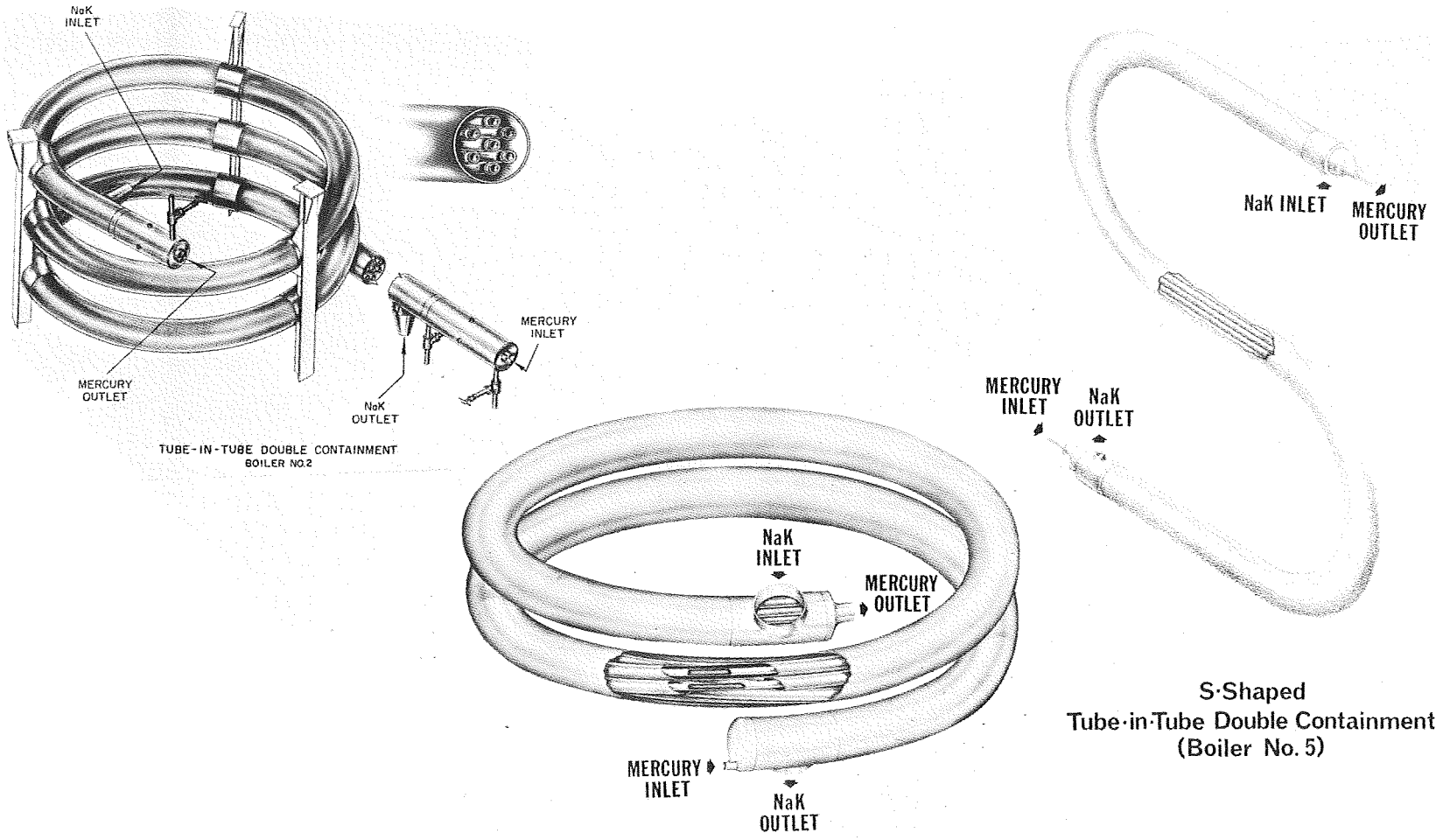

Figure 3.- Tantalum-Stainless Steel Double Containment Boiler Configurations

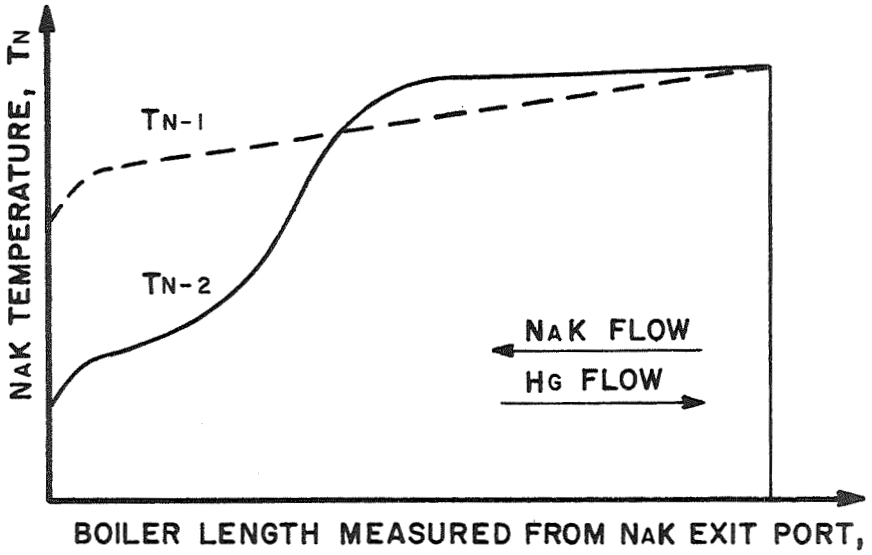

4A. COMPARISON OF TYPICAL NAK TEMPERATURE PROFILES OF A BOILER WITH DECONDITIONED (T_{N-1}) AND FULLY CONDITIONED (T_{N-2}) MERCURY SIDE HEAT TRANSFER SURFACES.

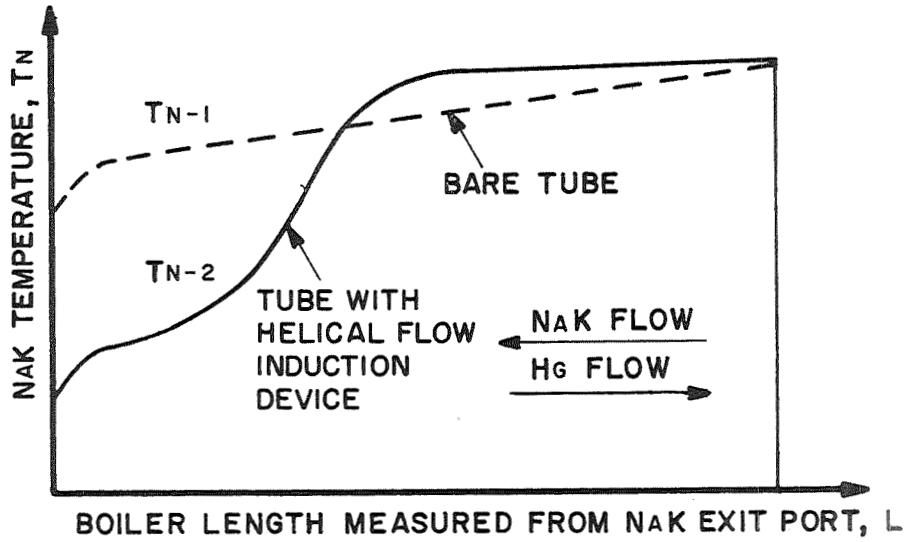

4B. COMPARISON OF TYPICAL NAK TEMPERATURE PROFILES OF A BOILER WITH FULLY CONDITIONED MERCURY SIDE HEAT TRANSFER SURFACES FOR TUBES WITH (T_{N-2}) AND WITHOUT (T_{N-1}) INTERNAL HELICAL FLOW INDUCTION DEVICES.

Figure 4.- Typical Boiler NaK Temperature Profiles

on the exterior surfaces from possible contaminants in the flowing NaK. This was accomplished by isolating the tantalum within a stainless steel envelope. One design utilized a metallurgically bonded bimetal tube which consisted of a tantalum liner inside a 316 stainless steel tube. The corrosion resistant tantalum was used to contain the flowing mercury and the external stainless steel surface protected the tantalum from possible NaK side impurities. The second, and chosen design, consisted of tantalum tubes contained within an oval shaped 321 stainless steel tube as shown in Figures 2E and 2F. The volume formed between the two tubes was filled with a high conductivity, non-flowing fluid (NaK) to assure good heat transfer. The resultant configuration termed "double containment," isolated the tantalum tube from the flowing NaK and additionally provided added protection against the possible intrusion of radioactive primary loop NaK into the working fluid. The stainless steel oval shape was chosen to minimize the static NaK volume while providing adequate space for the movement of the tantalum tubes relative to the stainless steel tube. This movement results from the large differential thermal expansion between the tantalum and stainless steel tubes. Since both boiler designs were initially considered to be of equal potential, it was decided to test both of them in a subscale SNAP-8 configuration simulating the plug insert section of the boiler.

A single tube experimental SNAP-8 boiler (SF-A1), utilizing the concentric bimetal tantalum-stainless steel tube configuration was successfully developed and tested in a seventh scale loop. This test enabled the evaluation of the structural reliability of the bimetal tube joint, verification of the integrity of the tantalum-stainless steel tube bond, and the evaluation of the heat transfer characteristics of the helical flow passage geometry. This experimental boiler exhibited excellent heat transfer characteristics and the results were in relatively good agreement with the predictions based on idealized wetting, and non-wetting two-phase flow models. From analysis of the test data, it was concluded that tantalum-316 stainless steel bimetal tubes bonded by either hot coextrusion or explosive bonding, demonstrated the potential for providing up to 40,000 hours SNAP-8 boiler mercury containment tube life. The

coextruded bond was preferred because the product contains no pre-existing sites for debond growth as does the bimetal tube fabricated by explosive bonding.

Although the bimetal tube and the double-containment concepts both appeared to be acceptable for mercury service, the double containment configuration was chosen for the full size prototype design because of its higher reliability for man-rated applications.

The overall dimensions of the boiler are defined by NaK shell O.D. and length. These dimensions and the available space in the combined SNAP-8 Electrical Generating System's assembly envelope were the determining factors for the boiler design geometry. The boiler configuration, used in the bread-board power conversion system tests, is the 7-tube concept shown in Figure 2B.

The selection of Hg flow passage internal geometry for the tantalum-stainless steel boilers was based on the results of single tube and full scale boiler tests. The helical multipassage plug insert (MPP) and the helical turbulator swirl wire (SW) tube geometry, as shown in Figure 5, was used in the tantalum-stainless steel boiler design. The effect of different helical flow induction devices on two-phase flow heat transfer is discussed in the following section.

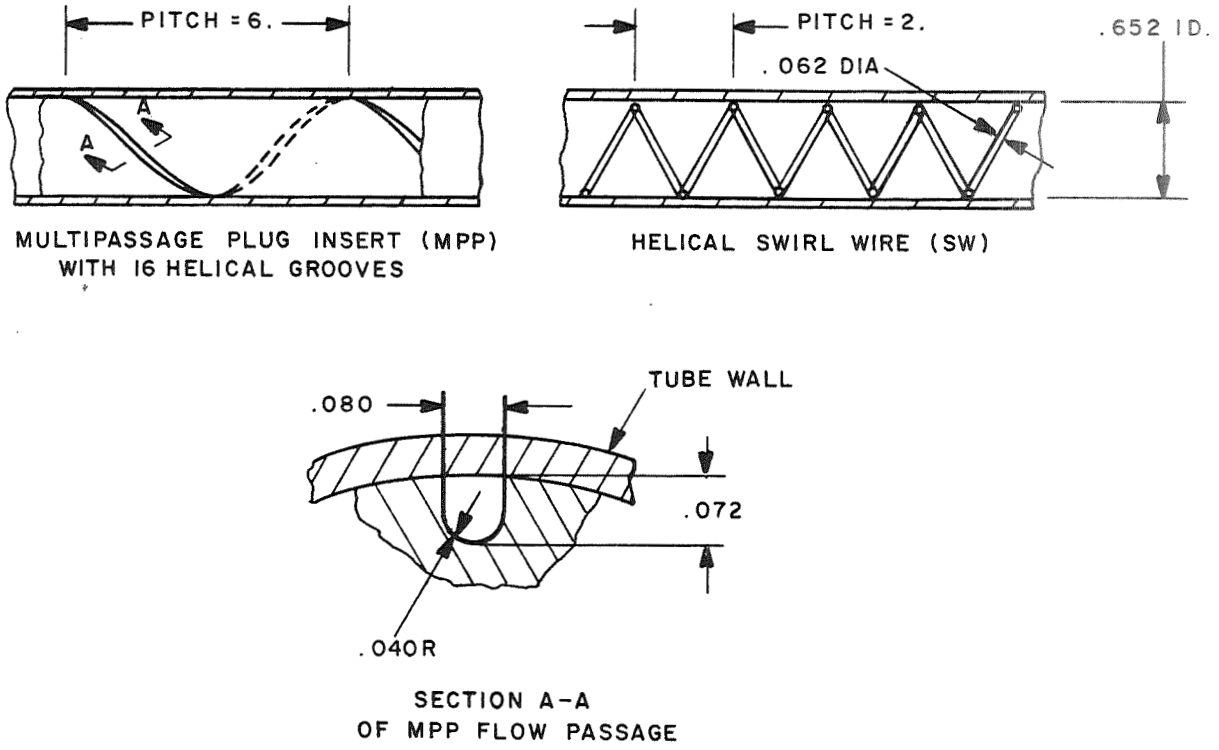

Figure 5.- Mercury Tube Internal Geometry

3.0 HELICAL FLOW INDUCTION DEVICES AND THEIR EFFECT ON BOILER HEAT TRANSFER

In a "once through" boiler the working fluid is preheated, vaporized, and superheated while it is passing through the boiler tubes. Heat transfer effectiveness in the boiler vapor quality region is dependent on the two-phase flow regime that is induced by the flow passage geometry. In the case of the SNAP-8 reference boiler, both the NaK side film resistance and the composite double containment tube wall resistance are considered constant. Heat input into the mercury is governed by the Hg-side film conductance which is highly dependent on the two-phase flow dynamics in the Hg tube. A comparison of "once through" Hg boiler NaK temperature profiles in a bare tube and in tubes provided with a helical multipassage plug insert and helical swirl wire turbulators is depicted in Figure 4B. Heat transfer, as indicated by the small gradient of the bare tube NaK temperature profile, is attributed to a linear two-phase flow pattern. It is characterized by a slug flow boiling regime in the low vapor quality region (x = 0 to 12%) and a stratified two-phase flow boiling regime induced by the external gravitational field. Both flow regimes are associated with low film conductances and extremely long tube lengths are required to accomplish Hg vaporization.

The liquid phase should be in contact with the heat transfer surface to achieve maximum heat fluxes. A divided linear two-phase flow regime defined by an annular liquid layer contiguous to the heated tube wall with a turbulent vapor core is the optimum. Such an idealized two-phase flow regime was the basis for establishing three boiling modes in the low quality vapor region under heat transfer surface wetting conditions by the mercury. The definition of these boiling modes and their analytical correlations are provided in Section 4.3

The divided two-phase flow regime cannot be realized in a bare tube. To approach the idealized divided two-phase flow, helical turbulence promoters are provided. The creation of a helical flow pattern permits the use of its tangential velocity component to accelerate the liquid phase towards the heated tube wall. This acceleration makes boiler operation independent of the

external gravity environment. Consequently, boiler performance should not be affected by external gravity environments. As shown in Figure 4B, the relatively large NaK temperature gradients demonstrate the effectiveness of these helical flow turbulence promoters in improving boiling heat fluxes.

Various types of helical flow turbulence promoters were utilized in the early experimental and full scale boilers. These included single and multi-passage plug inserts, twisted tapes, swirl wires and single fluted helices. The plug inserts were placed in the mercury inlet and tube section and were designed to contain the liquid-vapor interface and quality vapor region (up to approximately 12% vapor quality). In both the single passage plug insert and the parallel multipassage plug insert, the flow passages were helical with a relatively small flow cross-sectional area commensurate with the vapor volume flow.

The purpose of the plug insert is to minimize or eliminate the slug flow boiling length, promote early vortex flow boiling and introduce the vortex flow pattern into the unplugged tube section. A single passage plug insert is preferred to obtain a relatively high heat flux in the initial vapor quality section. The single helical flow passage can be designed with a relatively small pitch to provide a high working fluid radial acceleration force. However, the single flow passage plug insert results in an excessive pressure loss and pressure loss variations over the boiler NaK inlet temperature band prescribed for the SNAP-8 system. This plug insert geometry also gives excessive pressure drop during the initial mercury injection period. To minimize these pressure loss problems, the helical parallel multipassage design configuration was selected. This geometry is characterized by a reduced pressure loss and less pressure loss variation with a change in NaK inlet temperature.

The vortex flow promoters considered for the boiler unplugged tube section were twisted tapes, swirl wires and single fluted helices. Each promotes the helical flow pattern to a certain degree. Twisted tapes and helical swirl wires were investigated experimentally in an isothermal N_2-Hg test facility to determine their suitability. Twisted tapes, because of their relatively large minimum pitch limitations, were not found to be suitable for

effective working fluid radial acceleration. A better helical flow pattern was observed with helical wire turbulators. Fabrication simplicity and their successful application in early SNAP-8 programs was the basis for their selection for the SNAP-8 boiler. A true helical flow pattern, obtained by means of single fluted helix (helical strip wound on center bar), was successfully investigated in an experimental single tube boiler. The single fluted helix eliminates the axial vapor core flow associated with a swirl wire. The axial vapor core flow is a contributing factor for liquid droplet carryover. In a true helical passage, the development of axial vapor core flow is prevented by the helical strip and the center bar. As a result, mercury droplets contained in the vapor flow are forced against the helical channel boundaries and are vaporized.

3.1 Helical Flow Passage Geometry

The geometric constants for a tube containing a helical swirl wire (SW) turbulator are derived from the definition of a true helical flow passage geometry. Such a geometry can be obtained by winding a helical strip of minimum thickness on a center bar and inserting it in a tube as shown in Figure 6. This geometry represents a single fluted helix defined by:

D = tube internal diameter

D_B = center bar diameter

t = helical strip thickness

p = helical pitch

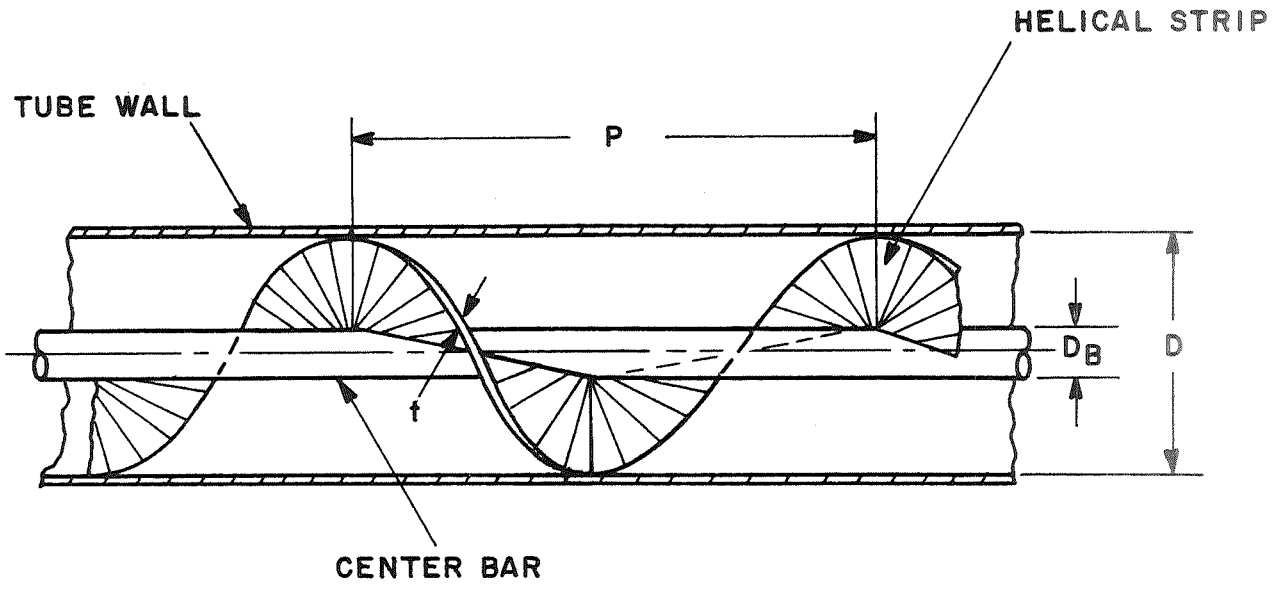

Figure 6.- Single Fluted Helix Geometry

In accordance with Reference (6) the SFHX geometric parameters are:

$$r_o = \frac{D}{2} = \text{tube radius}$$

$$r_b = \frac{D_B}{2} = \text{center bar radius}$$

$$\omega' = \frac{2\pi}{p} = \text{a constant}$$

$$p_{orth,T} = 2\pi\ r_o^2\ \omega' = \text{orthogonal pitch, tube ID}$$

$$p_{orth,B} = 2\pi\ r_b^2\ \omega' = \text{orthogonal pitch, bar diameter}$$

$$Z_T = \frac{2\pi\ r_o}{\left[1 + (r_o\ \omega')^2\right]^{1/2}} - t = \text{wetted perimeter portion on tube ID}$$

$$Z_B = \frac{2\pi\ r_b}{\left[1 + (r_b\ \omega')^2\right]^{1/2}} - t = \text{wetted perimeter portion on bar diameter}$$

$$\theta_B = \frac{2\pi}{1 + (r_b\,\omega')^2} = \text{bar circular projection angle in radians}$$

$$\theta_T = \frac{2\pi}{1 + (r_o\,\omega')^2} = \text{tube circular projection angle in radians}$$

$$Y = \left[r_o^2 + r_b^2 - 2\,r_o r_b \cos\frac{\theta_B - \theta_T}{2}\right]^{1/2} = \text{wetted perimeter portion on helical strip}$$

$$P_W = Z_T + Z_B + 2Y = \text{Total wetted perimeter of helical flow cross section}$$

$$A_{hel} = \frac{p^2}{2\pi}\sqrt{1 + (\omega'\,r_o)^2} - \sqrt{1 + (\omega'\,r_b)^2} - t\,(r_o - r_b) = \text{helical flow cross section area}$$

$$De_{hel} = \frac{4\,A_{hel}}{P_W} = \text{equivalent diameter, helical}$$

$$A_{lin} = \frac{\pi}{4}(D^2 - D_B^2) = \text{linear cross section}$$

$$De_{lin} = D_T - D_B = \text{equivalent diameter, linear}$$

$$De_{tan} = \frac{2\,(r_o - r_b)\,p}{[(r_o - r_b) + p]} = \text{equivalent diameter, tangential}$$

The flow cross-section of the helical geometry is bounded by the wetted perimeter of the surfaces comprised of the center bar, tube ID and helical strip. A true helical flow pattern, consisting of axial and tangential velocity components, is obtained. In the case of a helical swirl-wire geometry, a partial helical flow is induced by the wire drag effect, and part of the flow, because of the absence of a solid helical boundary, assumes a linear flow pattern. To calculate the swirl-wire tube geometric parameters, the helical flow geometric correlations were modified. The absence of the center bar was accounted for by assuming $D_B = 0$. The partial linear flow effect was neglected by assuming an imaginary helical strip thickness t = 0.001 inch to use the heat and momentum transfer correlations developed for the helical flow insert.

4.0 HEAT AND MOMENTUM TRANSFER CORRELATIONS

Heat transfer in the boiler is dependent on the local overall conductance between the flowing NaK and Hg. Substituting the true oval/round tube geometry (see Figure 2) by its equivalent round/round tube geometry as shown in Figure 7, the overall conductance is:

$$U = \frac{1}{R + \frac{1}{h_H}} \qquad \text{(Eq. 4.0 -1)}$$

where:

$$R = \frac{R_1}{R_4}\frac{1}{h_N} + \frac{R_1}{R_{M34}}\frac{R_4-R_3}{k_{SS}} + \frac{R_1}{R_{M23}}\frac{R_3-R_2}{k_{ST}} + \frac{R_1}{R_{M12}}\frac{R_2-R_1}{k_{TA}} \qquad \text{(Eq. 4.0 -2)}$$

where:

h_H = mercury side film conductance

k_{SS}, k_{ST} and k_{TA} are the thermal conductance of the stainless steel tube, stagnant NaK and the tantalum tube, respectively, and h_N is the flowing NaK film conductance. $R_{Mi,j}$ is the mean radius of the individual composite wall materials determined from

$$R_{Mi,j} = \frac{R_j - R_i}{\ln (R_j/R_i)} \qquad \text{(Eq. 4.0 -3)}$$

The approximation of the oval/round tube geometry in terms of the round/round tube geometry is shown in 10.1 of the Appendix. This approach simplifies the boiler design analysis as it allows the use of a one dimensional nodal network in the computer code.

Under SNAP-8 steady state operating conditions, the variations of NaK side transport properties and the double containment wall material thermal conductivities are relatively small. Thermal resistances of the NaK side and the double containment wall can be assumed as constants and lumped together as provided in Equation 4.0-1. Local heat transfer in various

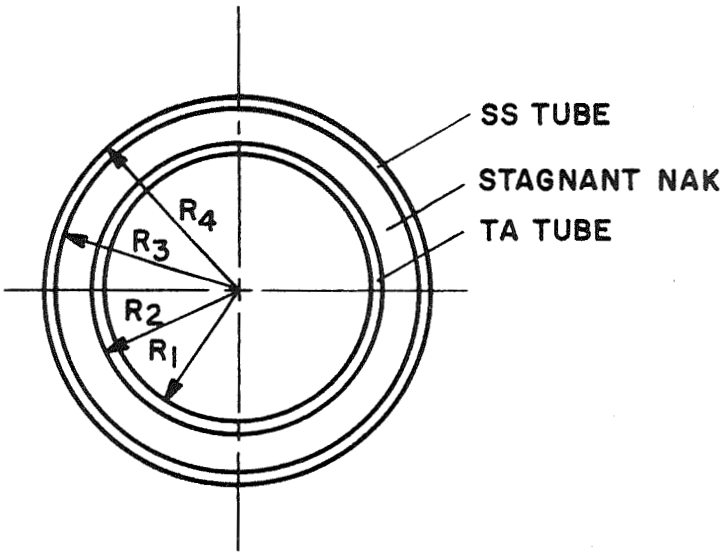

Figure 7.- Concentric Double Containment Ta-SS Tube Geometry

regions of the boiler are only functions of the Hg side film conductance. In the Hg preheat and wetted boiling region, film conductances are large ($h_H \geq 7000$ Btu/hr-ft^2-$^\circ$F), and heat transfer is governed by the combined NaK-side film and wall resistance. In the dry wall boiling and vapor superheat region, film conductances are small (h_H = 95 to 60 Btu/hr-ft^2-$^\circ$F), and heat transfer is governed by the Hg-side film resistance.

4.1 NaK-Side Film Conductance and Pressure Drop

To determine the NaK side film conductance, a reference is made to the boiler cross-section geometry shown in Figure 2. Figure 2 depicts a cross-section of the NaK in-line flow through a rod bundle configuration as defined by the equidistant triangular tube spacing (S) and stagnant NaK containment tube external diameter (D). Dwyer and Tu's semi-empirical correlation for fully established turbulent flow was selected for the film conductance determination (see Reference 12 and 13):

$$h_N = \frac{k_N}{De_N}\left[0.93 + 10.81\,\frac{S}{D_N} - 2.01\left(\frac{S}{D_N}\right)^2 + 0.252\left(\frac{S}{D_N}\right)^{0.278}\left(\bar{\Psi}\,Pe\right)^{0.8}\right]$$

(Eq. 4.1 -1)

where:

$$\bar{\Psi} = 1 - \frac{1.82}{Pr \left[\frac{\epsilon_M}{\nu}\right]^{1.4}_{max}} \qquad \text{(Eq. 4.1 -2)}$$

De_N = flow passage equivalent diameter

k_N = bulk NaK thermal conductivity

The maximum ratio of eddy momentum diffusivity to the kinematic viscosity $(\epsilon_M/\nu)_{max}$ as a function of Reynolds (Re) number is provided in Figure 8. In the above correlation, the stagnant NaK containment tube external diameter (D) was assumed to be $2R_4$, which is consistent with the oval/round tube treatment discussed in the preceding section.

For the reference boiler cross-section geometry, the predicted NaK side conductance (h_N) was 2680 Btu/hr-ft^2-^{o}F. The analysis of experimental and full scale boiler data, however, showed that these boilers operated at 12% higher film conductance. This increase can be attributed to the placement of the tube support structure in the NaK stream. These structures disrupt the laminar boundary layer thus augmenting the film conductance. A helical wire was placed around the tube bundle, to eliminate NaK flow and temperature stratification, and it also contributed to increased NaK-side heat transfer coefficients. The helical turbulator coil around the tube bundle is shown in Figure 9.

The NaK side pressure loss consists of the sum of the following losses:

ΔP_{in} - NaK entrance loss

ΔP_{ex} - NaK exit loss

ΔP_S - pressure losses incurred by the tube bundle supports

ΔP_C - NaK turbulator coil pressure loss

ΔP_B - pressure loss incurred by the NaK flow through the curved passages

The total pressure drop is then expressed as:

$$\Delta P_T = \Delta P_{in} + \Delta P_{ex} + \Delta P_S + \Delta P_C + \Delta P_B \qquad \text{(Eq. 4.1 -3)}$$

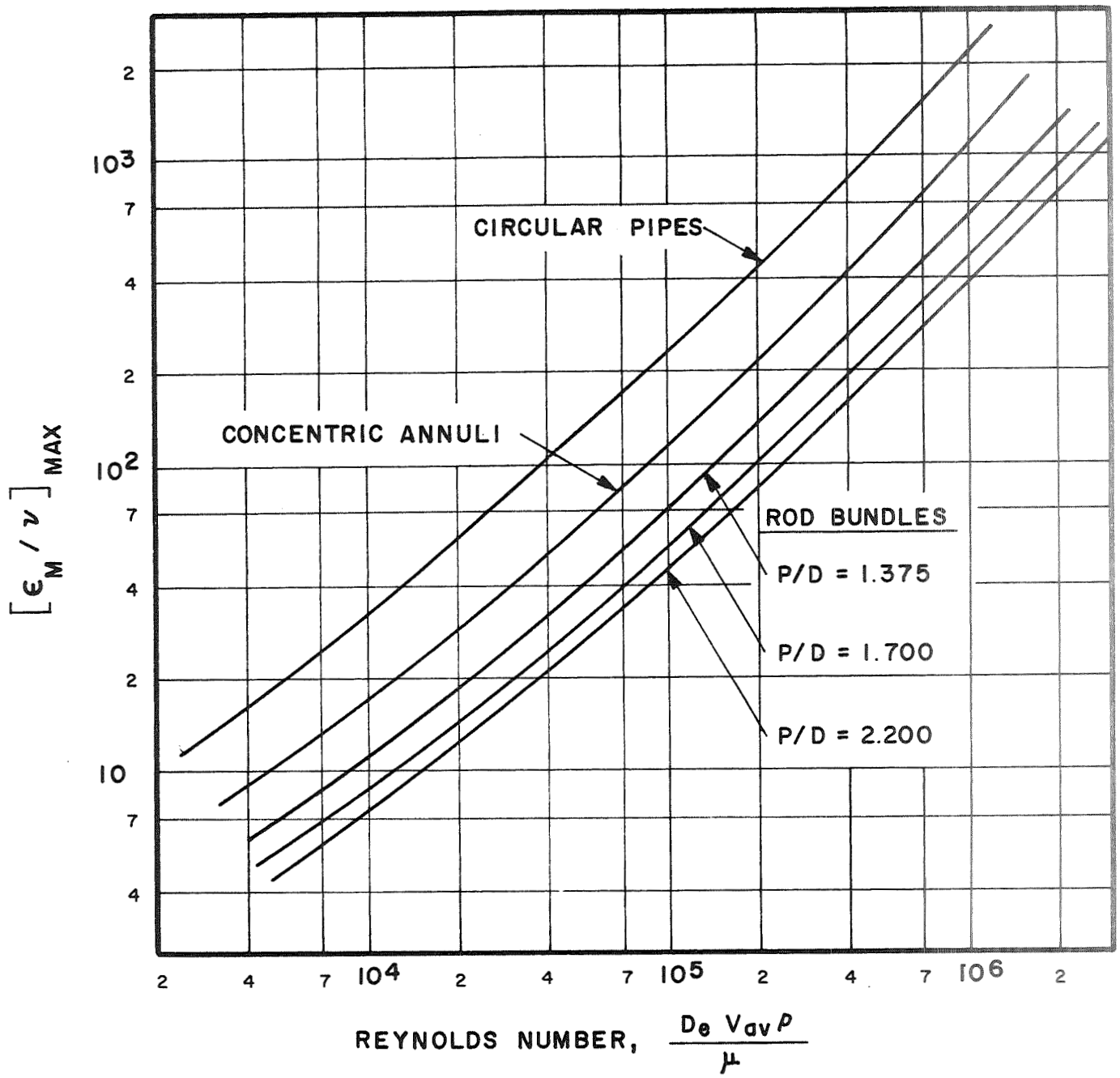

Figure 8.- Ratio of Eddy Momentum Diffusivity to the Kinematic Viscosity as a Function of Reynolds Number

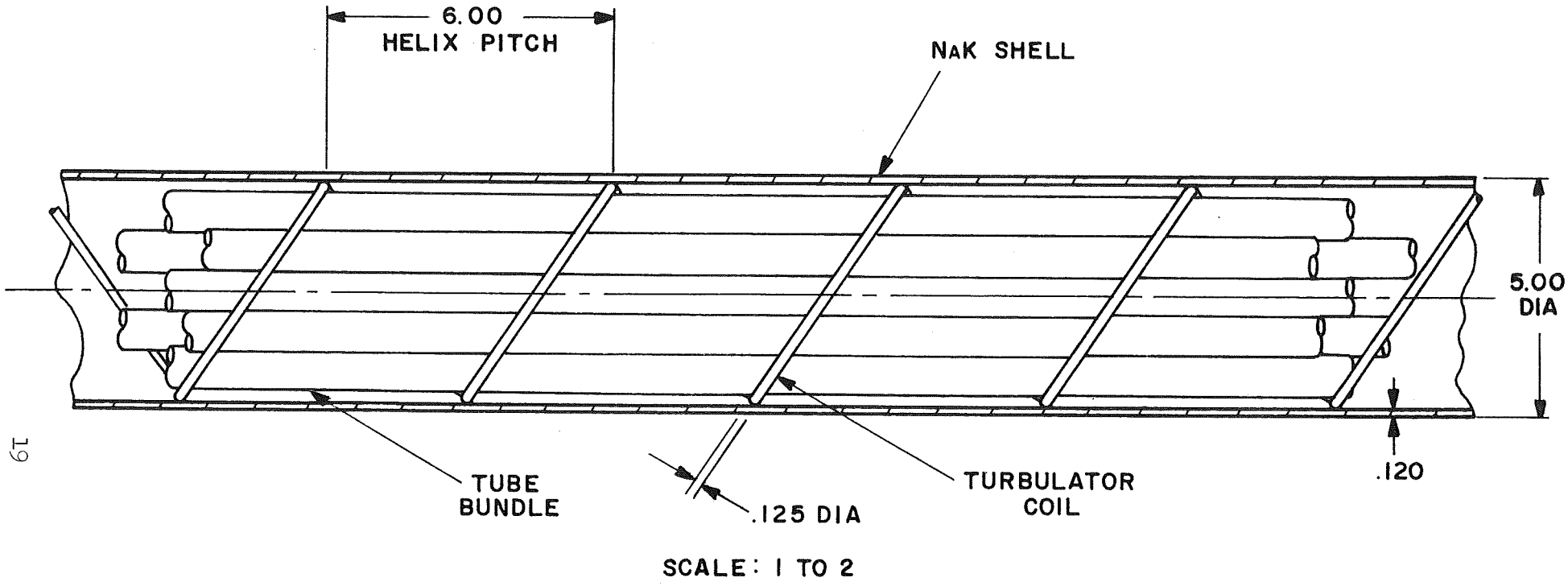

Figure 9.- BRDC Boiler No. 4 NaK Side Turbulator Coil

The velocity head method was used to calculate the individual losses. To proceed with this method, it was necessary to experimenatally determine the velocity head coefficients for the NaK turbulator coil (Figure 9), the Hg tube bundle support (Figure 2B) and the NaK inlet and exit sections (Figure 10). Two full-scale boiler experimental test sections were built and tested. A sample NaK-side pressure drop calculation is shown in 10.2 of the Appendix. Experimentally determined velocity head coefficients and the individually calculated losses in the boiler NaK flow passages are shown for BRDC No. 4. Figure 11 presents the NaK-side pressure loss as a function of NaK flow. The theoretically calculated pressure loss, as shown in Figure 11 (see 10.2 of the Appendix), is in excellent agreement with the experimental curve. At a NaK flow rate of 50,000 lbm/hr the 2.43 psi compares with the maximum allowable NaK-side pressure loss of 3.00 psi.

4.2 Preheat Section Design Correlations

For a given boiler design defined by the system NaK flow ($\dot{w}_N$) and mercury flow ($\dot{w}_{Hg}$), NaK inlet temperature (T_{Nbi}), mercury inlet (T_{Hbi}) and exit (T_{Hbo}) temperatures, mercury exit pressure (P_{Hbo}) and boiler cross-section geometry, the preheat section length is dependent on the available mercury preheat thermal potential and overall conductance (U) between the working fluids. The overall conductance was defined by the Equation 4.0-1, which requires the determination of the mercury side conductance from the following correlation (see Reference 12):

$$h_H = \frac{k_L}{De}\left[7.0 + 0.025\left(Pe - \frac{1.82\ Re}{(\epsilon_M/\nu)^{1.4}_{max}}\right)^{0.8}\right] \qquad \text{(Eq. 4.2 -1)}$$

where:

k_L = liquid Hg thermal conductivity

D_e = flow passage equivalent diameter

Re = Reynolds number

Pe = Peclet number

ϵ_M = Eddy diffusivity of momentum

ν = liquid Hg kinematic viscosity

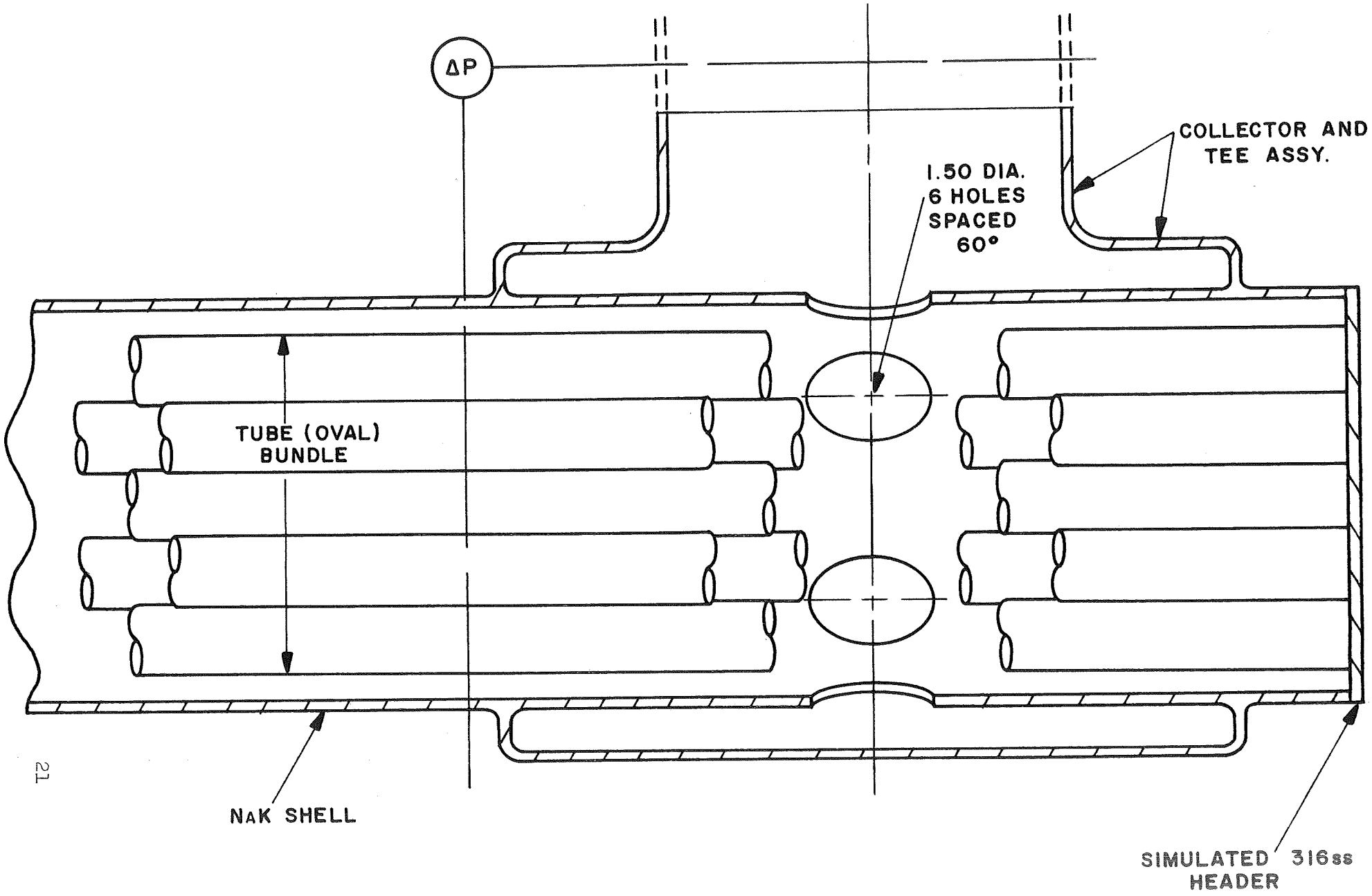

Figure 10.- BRDC Boiler No. 4 NaK Inlet and Outlet Flow Test Section

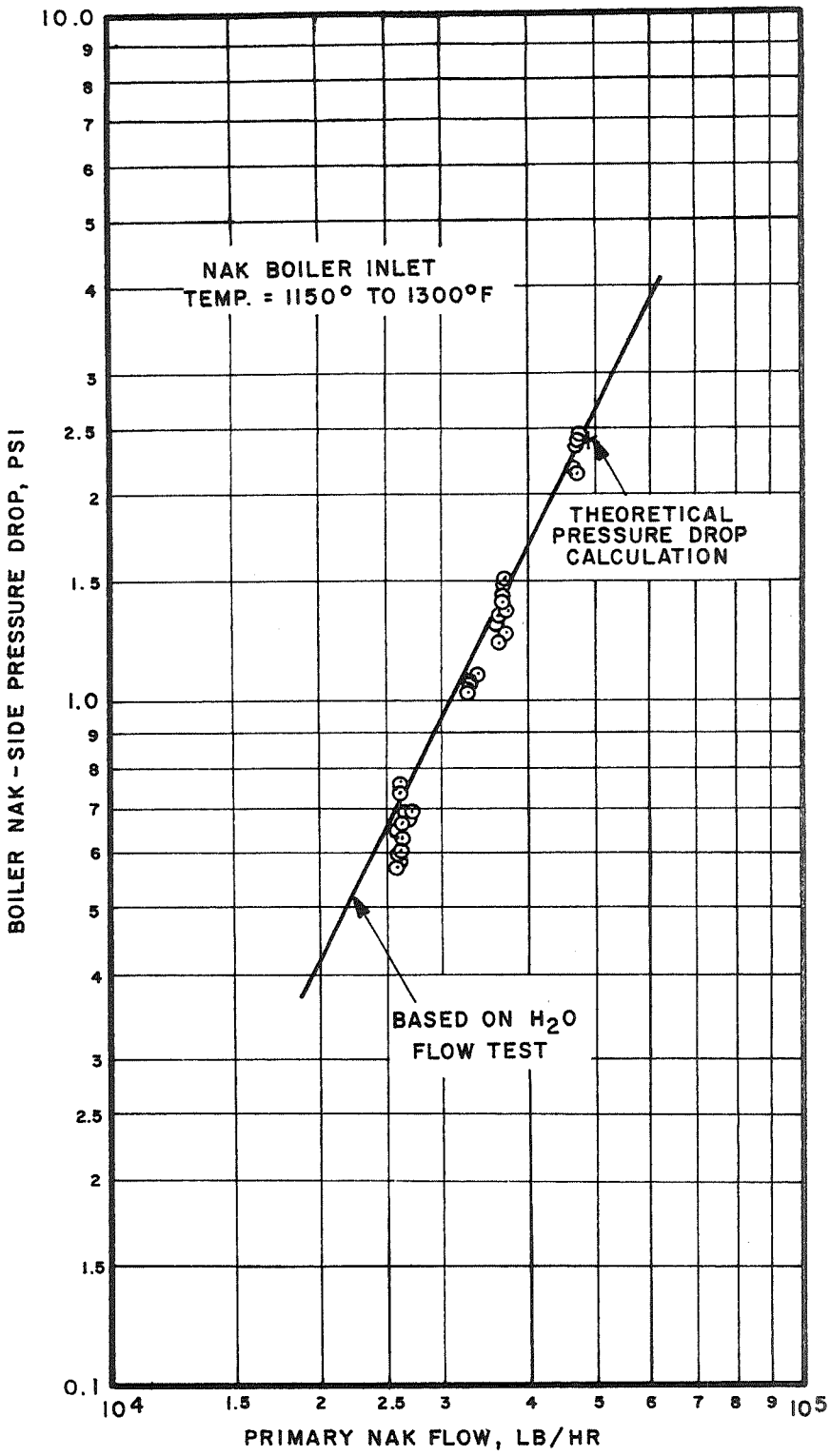

Figure 11.- BRDC Boiler No. 4 Nak-Side Pressure Drop Graph from H_2O Flow Test Data

The ratio (ϵ_M/ν) as a function of the Reynolds number (Re) is provided in Figure 8. Its value must be evaluated in the light of the critical Peclet (Pe) number as provided in Table I. As the Peclet number is increased, the critical value is that number at which eddy transport begins to assert itself in contributing to the total convective heat transfer rate. The thermal potential conditions in the preheat section are depicted in Figure 12. In this scheme, the NaK exit temperature (T_{Nbo}) can be determined from an overall heat balance and the preheat section inlet temperature difference. Therefore, the NaK inlet temperature difference is as follows:

$$\Delta T_{in} = T_{Nbo} - T_{Hbi} \qquad \text{(Eq. 4.2 -2)}$$

Table I. Critical Peclet Numbers

			Δ Rod Bundles		
N_{Pr}	Tubes	Annuli*	P/D = 1.375	P/D = 1.700	P/D = 2.200
0.005	117	270	460	622	770
0.01	131	300	530	720	890
0.02	144	330	582	800	1000
0.03	150	345	603	840	1056

* For heat transfer through either the inner or outer wall

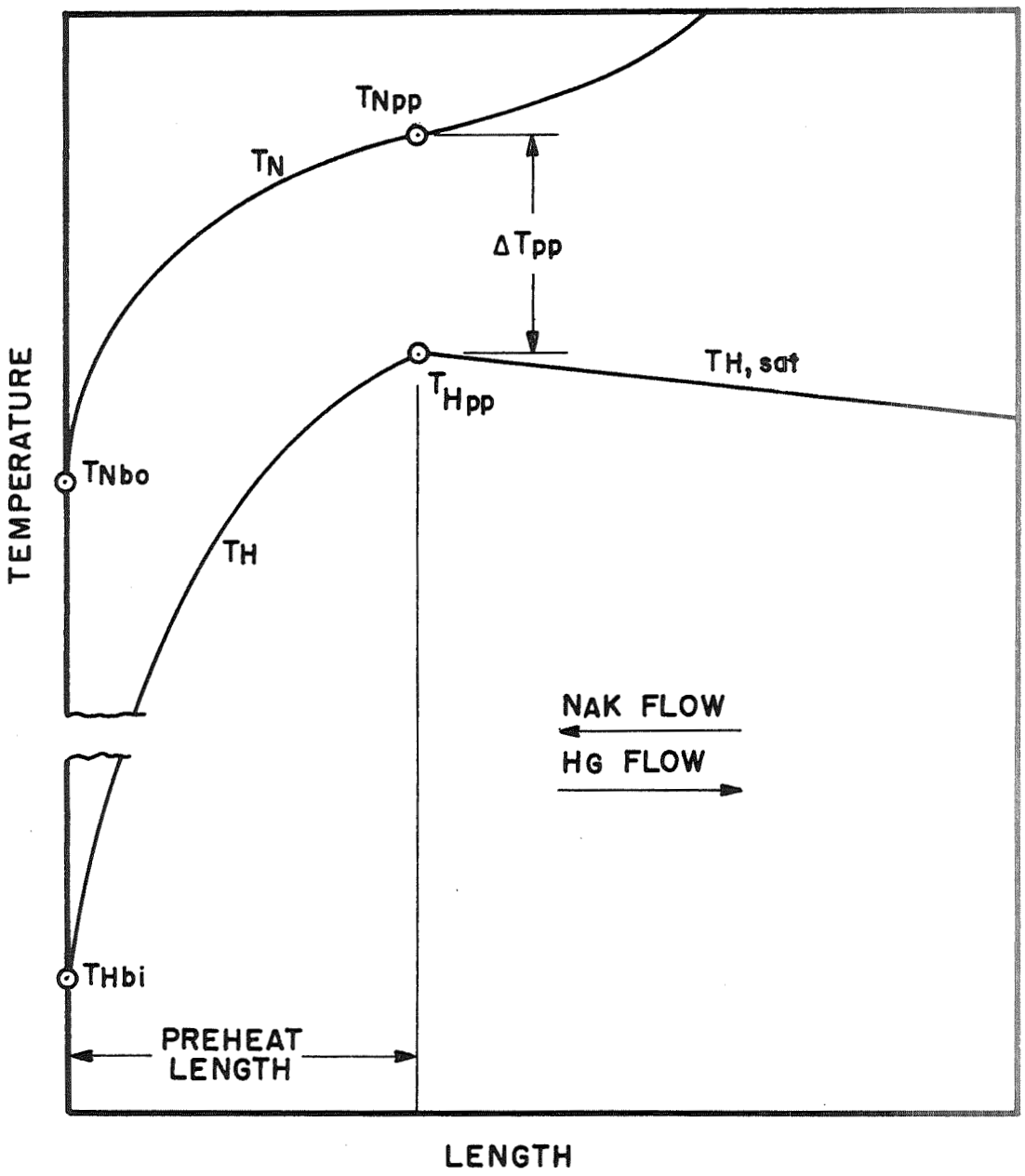

Figure 12.- Preheat Section NaK (T_N) and Mercury (T_H) Temperature Profiles

The preheat section exit temperature difference (ΔT_{pp})

$$\Delta T_{pp} = T_{Npp} - T_{Hpp} \qquad \text{(Eq. 4.2-3)}$$

is, however, not available because the mercury saturation temperature (T_{Hpp}) at the liquid-vapor interface is dependent on the local pressure which is a function of downstream pressure loss and the boiler exit pressure. The preheat section exit temperature difference (ΔT_{pp}), denoted in this text as "pinch point" temperature difference, is determined by an iterative process, which assumes convergent mercury inlet pressure and preheat section pressure loss values to meet the prescribed boiler exit pressure. For an assumed boiler inlet pressure (P_{Hbi}) and preheat section pressure loss (ΔP_{PH}) the mercury temperature at the liquid-vapor interface is:

$$T_{Hpp} = f\,(P_{Hbi} - \Delta P_{PH}) \qquad \text{(Eq. 4.2 -4)}$$

The preheat rate (q) is:

$$q = \dot{w}_H\, c_{pH}\, (T_{Hpp} - T_{Hbi}) \qquad \text{(Eq. 4.2 -5)}$$

The NaK temperature (T_{Npp}) at the liquid-vapor interface is:

$$T_{Npp} = T_{Nbo} + \frac{q}{\dot{w}_N\, c_{pN}} \qquad \text{(Eq. 4.2 -6)}$$

where:

$\dot{w}_H$ = mercury flow rate

$\dot{w}_N$ = NaK flow rate

c_{pH} = liquid mercury specific heat

c_{pN} = NaK specific heat

Inserting the calculated T_{Hpp} and T_{Npp} values from Equation 4.2-4 and 4.2-6, respectively, into Equation 4.2-3 and using Equation 4.2-2, the available log mean temperature may be obtained as follows:

$$\Delta T_M = \frac{\Delta T_{in} - \Delta T_{pp}}{\ln(\Delta T_{in}/\Delta T_{pp})} \qquad \text{(Eq. 4.2 -7)}$$

Noting that mercury film conductance (h_H) may be derived from Equation 4.2-1, the overall conductance (U) can be determined from Equation 4.0-1. Thus, the available preheat flux (q") is:

$$q'' = U \Delta T_M \qquad \text{(Eq. 4.2 -8)}$$

The required preheat length can be determined from:

$$L_{PH} = \frac{q}{N_1 P_W q''} \qquad \text{(Eq. 4.2 -9)}$$

where:

N_1 = mercury tube count

P_W = wetted perimeter

q = preheat rate from Equation 4.2 -5.

Pressure loss in the preheat section is determined from the conventional Darcy pressure loss correlation:

$$\Delta P = f \frac{L}{De} \frac{G^2}{2 g_c \rho_o} \qquad \text{(Eq. 4.2 -10)}$$

where:

$$f = \frac{0.316}{Re^{.25}} \qquad \text{(Eq. 4.2 -11)}$$

De = flow passage equivalent diameter

G = specific mass velocity

g_c = gravitational constant

ρ_o = liquid mercury density

4.3 Vapor Quality Section Design Correlations

The determination of the vapor quality section length is based on two-phase flow heat and momentum transfer correlations established during early tests on refractory metal boilers. The validity of these design correlations was successfully supported by the test results of experimental and full scale tantalum-stainless steel boilers. To justify this judgment, comparison of test data with design predictions is depicted in Figure 13. The NaK temperature profile in Figure 13 is subdivided in 10% vapor quality increments (⊙——⊙) from x = 0 to x = 100%. This region comprises the vapor quality section and contains the two-phase flow regimes. The preceding and following tube lengths are the mercury preheat and superheat sections, respectively. An additional theoretical curve (T_H) is the mercury temperature which shows the sensible heat addition up to the preheat length termination point (ΔT_{pp}). In the vapor quality region, T_H is the vapor saturation temperature, a function of the saturation pressure, and thereafter it represents the vapor superheat temperature. The pinch point temperature difference (ΔT_{pp}) is the available thermal potential for the incipient mercury boiling in the MPP section. The theoretical NaK temperature profile (T_N) is in excellent agreement with the measured NaK shell tube wall temperatures, and both the predicted NaK temperature profile (T_N) and the pressure profile (P_H) meet the boiler terminal temperature and pressure measurements, respectively. The pressure profile (P_H) also agrees with the pressure measurement at the end-point of the multipassage plug insert.

The vapor quality region containing a high NaK temperature gradient ($\frac{\partial T_N}{\partial L}$) is postulated as a wetted boiling regime for the vapor quality regime from 0 to 88%. Heat and momentum transfer correlations for this regime are derived from a separated two-phase flow model. The simplified geometry of such a model can be visualized in a bare tube when the liquid phase in the form of a laminar concentric annular film is placed on the tube wall and is flowing simultaneously with the turbulent vapor core. These separated flow correlations were modified and applied to the helical flow passage geometry.

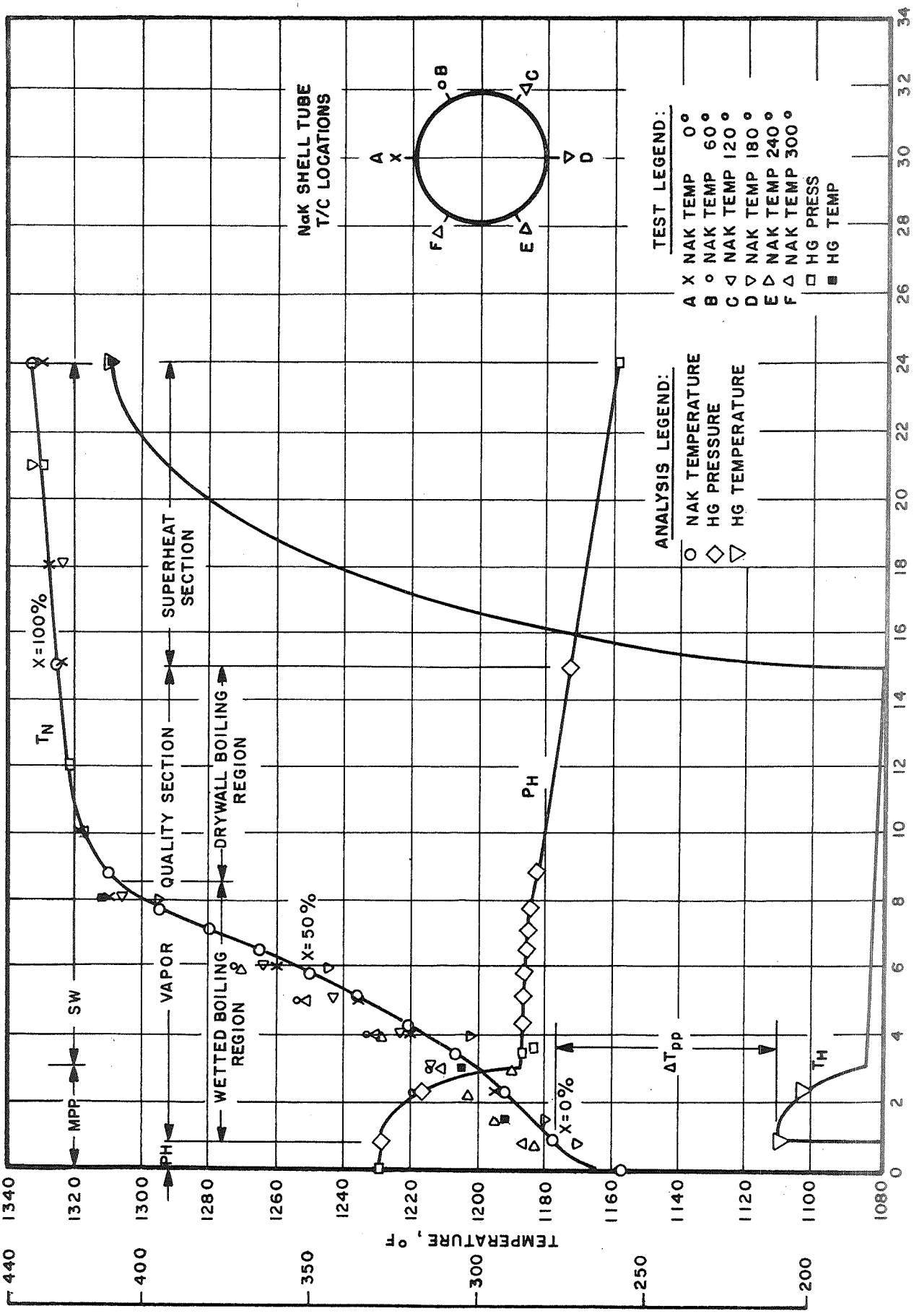

Figure 13.- Typical SNAP-8 Ta-SS Boiler Temperature and Pressure Profiles

In order to evaluate the boiling film conductance of a separated two-phase flow model, three boiling modes were postulated in the liquid layer contiguous to the tube wall. The first mode consists of a superheated liquid layer that is heated from the tube wall and loses heat from the liquid-vapor interface by evaporative heat transfer. Heat transmission through the liquid layer itself is achieved by conduction. The second mode is defined by a superheated liquid layer with wall heat addition and a uniform volume heat sink representing volume boiling. The third mode is defined by a superheated liquid layer with wall heat addition and a volume heat sink that varies linearly from a maximum value at the wall to zero at the liquid-vapor interface. No liquid-vapor interface evaporative heat transfer occurs in the last two modes. The general differential equation defining these three boundary value problems is:

$$\bar{u}\,\frac{\partial t}{\partial x} = \alpha\,\frac{\partial^2 t}{\partial r^2} - \frac{S}{\rho_o\, c_{pf}} \qquad \text{(Eq. 4.3 -1)}$$

where:

r = radial distance

x = axial distance

t = temperature

α = thermal diffusivity

S = volumetric heat sink function

ρ_o = liquid density

c_{pf} = liquid specific heat

$\bar{u}$ = velocity

In all cases $\partial t/\partial x = 0$. For the first mode $S = 0$, for the second mode $S = S_m$, and for the third mode $S = So\ (1 - r/\delta)$, where S_m and So are the mean volumetric heat sink and volumetric heat sink evaluated at the tube wall respectively and $\delta = r_o - r_1$ is the liquid layer thickness bounded by the tube internal radius (r_o) and the liquid-vapor interface radius (r_1). A temperature solution was derived for each heat transfer mode. Next, the difference between the wall and liquid-vapor interface

temperatures was substituted into the Nusselt modulus equation:

$$Nu = C \frac{D}{\delta} \qquad \text{(Eq. 4.3 -2)}$$

where:

D = tube internal diameter

δ = liquid layer thickness

C = 1 for heat loss at the liquid-vapor interface

C = 2 for a uniform volume heat sink

C = 3 for heat sink that varies linearly from a maximum value at the wall to zero at the liquid-vapor interface.

The solution of Equation 4.3.-2 requires prior determination of the liquid layer thickness in terms of local vapor quality. The liquid layer thickness is obtained from the momentum transfer correlations for the separated two-phase flow regime in the plug insert and swirl wire tube sections, respectively. These correlations are provided in Sections 4.3.1 and 4.3.2.

The vapor quality region at $x \geq 88\%$ is represented by a relatively small NaK temperature gradient $(\frac{\partial T_N}{\partial L})$ which indicates significantly smaller decreasing heat flux with increasing vapor content. This region is postulated as a mixed droplet-vapor two-phase flow dry wall boiling regime. Under helical flow conditions, when the annular liquid film is not present at the tube wall, the liquid phase is concentrated in the form of droplets in the vapor stream, which intermittently contact the hot wall. Droplet concentration at the tube wall is caused by the helical flow radial acceleration component. The dry wall boiling heat transfer correlations are, therefore, derived from a model considering droplet vaporization on a hot plate.

4.3.1 Multipassage Plug Insert

The purpose of the helical multipassage insert (MPP) is to induce early vortex two-phase flow in the MPP flow passages and to provide sufficient vapor volume flow at the inlet to the swirl wire (SW) tube section for the purpose of sustaining the helical two-phase flow pattern. The determination of the mercury vapor state conditions at the MPP termination point is based on Koestel's (see Reference 2) semi-empirical criteria which provides, that in the design of mercury boilers, the quantity;

$$\rho_l \, u_l^2 = 142 \, \frac{\text{lbm}}{\text{ft sec}^2} \qquad \text{(Eq. 4.3.1-1)}$$

can be considered a critical value, below which the forced convection pool boiling Nusselt numbers should be applied, and above which, vortex boiling Nusselt numbers should be applied. In the above correlation ρ_l and u_l are the vapor density and the vapor linear velocity, respectively, in the SW tube section next to the MPP termination point. Data obtained from SNAP-8 experimental boilers indicate that the constant, 142, is conservative and can be reduced to 115 without detrimental effect on boiler performance stability. The required MPP length is dependent on incipient boiling heat flux which is governed by the available pinch point temperature difference (ΔT_{pp}). A high ΔT_{pp} results in a relatively short MPP design length, a low MPP pressure drop (see Figure 14), and stable boiler performance characteristics. For the reference boiler MPP cross-section geometry (see Figure 2B) and a MPP length of 3 feet, as used in experimental boiler tests, Figure 15 depicts the ΔT_{pp} plotted in terms of the MPP vapor exit quality (x_{PL}). It shows that at least $\Delta T_{pp} = 40^{\circ}F$ and $x_{PL} = 11\%$ are required to hold the boiler exit pressure variation within acceptable limits (0 to ± 5 psi), under prescribed system operating conditions. The SNAP-8 MPP design length was defined by the pinch point temperature difference and MPP vapor exit quality of $40^{\circ}F$ and 11% respectively. These values are referred to as the low boiler NaK inlet temperature schedule that must be used for the MPP and total boiler length determination. The effect

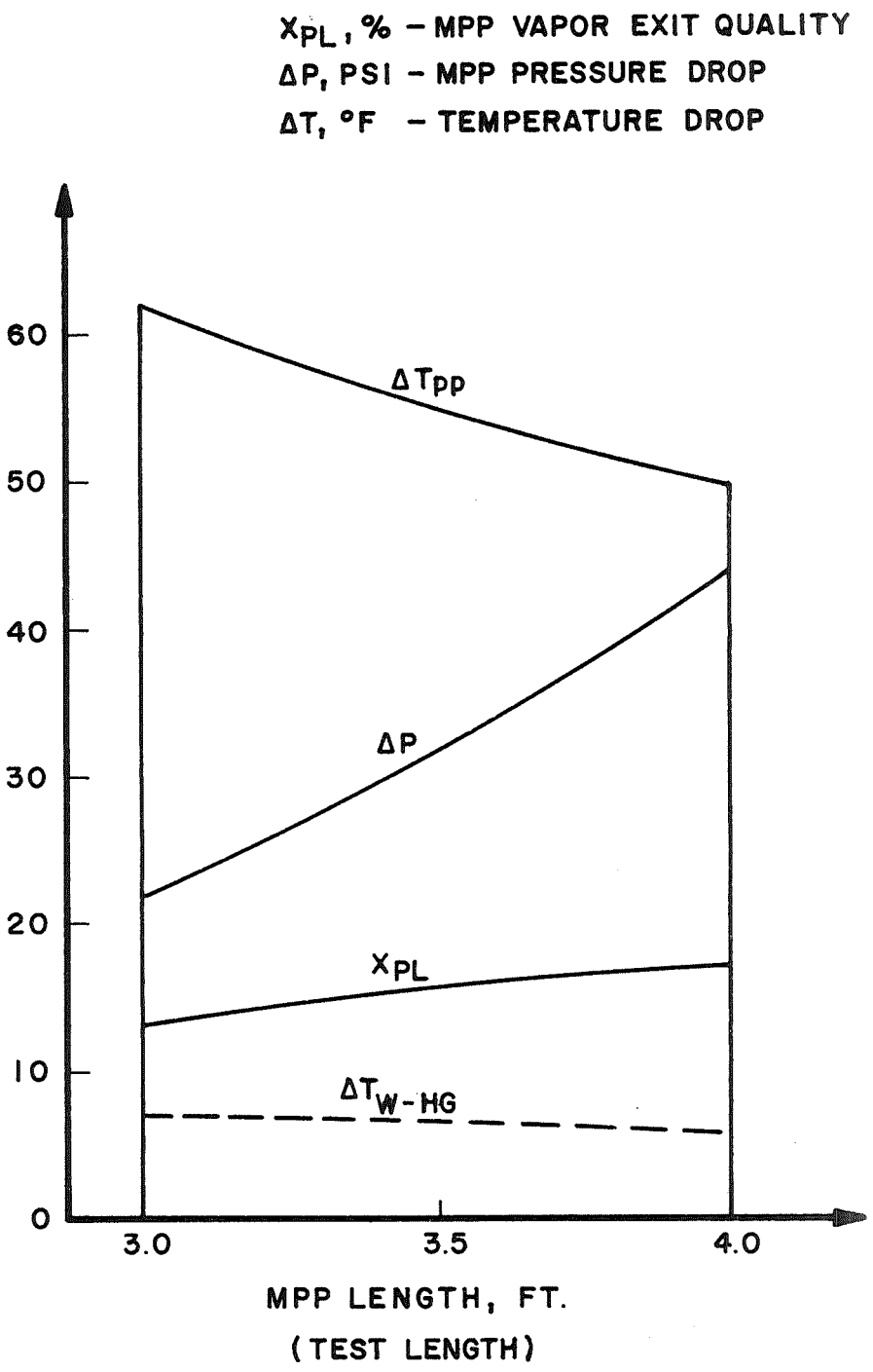

Figure 14. MPP Operating Parameter Versus MPP Length

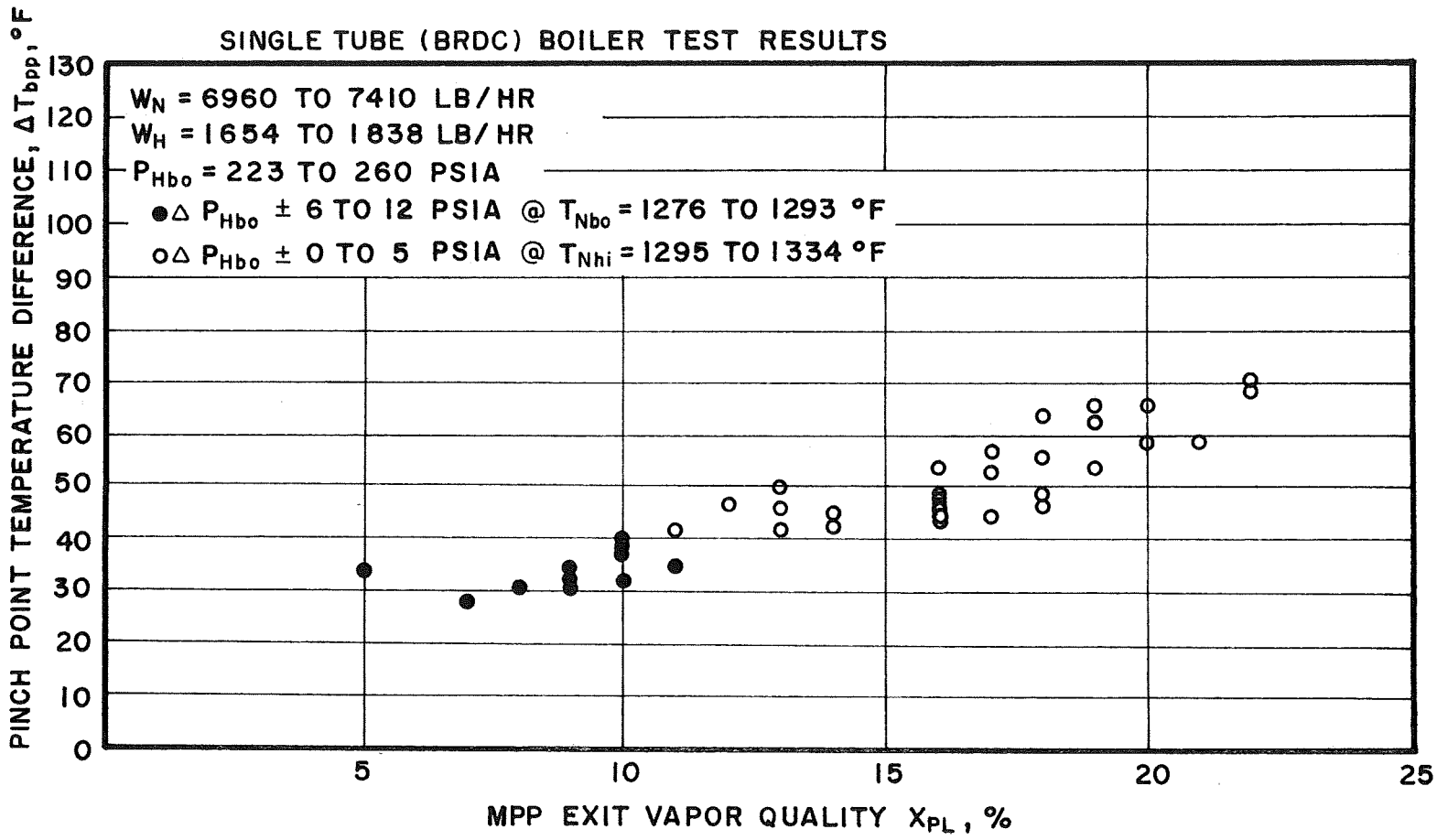

Figure 15. Pinch Point Temperature Difference Versus MPP Exit Vapor Quality (MPP Length = 3 feet)

of the MPP length variation on pinch point temperature difference (ΔT_{pp}), MPP pressure drop (ΔP), and the vapor exit quality (x_{PL}) under SNAP-8 system nominal operating conditions is shown in Figure 14. It also shows the magnitude of ΔT_{pp} in relation to temperature drop across the mercury side film, which is denoted by ΔT_{W-HG}.

To obtain the boiling film conductance, the local liquid layer thickness (Equation 4.3-2) must be determined in the MPP geometry as shown in Figure 16. From the shear stress-pressure drop and shear stress-strain equations, one can obtain an equation for the velocity profile in the liquid layer as follows for $r_1 < r < r_o$;

$$V = \frac{1}{4\,\mu_o} \frac{\partial p}{\partial x} (r^2 - r_o^2) \qquad \text{(Eq. 4.3.1-2)}$$

Upon integration from r_o to r_1, the liquid mass flow rate, $\dot{w}_o$, can be obtained as follows:

$$\dot{w}_o = \frac{\beta\,\rho_o}{8\,\mu_o} \left[-\frac{1}{2} (r_o^4 - r_1^4) + r_o^2 (r_o^2 - r_1^2) \right] \left(\frac{\partial P}{\partial X}\right)_o \qquad \text{(Eq. 4.3.1-3)}$$

where:

V = velocity profile in liquid layer

μ_o = liquid viscosity

$\left(\frac{\partial P}{\partial X}\right)_o$ = axial frictional pressure gradient in liquid phase

r = radial distance

r_o = inside radius of tube

r_1 = radial distance to interface between two phases

$\dot{w}$ = liquid mass flow rate

ρ_o = liquid density

β = angle subtended by the insert helical groove (see Figure 16)

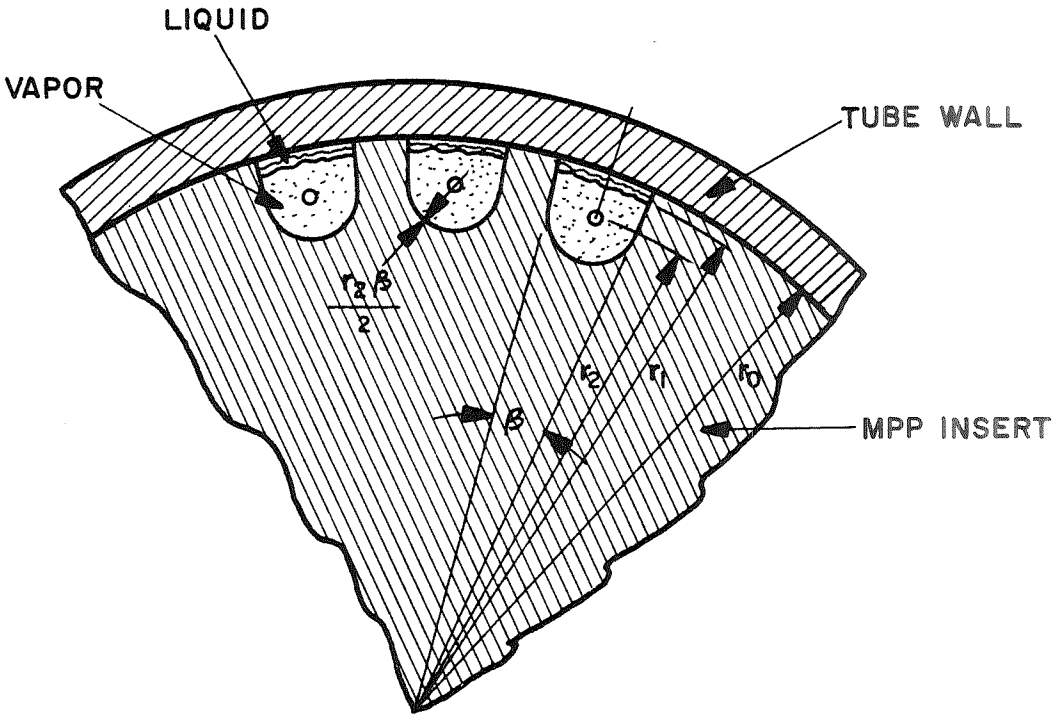

(A) SCHEMATIC DIAGRAM OF MPP INSERT CROSS SECTION

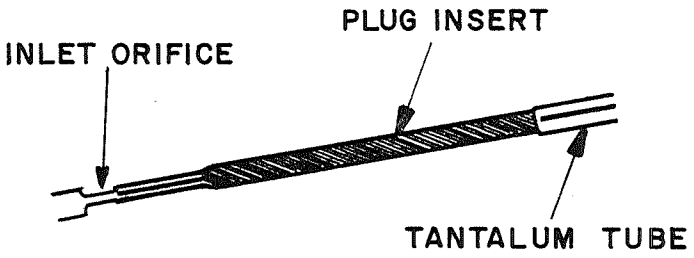

(B) ARRANGEMENT OF INLET ORIFICE, TANTALUM PLUG AND TANALUM TUBE

Figure 16.- Tantalum Plug Insert

The pressure drop equation for the turbulent vapor core in the MPP is:

$$\left(\frac{\partial p}{\partial X}\right)_1 = \frac{\xi_{INT}\, \rho_1\, V^2}{4\, R_h\, 2\, g_c} \qquad \text{(Eq. 4.3.1-4)}$$

where:

ξ_{INT} = friction factor for interface between the liquid and vapor phase

ρ_1 = vapor density

V = average vapor velocity

R_h = hydraulic radius

g_c = gravitational constant

In this analysis, it is postulated that the viscous liquid-turbulent vapor interface velocity is small compared to the average vapor velocity, V, and is thus neglected. The geometric bounds of the idealized passage in the MPP are arcs of circles and radial segments. Thus, the hydraulic radius definition is:

$$R_h = \frac{(r_1^2 - r_2^2)\,\frac{\beta}{2} + \frac{\pi}{8}\,(\beta\, r_2)^2}{\beta r_1 + 2\,(r_1 - r_2) + \frac{\pi}{2}\,\beta\, r_2} \qquad \text{(Eq. 4.3.1-5)}$$

where:

r_2 is the radial distance to the center of the arc defining the inner bounds of the MPP passage.

The mean vapor velocity squared, V^2, can be expressed in terms of the following continuity equation:

$$V^2 = \frac{\dot{w}_1^2}{(\text{flow area})^2\, \rho_1^2} = \frac{\dot{w}_1^2}{\rho_1^2\left[(r_1^2 - r_2^2)\,\frac{\beta}{2} + \frac{\pi}{8}\,(\beta\, r_2)^2\right]^2} \qquad \text{(Eq. 4.3.1-6)}$$

where:

$\dot{w}_1$ is the vapor flow rate. By substitution of Equation 4.3.1-5 and 4.3.1-6 into 4.3.1-4 we obtain:

$$\left(\frac{\partial p}{\partial x}\right)_1 = \frac{\xi_{INT}}{8\, g_c}\,\frac{\dot{w}_1^{\,2}}{\rho_1}\,\frac{\left[\beta\, r_1 + 2\,(r_1 - r_2) + 1/2\,\pi\,\beta\, r_2\right]}{\left[(r_1^{\,2} - r_2^{\,2})\,\frac{\beta}{2} + \frac{\pi}{8}\,(\beta\, r_2)^2\right]^3} \qquad \text{(Eq. 4.3.1 -7)}$$

By noting that in a parallel flow circuit, the pressure drop terms in Equation 4.3.1-3 and 4.3.1-7 are equal, one can obtain the following:

$$\left(\frac{\partial p}{\partial x}\right)_o = \left(\frac{\partial p}{\partial x}\right)_1 \qquad \text{(Eq. 4.3.1 -8)}$$

which results in the following:

$$\frac{128}{\xi_{INT}\beta}\,\frac{Y}{X}\,\frac{\left[(\rho^2 - \rho_2^{\,2})\,\frac{\beta}{2} + \frac{\pi}{8}\,(\beta\,\rho_2)^2\right]^3}{\left[\beta\,\rho + 2\,(\rho - \rho_2) + \pi\,\beta\,\rho_2\right]} = (1 - \rho^2)^2 \qquad \text{(Eq. 4.3.1 -9)}$$

where:

$$X = \frac{\bar{x}\,\rho_o\,\mu_1}{(1-\bar{x})\,\rho_1\,\mu_o} \qquad \text{(Eq. 4.3.1 -10)}$$

$$Y = \frac{N_1\,N_2\,r_o\,\mu_1}{12\,\bar{x}\,\dot{w}_H} \qquad \text{(Eq. 4.3.1 -11)}$$

$$\rho = \frac{r_1}{r_o} \qquad \text{(Eq. 4.3.1 -12)}$$

$$\rho_2 = \frac{r_2}{r_o} \qquad \text{(Eq. 4.3.1 -13)}$$

$$\dot{w}_H = \dot{w}_o + \dot{w}_1 \qquad \text{(Eq. 4.3.1 -14)}$$

$\bar{x}$ = local average vapor quality by weight

N_1 = number of mercury tubes

N_2 = number of mercury passages in the MPP

The interface frictional pressure drop coefficient (ξ_{INT}) determination for Equation 4.3.1-9, is discussed in Section 4.3.5. Using the reference boiler design parameters and MPP geometry, $\xi_{INT} = 0.55$.

Inserting the calculated values from Equation 4.3.1-10 and 4.3.1-11 into Equation 4.3.1-9 the nondimensional liquid layer thickness defined by Equation 4.3.1-12 can be calculated. Rho (ρ) is the root of the nonlinear correlation defined by Equation 4.3.1-9. Thus, the local liquid layer thickness determined as follows:

$$\delta = (1 - \rho)\, r_o \qquad \text{(Eq. 4.3.1 -15)}$$

and inserted in the following correlation to obtain the mercury liquid film conductance (h_H).

$$h_H = \frac{k_L}{De}\, C\, \frac{D}{\delta} \qquad \text{(Eq. 4.3.1 -16)}$$

where:

k_L = liquid thermal conductivity at saturation temperature

De = MPP flow passage equivalent diameter

D = inside tube diameter

As indicated in Section 4.3 the values for C can range from 1 to 3 depending on the specific nucleation process in operation. In the multipassage plug insert region, a value of C = 1 was most representative for the experimental test results.

The local overall conductance (U) can be determined from Equation 4.0-1 and the local boiling heat transfer parameters and corresponding MPP length can be calculated in accordance with the procedure discussed herein.

The two-phase flow frictional pressure drop $(\partial p/\partial x)_{TF}$ is generalized as follows. The frictional pressure drop in the MPP passage, if completely filled with the available vapor, $\bar{x}\ \dot{w}_{Hg}$, would be:

$$\left(\frac{\partial p}{\partial x}\right)_{\text{all vapor}} = \frac{\xi\ \bar{x}\ \dot{w}_H^{\,2}}{8\ g_c\ \rho_1^{\,2}} \frac{\left[\beta\ r_o + 2\ (r_o - r_2) + \frac{\pi}{2}\ \beta\ r_2\right]}{\left[(r_o^{\,2} - r_2^{\,2})\ \frac{\beta}{2} + \frac{\pi}{8}\ (\beta\ r_2)^2\right]^3} \qquad \text{(Eq. 4.3.1 -17)}$$

Upon dividing Equation 4.3.1-7 by Equation 4.3.1-17, one obtains the two-phase flow factor:

$$\Phi = \frac{(\partial p/\partial x)_{TF}}{(\partial p/\partial x)_{\text{all vapor}}} \qquad \text{(Eq. 4.3.1 -18)}$$

$$= \frac{\xi_{INT}}{\xi}\left[\frac{\beta\ \rho + 2\ (\rho - \rho_2) + \frac{\pi}{2}\ \beta\ \rho_2}{\beta + 2\ (1 - \rho_2) + \frac{\pi}{2}\ \beta\ \rho_2}\right]\left[\frac{(1 - \rho_2)^2\ \frac{\beta}{2} + \frac{\pi}{8}\ (\beta\ \rho_2)^2}{(\rho^2 - \rho_2^{\,2})\ \frac{\beta}{2} + \frac{\pi}{8}\ (\beta\ \rho_2)^2}\right]^3$$

Using the values previously defined for Equation 4.3.1-9 we can obtain the following:

$$(\partial p/\partial x)_{TF} = \partial p/\partial x_1$$

Thus, the two-phase pressure drop correlation results in the following equation:

$$\Delta P_{TF} = \Phi\ \xi\ \frac{\Delta L}{\cos\ \alpha_B\ De}\ \frac{\bar{x}\ G^2}{2\ g_c\ \rho_1} \qquad \text{(Eq. 4.3.1 -19)}$$

where:

$\bar{x}$ = average local vapor quality

G = specific mass velocity

De = equivalent diameter

ΔL = flow passage axial length corresponding to local vapor quality increment

$\alpha_B = \tan^{-1}\frac{\pi D}{p}$ = MPP passage helical angle

ρ_1 = vapor phase density

ξ = all vapor flow frictional pressure drop coefficient in helical flow passages (see Equation A10.3-22 in Appendix)

D = tube ID

p = helix pitch

g_c = gravitational constant

4.3.2 Swirl Wire Tube Wetted Boiling Region

The wetted boiling correlations employed in the MPP are also applied in the swirl wire (SW) tube section up to a vapor quality point of 88%, the limiting condition for a high NaK temperature profile gradient as shown in Figure 13. The inlet conditions in the SW tube section are those established at the MPP exit.

To obtain the mercury film conductance (Eq. 4.3-2), the liquid layer annular thickness at the tube wall is determined from a separated two-phase flow model as shown in Figure 17. Based on the liquid layer velocity profile (Eq. 4.3.1-2) and assuming $\beta = 2\pi$ in Equation 4.3.1-2, the liquid mass flow rate may be obtained as follows:

$$\dot{w}_o = \frac{\pi \rho_o}{4 \mu_o}\left[-\frac{1}{2}(r_o^4 - r_1^4) + r_o^2 (r_o^2 - r_1^2)\right]\left(\frac{\partial p}{\partial x}\right)_o \qquad \text{(Eq. 4.3.2-1)}$$

The pressure gradient for the turbulent vapor core at $0 < r < r_1$ is:

$$\left(\frac{\partial p}{\partial x}\right)_1 = \frac{\xi_{INT}\, \rho_1\, \nu_r}{(2\, r_1)(2\, g)} \qquad \text{(Eq. 4.3.2-2)}$$

where:

ν_r is vapor core velocity relative to the liquid-vapor interface.

Noting that the absolute vapor core velocity is:

$$\bar{u} = V_1 + \nu_r$$

where:

$$V_1 = \frac{1}{4\, \mu_o}\left(\frac{\partial p}{\partial x}\right)_1 (r_1^2 - r_o^2) \quad \text{(from Equation 4.3.1-2),}$$

the vapor core weight flow may be calculated as follows:

$$\dot{w}_1 = \pi\, r_1^2\, \rho_1 \left[\frac{1}{4\, \mu_o}\left(\frac{\partial p}{\partial x}\right)_1 (r_1^2 - r_o^2) + \nu_r\right] \qquad \text{(Eq. 4.3.2-3)}$$

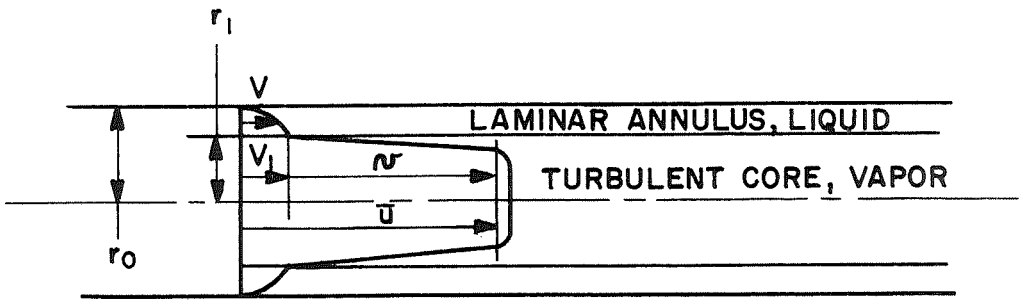

Figure 17.- Separated Two-Phase Flow Model

From the above equations we can obtain:

$$\nu^2 = \frac{\dot{w}_1^2}{\pi^2 r_1^4 \rho_1^2} + \frac{1}{2\mu_o}(r_o^2 - r_1^2)\left(\frac{\partial p}{\partial x}\right)_1 \frac{\dot{w}_1}{\pi r_1^2 \rho_1} + \frac{1}{16\mu_o^2}(r_o^2 - r_1^2)^2 \left[\frac{\partial p}{\partial x}\right]_1^2$$

(Eq. 4.3.2 -4)

The parallel flow circuit of a laminar annulus and a turbulent core provides:

$$\left(\frac{\partial p}{\partial x}\right)_o = \left(\frac{\partial p}{\partial x}\right)_1$$

Based on above the Equations 4.3.2-1, 4.3.2-2 and 4.3.2-4 we can obtain the following nonlinear correlation:

$$\frac{1}{2} X \left(\frac{\mu_o}{\mu_1}\right)\left(\frac{1-\rho^2}{\rho^3}\right) + \frac{4\pi}{\xi_{INT}} X Y \left(\frac{\mu_o}{\mu_1}\right) +$$

$$\left[\left(\frac{4\pi}{\xi_{INT}}\right)X^2 Y \left(\frac{\mu_o}{\mu_1}\right)^3 \left(\frac{1-\rho^2}{\rho^3}\right) + \left(\frac{4\pi}{\xi_{INT}}\right)^2 X^2 Y^2 \left(\frac{\mu_o}{\mu_1}\right)^4\right]^{1/2} = \frac{1}{\rho} \qquad \text{(Eq. 4.3.2-5)}$$

which then may be used to determine the non-dimensional liquid layer thickness (ρ). Inserting the latter in Equation 4.3.1-15, the true liquid layer thickness may be obtained. The X,Y and ρ values are defined by Equations 4.3.1-10 through 4.3.1-12, where $N_2 = 1$ for the SW tube section.

$$\left(\frac{\partial p}{\partial x}\right)_{\text{all vapor}} = \frac{\xi}{4\pi^2 r_o^5 \rho_l g_c} \dot{w}_l^2 \qquad \text{(Eq. 4.3.2-6)}$$

Denoting $\left(\frac{\partial p}{\partial x}\right)_{TF} = \left(\frac{\partial p}{\partial x}\right)_l$ and dividing $\left(\frac{\partial p}{\partial x_l}\right)$, as determined from Equations 4.3.2-2 and 4.3.2-4, into $\left(\frac{\partial p}{\partial x}\right)_{\text{all vapor}}$, the two-phase pressure drop factor Φ may be obtained as follows:

$$\Phi = \frac{\left(\frac{\partial p}{\partial x}\right)_{TF}}{\left(\frac{\partial p}{\partial x}\right)_{\text{all vapor}}}$$

$$= \frac{\xi_{INT}}{\xi}\left(\frac{r_o}{r_l}\right)^5 \left[1 - \left(\frac{2 r_l^2}{r_o^2 - r_l^2}\right)\left(\frac{\rho_l}{\rho_o}\right)\left(\frac{1 - \bar{x}}{\bar{x}}\right)\right]^2 \qquad \text{(Eq. 4.3.2 -7)}$$

where: ρ_o, ρ_l, and $\bar{x}$ are the liquid and vapor phase density and the average vapor quality in local vapor quality increments, respectively. Xi (ξ) is the frictional pressure drop coefficient for vapor flow only which is given by Equation 4.3.4-10. For the reference boiler SW tube section geometry, the interface frictional pressure drop coefficient $\xi_{INT} = 0.05$. Its determination is discussed in Section 4.3.5. The basic two-phase pressure drop correlation is provided by Equation 4.3.1-19.

4.3.3 Swirl Wire Dry Wall Boiling Tube Region

As discussed in Section 4.3 and shown in Figure 13, the bounds of the dry wall boiling regime are identified as being within the vapor quality area of 88 and 100%. Heat transfer correlations for this region were derived from the definition of stationary film boiling droplet vaporization models. In the model of the stationary droplet vaporization on a hot horizontal surface, the droplet is forced towards the surface by the gravity force similar to that developed by the radial acceleration in a helical flow pattern. In both cases, the droplets are supported by the high velocity vapor film at the wall. For this reason the stationary drop model detailed in Reference 4 was used to approximate the flow case.

The heat transfer from a tube wall to vaporize a liquid droplet contiguous to the wall is given by the following relation:

$$q = k_v \frac{(t_w - t_s)}{\delta} A_d \qquad \text{(Eq. 4.3.3-1)}$$

where:

k_v = vapor thermal conductivity

t_w = wall temperature

t_s = droplet saturation temperature

A_d = area of drop adjacent to the wall

δ = vapor film thickness

The heat transfer rate can also be defined in terms of conductance by the expression:

$$q = \bar{h} A_B (t_w - t_s) \qquad \text{(Eq. 4.3.3-2)}$$

where:

A_B is the heat transfer area per tube diameter length.

From Equations 4.3.3-1 and -2 the Nusselt modulus expression can be obtained as follows:

$$\frac{\bar{h}\, D}{k_v} = Nu = \frac{A_d}{A_B}\frac{D}{\delta}$$

The ratio A_d/A_B is defined by the relation;

$$\frac{A_d}{A_B} = \frac{n\,\pi\, r_d^{\,2}}{(\pi\, D)(D)} \qquad \text{(Eq. 4.3.3-3)}$$

where:

n = number (density) of droplets per tube diameter length

r_d = liquid droplet radius

From continuity;

$$n\,\pi\, r_d^{\,2}\, 2\, r_d = \bar{A}_\ell\, D \qquad \text{(Eq. 4.3.3-4)}$$

where the disk shaped droplets are 2 r_d units thick and $\bar{A}_\ell$ is the average liquid cross-section area and $\bar{A}_\ell$ D is the liquid volume per diameter length of tube. Thus, the liquid fraction y_ℓ can be expressed as follows:

$$y_\ell = \frac{\bar{A}_\ell}{\frac{\pi\, D^2}{4}} \qquad \text{(Eq. 4.3.3-5)}$$

From Equations 4.3.3-3 and -4 it can be shown that;

$$\frac{r_d}{D} = \left(\frac{Y_\ell}{8n}\right)^{1/3} \qquad \text{(Eq. 4.3.3-6)}$$

Based on the above correlations, the Nusselt number for dry wall boiling is defined as follows:

$$Nu = \frac{h\, De}{k_v} = \frac{6.6\, n\, (\frac{1}{8n}\,\bar{y})^{8/15}}{\left[(k_v\, \Delta T_F\, g)/(3600\, h_{fv}\, \rho_l^{\frac{1}{2}}\, \rho_o^{\frac{1}{2}}\, U_{tv}^3)\right]^{2/5}} \qquad \text{(Eq. 4.3.3-7)}$$

where:

$$\bar{y} = \frac{1 - \bar{x}}{1 + (\rho_o/\rho_l - 1)\,\bar{x}} \qquad \text{(Eq. 4.3.3-8)}$$

$$U_{tv} = \frac{\bar{x}\,G}{\rho_l}\,\frac{\pi\,D}{p} \qquad \text{(Eq. 4.3.3-9)}$$

For vapor quality when $0.10 < x < 1.0$

$$n = \frac{n_o\,x_o}{x} \qquad \text{(Eq. 4.3.3-10)}$$

where the calculations were made for the case, $n_o = 10$ and $x_o = .10$; these values were estimated on the basis of adiabatic mercury-air flow experiments in a glass tube (see Reference 10). The solution for the temperature drop (ΔT_F) across the dry wall boiling film resistance is obtained by the following equation:

$$\Delta T_F + R\,C_1\,\Delta T_F^{3/5} - \Delta T_B = 0 \qquad \text{(Eq. 4.3.3-11)}$$

Where:

ΔT_B is the available bulk NaK-to-Hg temperature difference

R is the resistance defined by Equation 4.0-2

and:

$$C_1 = \frac{12\,k_v}{De_h}\,\frac{6.6n\,(\frac{1}{8n}\,\bar{y})^{8/15}}{\left[(k_v\,g)/(3600\,h_{fv}\rho_l^{\frac{1}{2}}\rho_o^{\frac{1}{2}}\,U_{tv}^3\right]^{2/5}} \qquad \text{(Eq. 4.3.3-12)}$$

The Equation 4.3.3-11 is derived from the following heat flux correlation:

$$U\,\Delta T_B = h\,\Delta T_F$$

$$\therefore \quad \Delta T_F = \frac{U\,\Delta T_B}{h} \qquad \text{(Eq. 4.3.3-13)}$$

Inserting the expression for the overall conductance (U) from Equation 4.0-1 into Equation 4.3.3-13 one obtains:

$$\Delta T_F = \frac{\Delta T_B}{R\,h + 1} \qquad \text{(Eq. 4.3.3-14)}$$

Where:

$$h = \frac{C_1}{\Delta T_F^{2/5}} \qquad \text{(Eq. 4.3.3-15)}$$

The two-phase flow pressure drop factor (Φ_{gtt}) for the dry wall boiling regime is determined from the Martinelli-Nelson pressure drop correlation shown in Figure 18 where:

$$X_{tt} = \left(\frac{\rho_l}{\rho_o}\right)^{0.5} \left(\frac{\mu_o}{\mu_l}\right)^{0.1} \left(\frac{1 - \bar{x}}{\bar{x}}\right) \qquad \text{(Eq. 4.3.3-16)}$$

Thus, the two-phase flow pressure drop (ΔP_{TF}) can be calculated using Equation 4.3.1-19.

4.3.4 Swirl Wire Vapor Superheat Tube Section

The film conductance in the vapor superheat section is approximated by the linear addition of forced and free convection conductances.

$$h_{hel} = h_{forced} + h_{free} \qquad \text{(Eq. 4.3.4-1)}$$

The conductances in Equation 4.3.4-1 can be expressed in terms of the Nusselt moduli $Nu_{helical}$, Nu_{forced}, and Nu_{free}. Each of these moduli is defined in terms of different equivalent diameters which are defined in Section 3.1. The free and forced convection moduli are expressed and normalized on the basis of the Dittus-Boelter correlation, which represents a linear flow condition as follows:

$$Nu_{lin} = \frac{h_{lin}\,De_{lin}}{k_v} = .023\,(Re_{lin})^{0.8}\,(Pr)^{0.4} \qquad \text{(Eq. 4.3.4-2)}$$

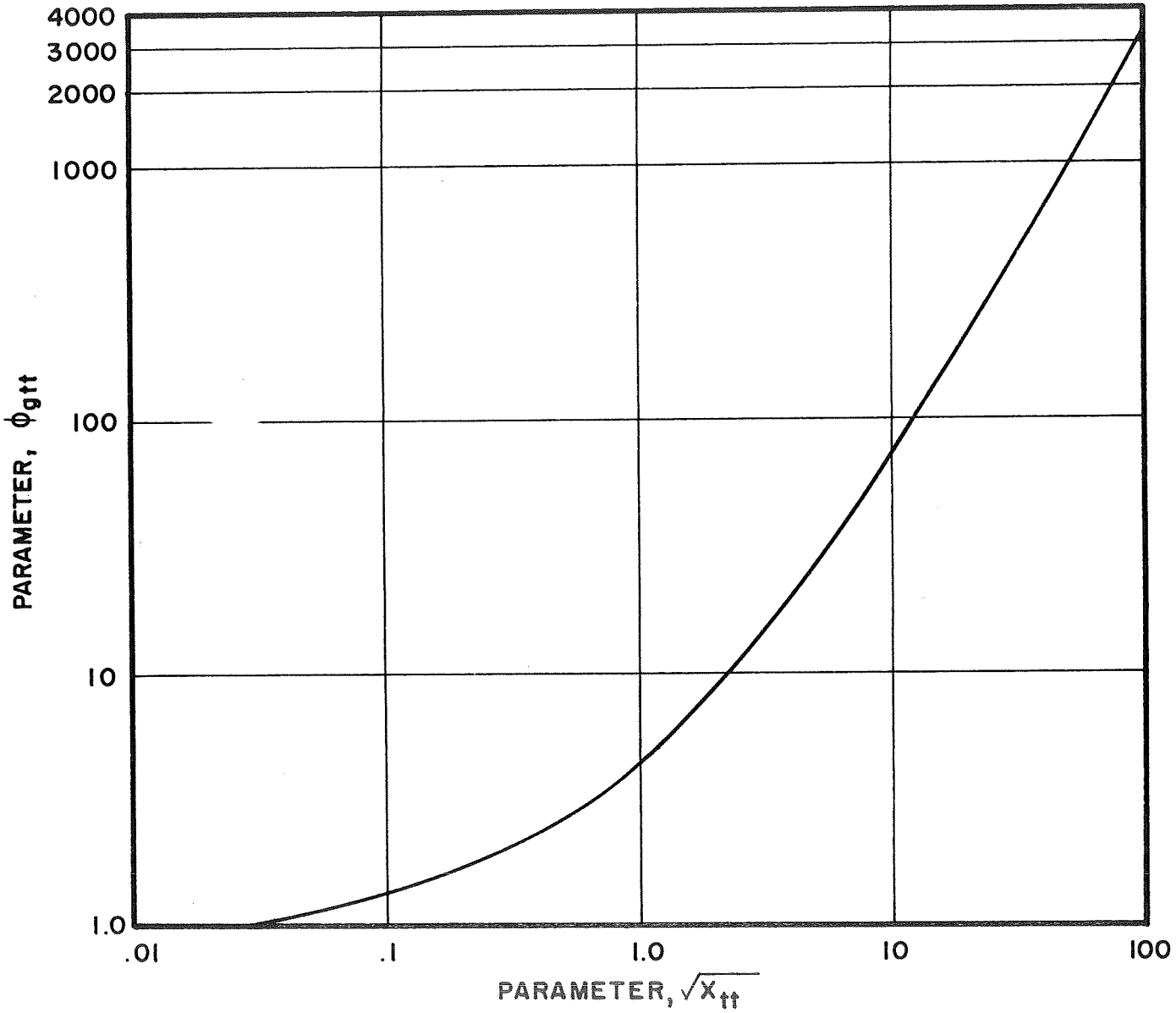

Figure 18.- Martinelli-Nelson Pressure Drop Correlation for Forced Convection Boiling Water (ASME Trans. V. 70, 1948)

For the helical flow passage, the actual flow path is longer than for a linear path. To arrive at the true forced convection conductance, the Nusselt modulus must be modified following the technique expressed in Reference 4. The Nussult moduli are therefore modified as follows:

$$Nu_{forced} = \frac{h_{forced}\, De_{hel}}{k_v} = Nu_{lin}\left[1+\left(\frac{\pi D}{p}\right)^2\right]^{0.4}\left(\frac{De_{hel}}{De_{lin}}\right)^{0.8} \qquad \text{(Eq. 4.3.4-3)}$$

From a mathematical model describing the free convection phenomena in a fluid that is circulating helically through a circular cross-section tube, the proposed free convection Nusselt modulus is:

$$Nu_{free} = \frac{h_{free}\, De_{tan}}{k_v} = Nu_{lin}\,(7.1)\frac{(\beta\,\Delta T_F)^{1/3}}{(Re_{lin})^{0.13}\,(Pr)^{0.07}}\left(\frac{\pi D}{p}\right)^{2/3}\left(\frac{De_{tan}}{De_{lin}}\right)^{2/3}$$

(Eq. 4.3.4-4)

where:

$\beta = 1/(T_{Hv} + 460)$ = volumetric expansion

and

Pr = Prandtl modulus, vapor

k_v = vapor thermal conductivity

The temperature drop (ΔT_F) across the film conductance is the root of the following non-linear correlation:

$$\Delta T_F^{1.333} + \frac{(Rh_F+1)\Delta T_F}{(R)\,(F)} - \frac{\Delta T_B}{(R)(F)} = 0 \qquad \text{(Eq. 4.3.4-5)}$$

Where:

R is the resistance defined by Equation 4.0-2

ΔT_B is the available bulk NaK-to-Hg temperature difference

and $$F = \frac{k_v}{De_{tan}} Nu_{lin} (7.1) \frac{\beta}{(Re_{lin})^{0.13}(Pr)^{0.07}} \left(\frac{\bar{u} D}{p}\right)^{2/3} \left(\frac{De_{tan}}{De_{lin}}\right)^{2/3} \quad \text{(Eq. 4.3.4-6)}$$

The Equation 4.3.4-5 is derived from the following heat flux correlation:

$$U \Delta T_B = h_{hel} \Delta T_F$$

$$\therefore \quad \Delta T_F = \frac{U \Delta T_B}{h_{hel}} \quad \text{(Eq. 4.3.4-7)}$$

Inserting the expression for the overall conductance (U) from Equation 4.0-1 into Equation 4.3.4-7 one obtains:

$$R\, h_{hel} \Delta T_F + \Delta T_F = \Delta T_B \quad \text{(Eq. 4.3.4-8)}$$

From the correlations provided by Equations 4.3.4-1, 4.3.4-3, 4.3.4-4, and 4.3.4-7, one can obtain:

$$h_{hel} = h_{forced} + F \Delta T_F^{1/3} \quad \text{(Eq. 4.3.4-9)}$$

Inserting Equation 4.3.4-9 into Equation 4.3.4-8, one can obtain Equation 4.3.4-5.

The frictional pressure drop coefficient for single phase helical flow is:

$$\xi = \left[\left(\frac{0.316}{Re_{hel}^{0.25}}\right) \left(\frac{A_{hel}}{A_{ax}}\right)^{1.75} \left(\frac{De_{hel}}{De_{ax}}\right)^{1.25} + 0.0584 \left(\frac{\pi D}{p}\right)^3 \left(\frac{D-t}{D+D_B}\right) \left(\frac{A_{hel}}{A_{ax}}\right)^{-0.25} \left(\frac{De_{ax}}{De_{hel}}\right)^{-0.25} \right] \cos \alpha_B \quad \text{(Eq. 4.3.4-10)}$$

The derivation of Equation 4.3.4-10 is provided in the Appendix (See 10.3).

4.3.5 Mercury Side Pressure Loss

The total boiler pressure drop (ΔP_{TOT}) consists of the sum of the following losses that are present in the boiler:

- ΔP_{REST} - The liquid phase pressure drop in the flow restrictor placed in the mercury end inlet tube
- ΔP_{PH} - The liquid phase pressure drop in the preheat section
- ΔP_{MPP} - The pressure drop through the MPP flow passages based on the wetting two-phase flow model
- ΔP_{SWW} - The pressure drop through the wetted SW tube region based on the wetting two-phase flow model
- ΔP_{SWD} - The pressure drop through the dry wall SW tube region based on the mixed droplet-vapor two-phase flow model
- ΔP_{SWSH} - The vapor phase pressure drop in the superheat section

The total pressure is then expressed as:

$$\Delta P_{TOT} = \Delta P_{REST} + \Delta P_{PH} + \Delta P_{MPP} + \Delta P_{SWW} + \Delta P_{SWD} + \Delta P_{SWSH} \qquad \text{(Eq. 4.3.5-1)}$$

The purpose of the flow restrictors placed in the individual tubes is to provide uniform equal mercury flow in a parallel tube network and to secure a positive pressure drop gradient with increasing flow in the boiler. The magnitude of the flow restrictor pressure drop depends on the thermal and dynamic conditions in the MPP and the SW tube sections.

The preheat section pressure drop is relatively very small and increases with flow during boiler startup. The pressure drop in the vapor quality region and in the superheat section is dependent upon boiling heat transfer characteristics imposed by the available NaK inlet temperature and the bulk pinch point temperature difference. Typical boiler pressure profiles, as predicted by the design correlations and confirmed by experimental test results, are depicted in Figure 19 for the low and high NaK inlet temperature operating conditions. This figure shows that the SW tube section pressure drop variation (ΔP_{SW} = 24 to 29 psi) as compared to the MPP vapor quality section pressure drop (ΔP_{MPP} = 16 to 41 psi) variations, is relatively small.

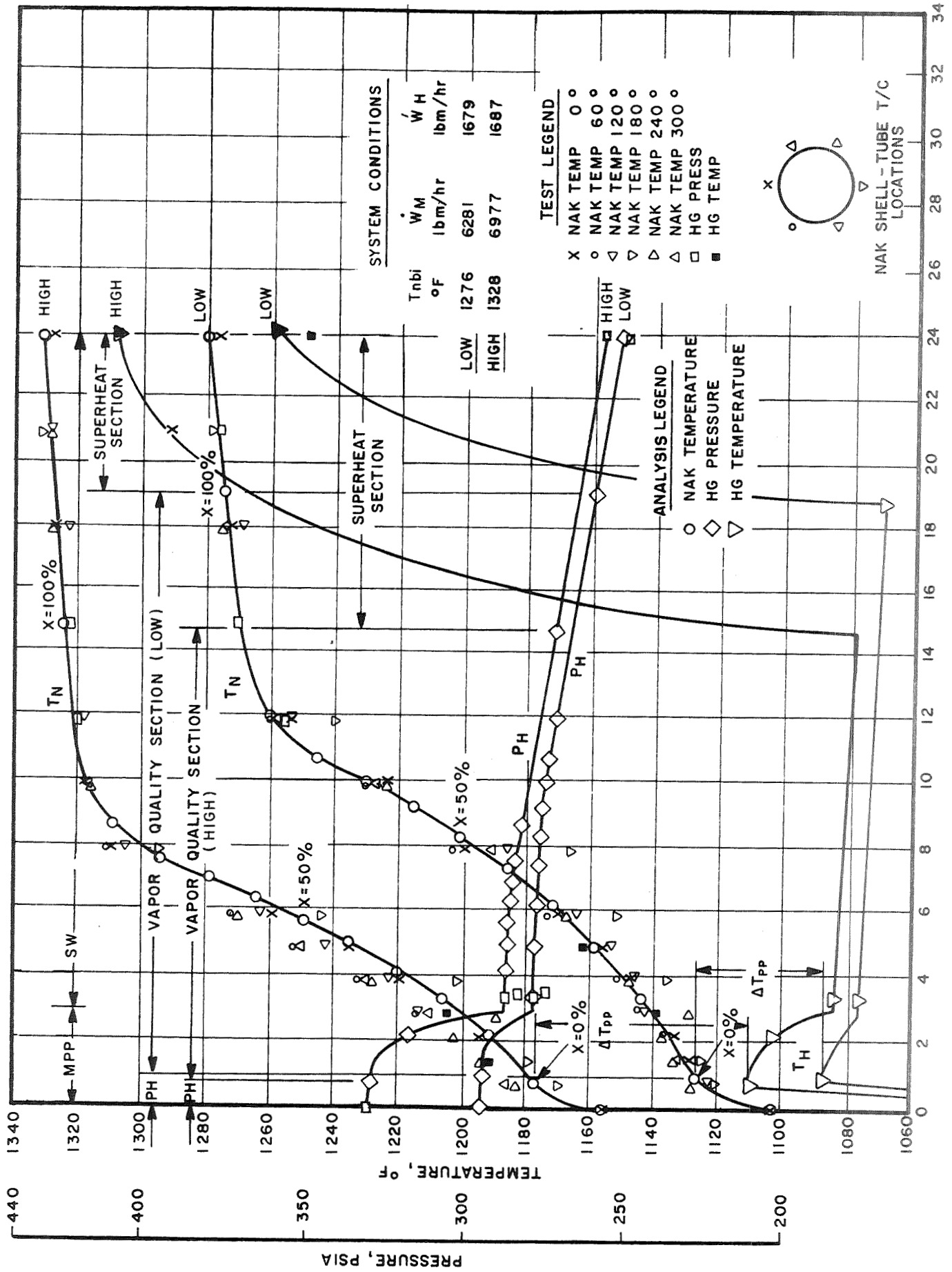

Figure 19.- SNAP-8 Experimental Boiler Temperature and Pressure Profiles for the High and Low NaK Temperature Schedule

Because of the large cross-section flow area, the SW section pressure drop is not significantly affected by the increased vapor flow exit quality from the MPP. The vapor flow increase through the relatively small MPP flow cross-section area, however, significantly affects the MPP pressure drop variation within the prescribed NaK inlet temperature band.

The most significant pressure drop variation in the boiler occurs during boiler startup. A typical pressure loss versus mercury flow plot obtained from test data is shown in Figure 20. In this plot, ΔP represents the net boiler pressure loss variation with no flow restrictors placed in the inlet end of each mercury tube. During startup, the initial exit pressure level is low and even though the mass flow is low, the volume flow in the MPP is very high. The pressure drop in the MPP vapor quality region increases markedly with increasing mercury flow due to rapid vapor volume buildup and a relatively high MPP vapor exit quality. When the mercury flow is increased further, the MPP boiling length and the pinch point temperature differences decreases. Consequently, the boiling heat flux and vapor phase flow also decrease and the boiler pressure drop (ΔP) curve assumes a negative slope. This pressure drop versus flow behavior is a typical characteristic of a "once through" boiler. The unstable character of this negative slope pressure gradient was eliminated by including a fixed orifice at the inlet to each flow passage. The orifice was designed to assure:

$$\frac{\partial(\Delta P_T)}{\partial \dot{w}_H} \geq 0 \text{ for } 0 < \dot{w}_H < \dot{w}_{H\,max} \qquad \text{(Eq. 4.3.5-2)}$$

The size of the restrictor flow passage must be such that when its pressure drop is added to the boiler net pressure drop, the total pressure drop satisfies the conditions in Equation 4.3.5-2.

The pressure drop characteristics for one boiler are depicted in Figure 21. This figure shows the selected flow restrictor size and its effect on the negative pressure drop gradient.

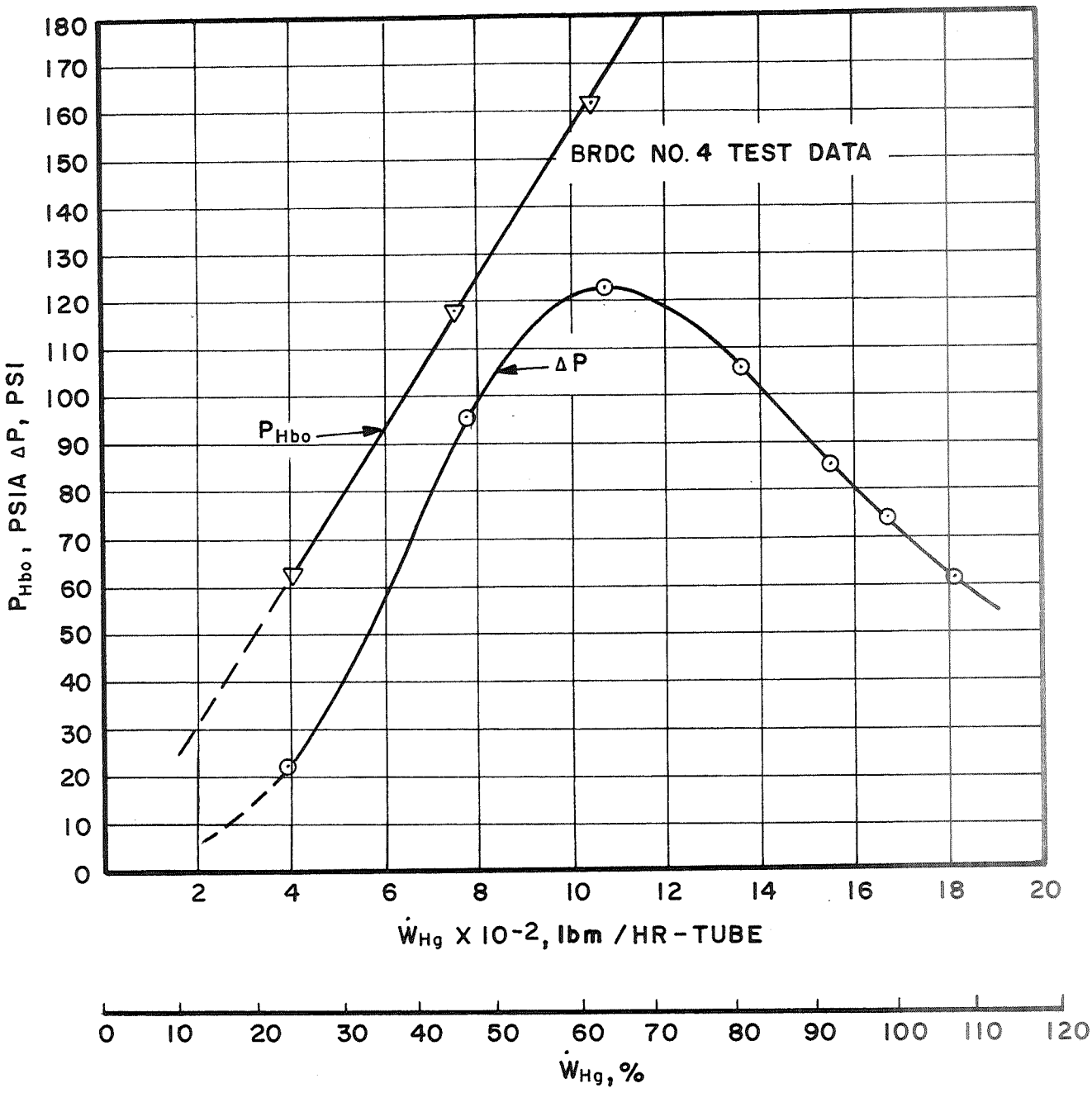

Figure 20.- Net Boiler Pressure Drop (ΔP) and Exit Pressure (P_{Hbo}) Versus Mercury Flow

The pressure drop correlation for the preheat section is defined by Equation 4.2-10. The general two-phase flow pressure drop correlation for the helical flow passage is expressed as follows:

$$\Delta P_{TF} = \Phi_{gtt}\ \xi\ \frac{\Delta L}{\cos \alpha_B\ De_h}\ \frac{\bar{x}\ G^2}{2\ g_c\ \rho_v} \qquad \text{(Eq. 4.3.5-3)}$$

Where:

Φ_{gtt} is the two-phase flow pressure drop factor

ξ is the "vapor flow only" frictional pressure drop coefficient

The helical flow passage length is defined by $\Delta L/\cos \alpha_B$, where αB is the mean helix angle. The correlation for single phase pressure drop coefficient (ξ) is defined by Equation 4.3.4-10. The determination of the two-phase flow pressure drop factor (Φ_{gtt}) for a mixed droplet vapor flow model used in the dry wall boiling regime is defined by Equation 4.3.3-16 and Figure 18.

The definition of the two-phase pressure drop factor for a divided two-phase flow model used in a wetted boiling regime is provided by Equations 4.3.1-18 and 4.3.2-7 for the MPP and SW tube regions, respectively. To utilize these correlations, one must determine the liquid-vapor interface frictional pressure drop coefficient (ξ_{INT}). The liquid-vapor interface friction is the result of the drag forces created between the annular laminar liquid film flow adjacent to the tube wall and the turbulent vapor core. Theoretically, such an interface can be visualized as a rough liquid mercury surface consisting of random wave heights (ϵ) and a distance (ℓ) between the wave maximum amplitudes. On this basis one can postulate that the ratio of frictional pressure drop coefficients between a rough surface (ξ_{INT}) and smooth surface (ξ) can be expressed as:

$$\frac{\xi_{INT}}{\xi} = f\left(\frac{\epsilon}{\ell}\ ,\ \frac{\epsilon}{R}\ ,\ Re\right) \qquad \text{(Eq. 4.3.5-4)}$$

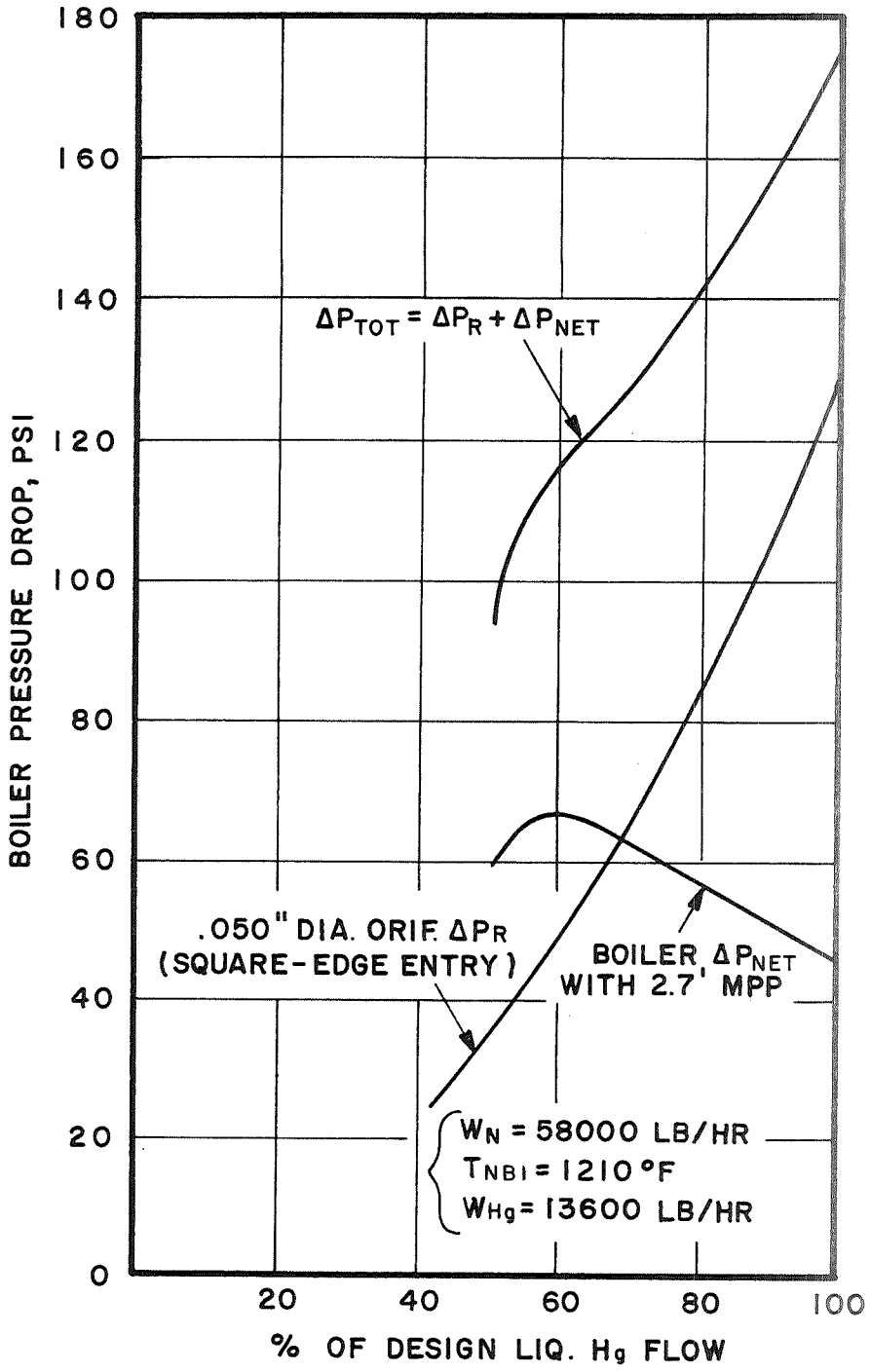

Figure 21.- BRDC Boiler No. 5 (12 Tube) Pressure Drop Versus Percent H_g Flow

Where: ϵ, ℓ, R and Re are the average radial and axial surface roughness parameters, cylindrical surface radius, and vapor core Reynolds number, respectively. In the absence of an explicit correlation for ξ_{INT}, its determination was studied in the light of experimental SNAP-8 boiler test results. Utilizing the NaK and Hg flow and their terminal state conditions (temperature, pressure) in conjunction with the MPP exit pressure, as determined from the test, various ξ_{INT} values were introduced in a boiler design computer code (see Reference 14) to arrive at a measured NaK temperature profile shape and to meet the measured Hg side pressure values at the boiler inlet, MPP exit, and the boiler exit. The convergence of this semi-analytical method, was used to provide the interface frictional coefficient values and their applicability criteria as follows:

$\xi_{INT} = 0.05$	for the SW tube wetted boiling region up to a vapor quality of 88%, a mercury flow of 100% of rated, and a MPP exit vapor quality range of from 11 to 20%.
$\xi_{INT} = 0.55$	for the MPP wetted boiling region, an exit vapor quality range of from 11 to 20%, and a mercury flow of 100% of rated.

The relatively very high value of the liquid-vapor interface frictional pressure drop coefficient in the MPP section is supported by the Geoscience, Ltd., mercury boiling experiment conducted in a tube which was equipped with a transparent window. It showed an extremely rough and spongy liquid film surface adjacent to the vapor core at low vapor quality ($\bar{x} < 15\%$).

The semi-analytical method was also used to determine the interface frictional pressure drop coefficient in terms of mercury flow in the MPP vapor quality region. The results are shown in Figure 22. These ξ_{INT} values are provided for the purpose of the boiler off-design pressure loss determination (see Figure 20).

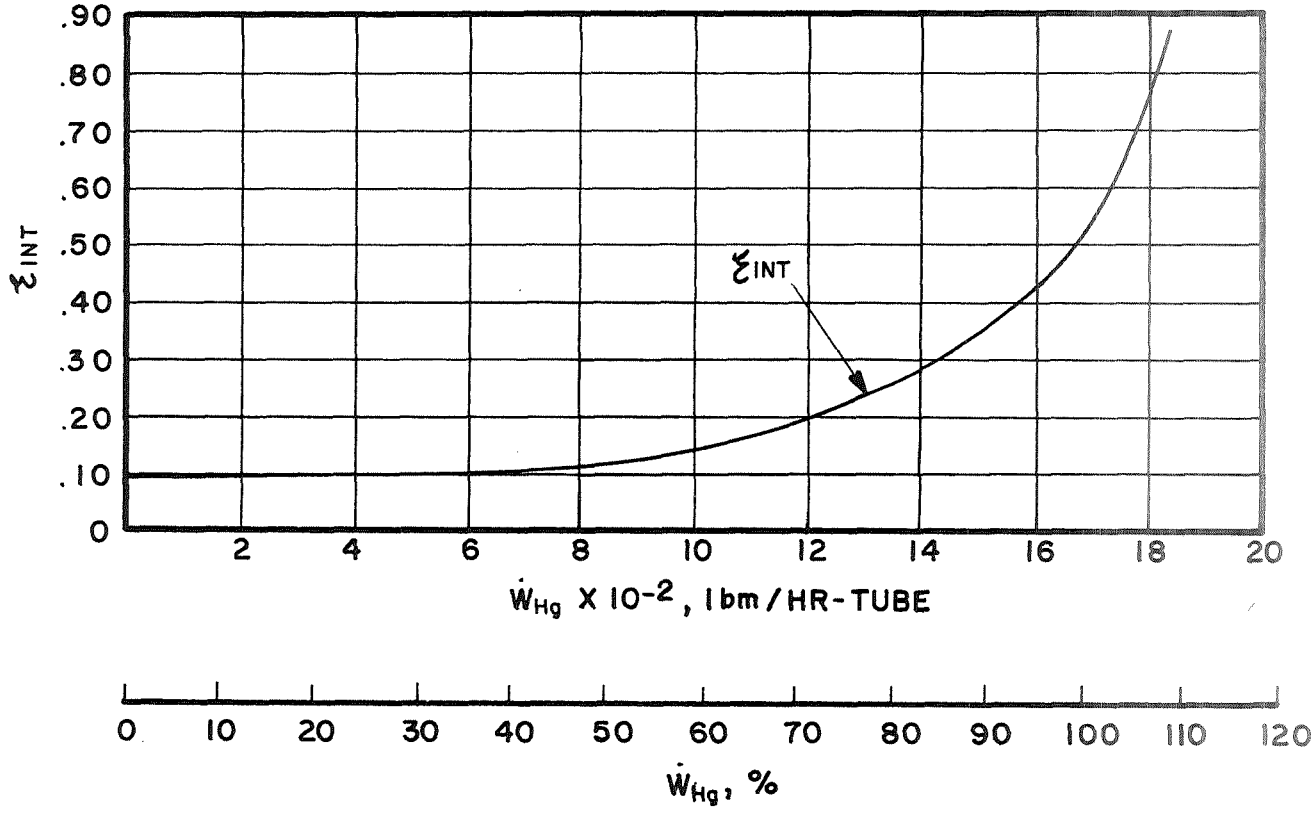

Figure 22.- MPP Vapor Quality Section Interface Frictional Pressure Drop Coefficient (ξ_{INT}) Versus Mercury Flow ($\dot{W}_{Hg}$)

5.0 COMPUTER DESIGN TECHNIQUE

The heat and momentum transfer correlations and their applicability criteria were coded for design and off-design performance analysis. The basic method of the analysis was to subdivide the boiler length into a series of small nodal increments and to write the coupling heat and momentum transfer correlations for each length element. The preheat and superheat sections were subdivided by taking equal increments of the mercury temperature rise. Similarly, the vapor quality region was subdivided by taking equal increments of the vapor quality. The solution of the coupling equations in each node provides the local thermal and dynamic operating parameters, the node length, and the node boundary state conditions. The latter conditions serve as input values for the following node calculations. In the case of design analysis, the program utilizes different given flow passage cross-section geometries in conjunction with given system performance requirements. The program calculates the plug insert length, the boiler over-all length, and the operating thermal and dynamic parameters. In the case of off-design performance analysis, the program utilizes given boiler cross-section and length geometry and determines the off-design performance characteristics at various system operating conditions.

A detailed description of the program structure, the flow charting and the input instructions are provided in a separate self-contained users manual titled "BODEPE - IBM 360 Code for SNAP-8 Boiler Heat and Momentum Transfer Analysis" (Reference 14).

6.0 EXPERIMENTAL BOILER TEST RESULTS

Three experimental tantalum-stainless steel boilers were built and tested during development. These boilers were of the single tube-in-tube configuration. The mercury side flow passage geometry was identical to the one used in parallel multitube full-scale boilers. The NaK-side flow cross-sectional area in these boilers was designed for a NaK-side film conductance identical to a full scale boiler. The purpose of these experimental boilers was to confirm and improve the theoretical design approach and provide a solid basis for the full scale boiler design and performance evaluation.

The first experimental tantalum-stainless steel double containment boiler (SB-1) was 30 feet long with a 4 foot long multipassage plug insert. It was tested in support of full scale boiler performance evaluation (BRDC Nos. 1 and 2) and to check out and compare the original dry wall boiling predictions. Typical test results of the SB-1 boiler are shown in Figure 23. It shows the measured NaK shell-tube temperatures, the NaK and Hg terminal temperatures, and the Hg terminal pressures that are superimposed by the theoretical performance predictions. Because the dry wall boiling profile (TN-BODEAN) which was determined from the drop with dry wall boiling heat and momentum transfer correlations falls significantly below the measured NaK shell-tube temperature (see References 1, 2 and 3) points (x), it is quite obvious that a more effective wetted boiling regime is present up to 11.6 feet of initial boiler length. T_N, P_{HG}, and T_{HG} are the profiles of the NaK temperature, Hg pressure and Hg temperature, respectively, as predicted by the design correlations presented in this report. In view of the relatively favorable agreement between the SB-1 boiler test results and the BODEPE code predictions, this code was utilized to investigate possible SB-1 boiler design modifications. Excessively long superheat length, relatively high pressure drop, and pressure drop variations over the NaK inlet temperature band, as experienced in both the full-scale boilers (BRDC Nos. 1 and 2) and the SB-1 boiler were attributed to excessive MPP length (4 ft) and the overall boiler (BRDC Nos. 1 and 2) and SB-1 lengths of 37 and 30 feet, respectively.

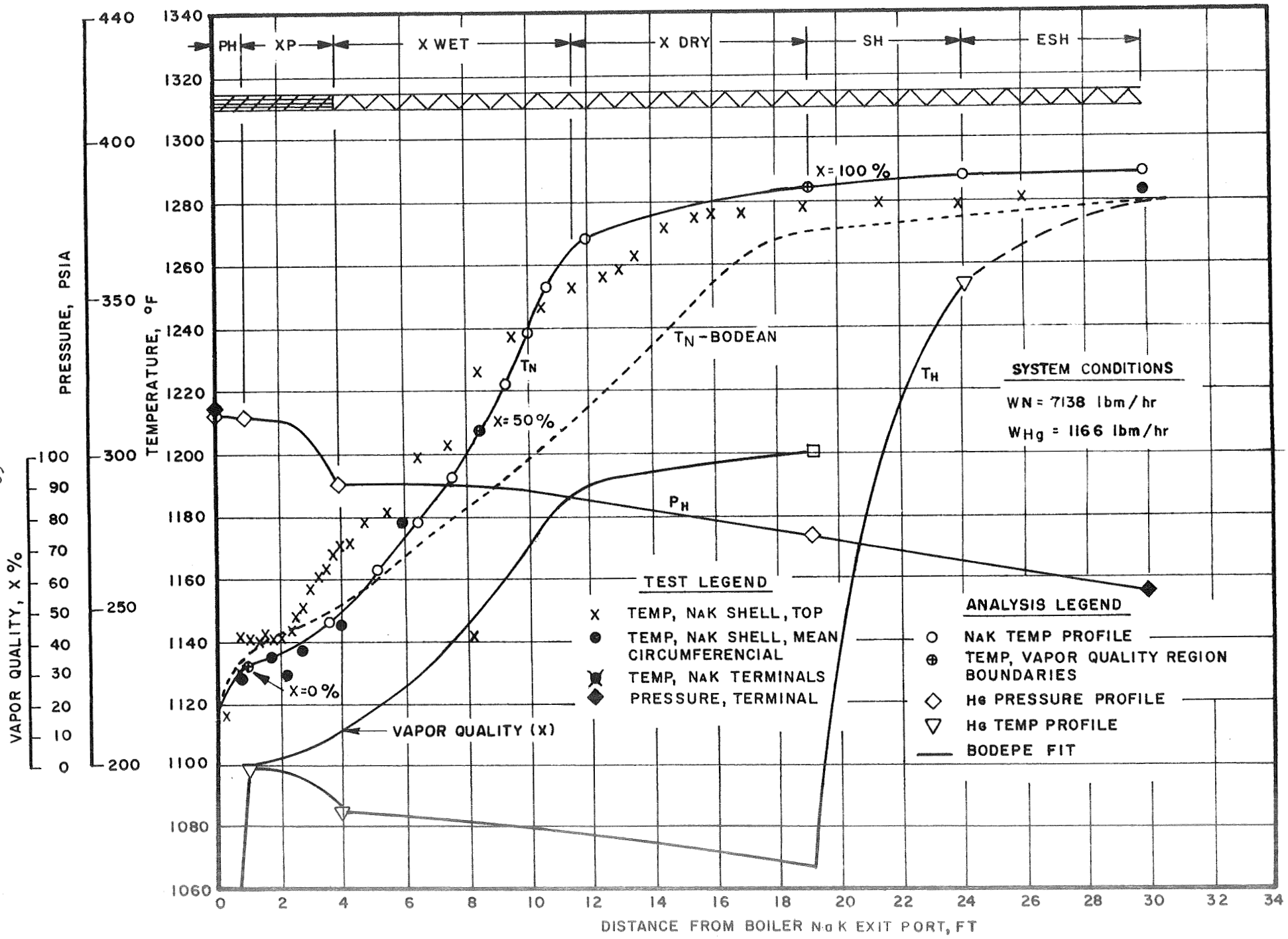

Figure 23.- SNAP-8 Experimental Boiler SB-1 Temperature and Pressure Profile

Based on design code predictions, the MPP and the overall length, in the second experimental boiler (SB-2) were reduced to 3 and 24 feet, respectively. The SB-2 boiler was designed and tested in direct support of a full scale boiler designated Bare Refractory-Double Containment No. 4 (BRDC No. 4). The predicted NaK and Hg temperature profile and the Hg pressure profile denoted by T_N, T_H, and P_H respectively, are shown in Figure 24. As shown by the superimposed test data, the performance of the SB-2 boiler was in excellent agreement with the design analysis.

Mercury boiling in a true helical flow passage contained in a bimetal tantalum-stainless steel tube was experimentally investigated in an experimental boiler, SF-1A. The explosively bonded tantalum-stainless steel tube with a single fluted helical flow passage (SFHX) demonstrated excellent heat transfer characteristics at systems operating conditions. The results are in relatively good agreement with the predictions based on idealized wetting and non-wetting two-phase flow heat and momentum transfer models. The comparison of the test data with theory is depicted in Figure 25.

Two sets of experimental data interpretation are shown in Figure 25. The profiles subscripted with "T" are the analytical performance predictions at the indicated conditions of mercury and NaK flows and inlet temperature for the test configuration. The test boiler contains internal instrumentation taps to measure both temperature and pressure at locations A, B and C. The temperature and pressure profiles are in very good agreement with the analytical performance predictions.

The second set of profiles are subscripted with "D". These profiles are predicted for a boiler tube without internal instrumentation taps. The difference in the profiles is caused by the frictional loss in pressure as the mercury passes the instrumentation taps. A multi-tube boiler of this configuration is expected to perform in accordance with the dashed (- - -) curves shown in this figure.

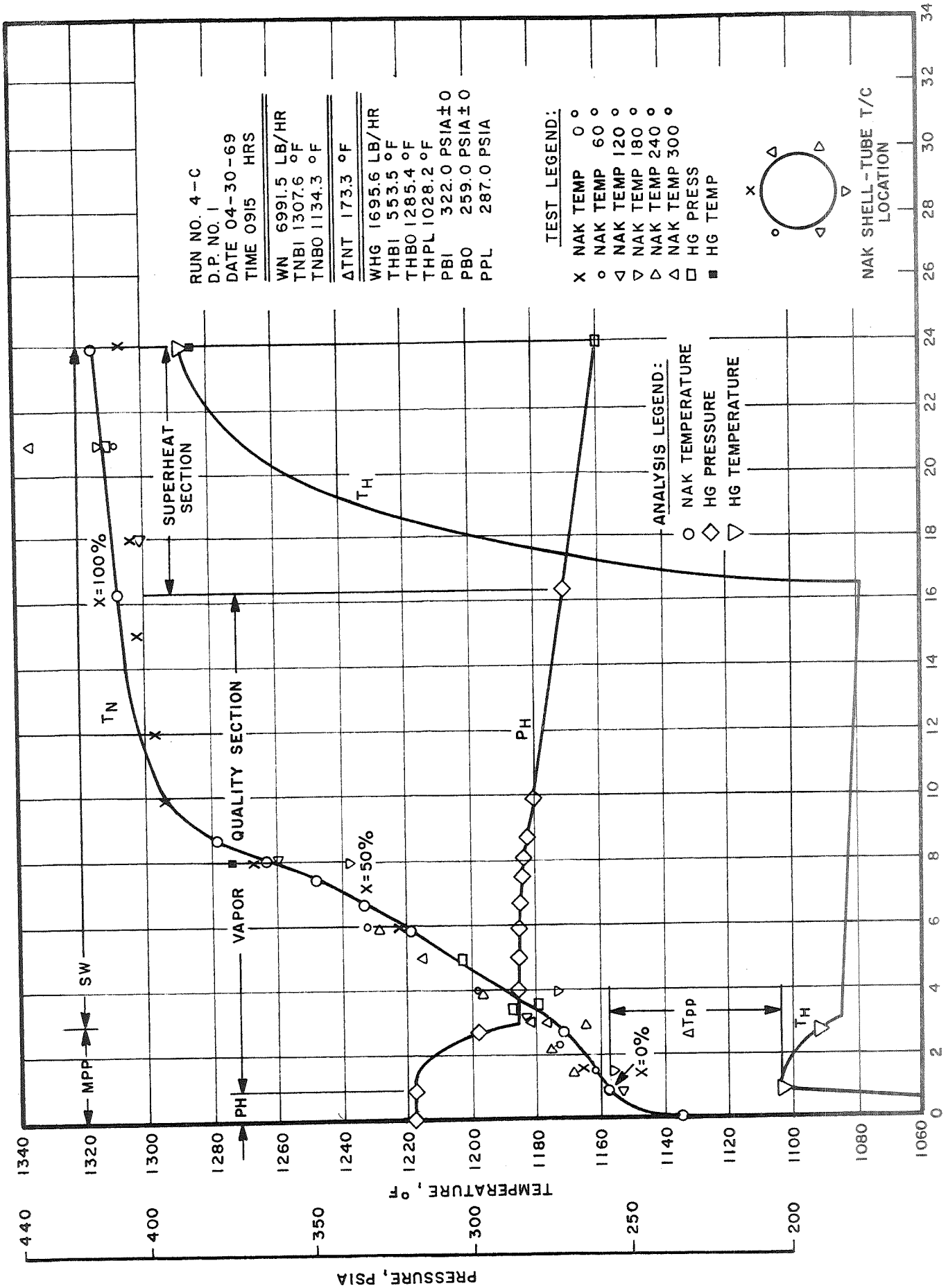

Figure 24.- SNAP-8 Experimental Boiler SB-2 Temperature and Pressure Profile, Normal NaK Temperature Schedule

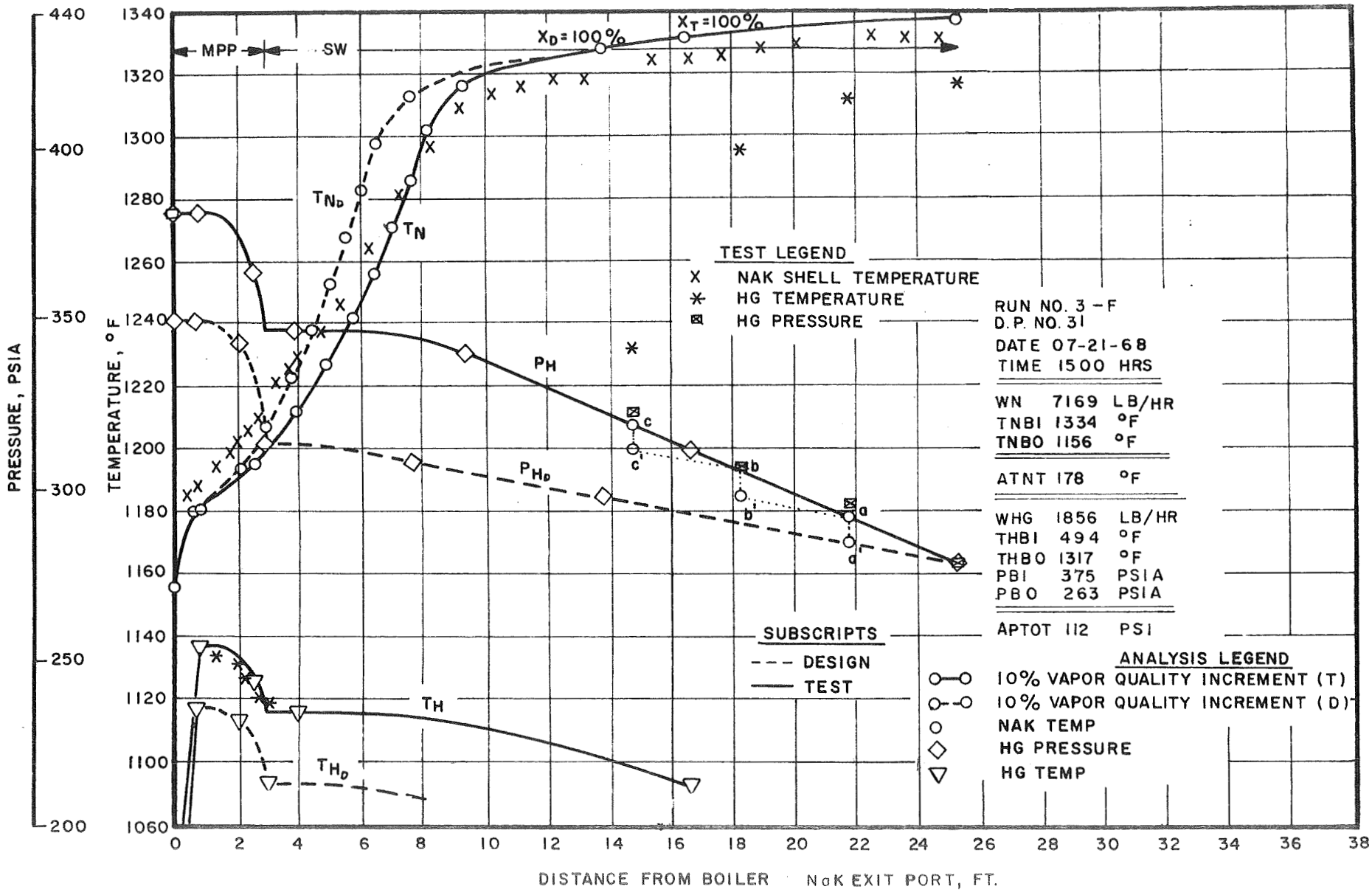

Figure 25.- SNAP-8 Experimental Boiler SF-1A Temperature and Pressure Profile

These data show that the boiler pressure drop reduction increases the heat transfer effectiveness $(\partial T/\partial L)_D > (\partial T/\partial L)_T$. The two-phase flow heat and momentum transfer characteristics of the single fluted helix are comparable with those of swirl wire tube geometry. It is postulated that the SFHX geometry is more effective in reducing or eliminating liquid carry-over through the boiler. Tantalum surface wetting in the MPP section, as suggested by the NaK temperature profile gradient, also implies that the MPP geometry, originally established to minimize slug-flow boiling, could be replaced by the simpler helical geometry. Such a geometry can be derived from the SFHX geometry by placing several parallel helical strips with a smaller helical angle on a larger center bar diameter. Such a plug insert would induce a higher fluid radial acceleration thus promoting more effective liquid phase evaporization at the tube wall.

Detailed evaluation of the test results of SB-1, SB-2, and SF-1A boilers can be found in References 15 through 17, respectively.

7.0 FULL SCALE BOILER TEST RESULTS AND DESIGN PREDICTIONS

All full-scale tantalum boilers tested used the same basic configuration. Seven (7) mercury containment tubes were placed in a NaK containing shell. NaK flow was counter to the mercury flow. The mercury tubes were in an equilateral triangular array (see Figure 2B). The first series of tantalum-stainless steel boilers, denoted by BRDC Nos. 1, 2, and 3, were designed with a 4 foot long MPP insert and an overall length of 37 feet. BRDC Boiler No. 1 was employed in system and endurance tests at the NASA W-1 facility and at the General Electric, Evandale, Ohio, test facility. A total test time of 15,125 hours and 6 startups were accumulated on this boiler. BRDC Boiler No. 2 was operated with a breadboard power conversion system for over 8700 hours and accumulated 27 startups. BRDC Boiler No. 3 operation in the NASA W-1 test facility resulted in 135 startups and a total test time of 157 hours. The performance characteristics of these boilers ranged from poor to excellent and were dependent on the boiler deconditioning (contamination) state. The effects of boiler deconditioning were experienced primarily in combined systems testing. Deconditioning was attributed to oil influx into the mercury loop and decomposition in the boiler. This was the most serious problem encountered in the boiler during combined systems operation. The possible mechanisms of boiler performance degradation and their analytical interpretations are provided in Reference 10.

Typical test data obtained during full conditioned BRDC Boiler No. 2 testing are shown in Figure 26. The figure shows a tabulation of measured NaK and Hg flow and their terminal state conditions. The NaK shell surface temperature measurements, as identified by different axial and circumferential thermocouple locations, are plotted in terms of boiler length. To compare these results with the BODEPE computer code predictions, the independent test parameters such as NaK and Hg flow and their inlet state conditions were introduced in the analysis to determine the analytical NaK and Hg temperature profiles and the Hg pressure profile in terms of boiler length. These calculated profiles are superimposed upon the test results for the purpose of comparison. In general, the calculated NaK profile (T_{NaK}) is in relatively good agreement with the measured NaK shell tube measurements. This is particularly true up to the first

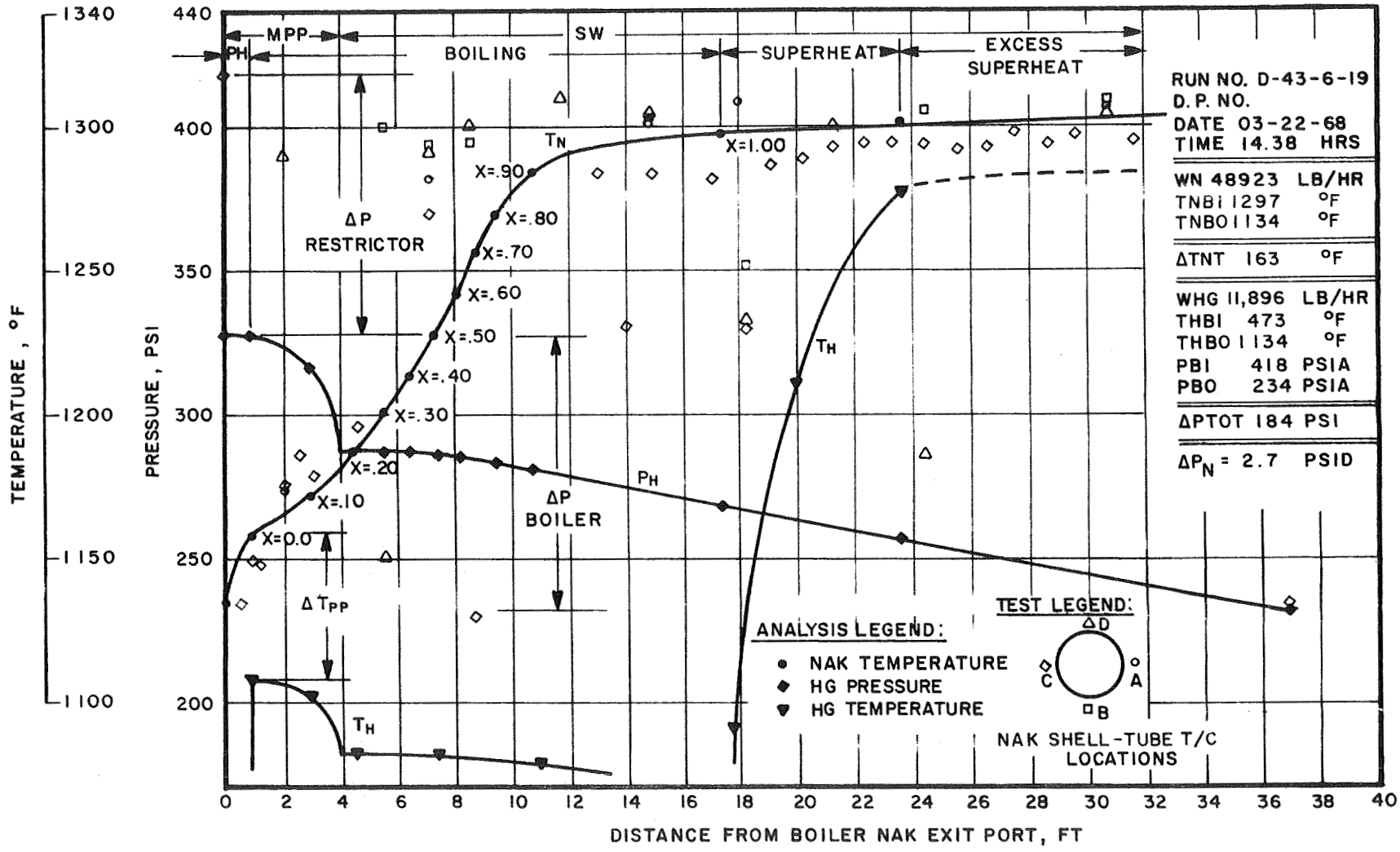

Figure 26.- SNAP-8 BRDC Boiler No. 2 Temperature and Pressure Profile

7-1/2 feet of boiler length and beyond 12-1/2 feet of boiler length. The discrepancy within the 7-1/2 through 12-1/2 foot length is attributed to an inaccuracy of thermocouple indications or NaK flow stratification, or both. When compared with the SB-1 profile, Figure 23, it can be seen that a more accurate experimental NaK temperature profile and consequently a better agreement with the BODEPE code results can be obtained from the better instrumented single tube boiler tests. Both the SB-1 and BRDC No. 2 boiler test results conclusively indicated excessive boiler superheat length (19.5 ft) and relatively high pressure loss (96 psi).

Based on the above conclusions and the SB-2 test results, the BODEPE code was utilized to modify the initial boiler design (BRDC Nos. 1, 2, and 3) MPP insert and overall boiler length. These modifications were incorporated in BRDC Boiler No. 4 which was employed in conjunction with the combined power conversion system tests. Typical BRDC Boiler No. 4 test results and corresponding design predictions are shown in Figure 27. To minimize or preclude NaK flow and temperature stratification, this boiler was provided with helical coil turbulators around the tube bundle (see Figure 9) and multiple radial NaK inlet and exit ports (see Figure 10). The effect of these features can be seen in a more uniform NaK shell temperature gradient as shown in Figure 27.

Test results of both the experimental and the full scale boilers verified that boiler designs can be based on heat and momentum transfer correlations derived from idealized wetting and non-wetting two-phase flow models with helical flow passages. To avoid the analytical difficulties encountered in determining the interface frictional pressure drop coefficient for a wetted boiling divided two-phase flow regime, a semi-empirical method was used. It was based on available experimental pressure data evaluation as described in Section 4.3.5.

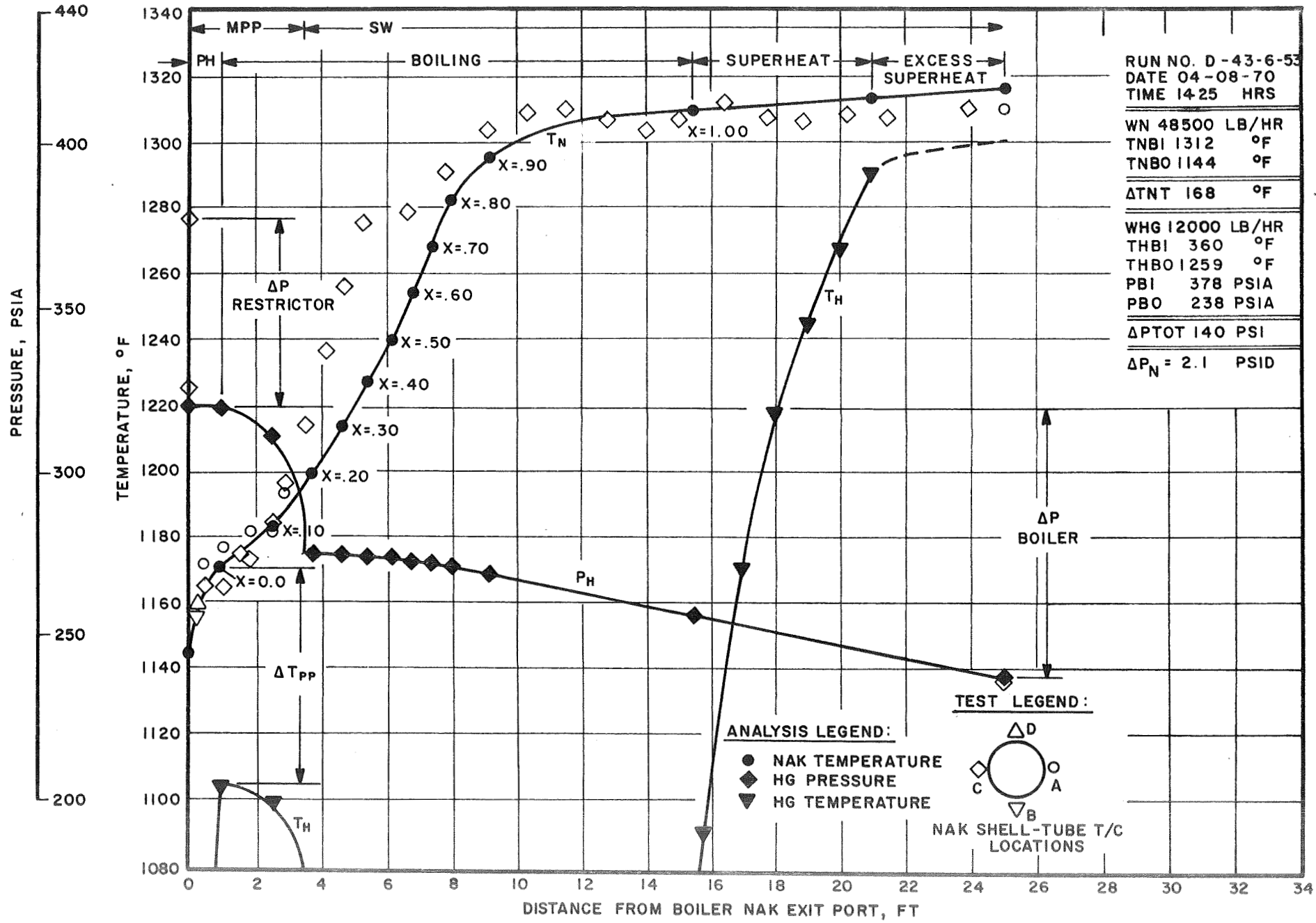

Figure 27.- SNAP-8 Boiler BRDC No. 4 Temperature and Pressure Profile

8.0 BOILER DESIGN FOR REVISED SYSTEM STATE POINT CONDITIONS

The final task in boiler development was to design a boiler for a higher electrical power output system.

The revised PCS-G system state point conditions are defined as follows:

Characteristic	Symbol	Units	Revised Value	Original Value
NaK Flow	$(\dot{W}_{NaK})$	lb/hr	57050	49500
Boiler Inlet NaK Temperature	$(T_{NaK,\ in})$	^{o}F	1185	1280
Mercury Vapor Flow	$(\dot{W}_{Hg,\ vap})$	lb/hr	13775	11800
Mercury Pressure at Boiler Outlet	$(P_{Hg,\ out})$	psia	146	254
Terminal Temperature Difference	ΔT_{term}	^{o}F	20	20
Minimum Pinch Point Temperature Difference	$(\Delta T_{pp,\ min})$	^{o}F	38	38
Duty	q	KW_t	600	517

The selected mercury flow containment geometry was identical to that of BRDC Boiler No. 4. To meet the revised state point conditons, the tube count was increased from 7 to 12 tubes which were placed equidistant in an annular NaK flow passage as shown in Figure 2C. The lower boiler operating pressure and increased mercury flow rate giving a greater volume flow dictated the increase in tube count.

A summary of the thermal design analysis is provided in Table II. It specifies the boiler cross-section geometry, the calculated MPP length, and the total length requirements for a low NaK inlet temperature schedule as well

Table II. SNAP-8 PCS-G BRDC No. 5

Boiler Design Characteristics and Operating Parameters

MECHANICAL

Design Concept	"Once through" mercury preheat, boiling and superheat
Boiler Type	Parallel counterflow NaK-to-Hg heat exchanger
Design Configuration	Parallel tube bundle-in-tube
Number of Hg Tubes	12
Hg Containment	In round Ta tube contained in oval 321 SS tube with stagnant NaK in annular space
Ta Tube Dimensions	.750 in. OD x .049 inch wall
Oval 321 SS Tube Dimensions	.880 in. x 1.45 in. x .049 inch wall
Effective MPP Length	2.7 ft, Tantalum
Number of Helical MPP Flow Passages	16
MPP Flow Passage Pitch	6 inch
MPP Flow Passage Cross-Section	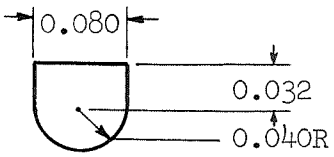
Swirl Wire Dimensions	.062 in. dia. x 2 in. pitch, 90% Ta-10% W
NaK Shell Tube Dimensions	7.625 in. OD x .120 in. wall, 316 SS
Length-Centerline to Centerline of NaK Inlet and Outlet	21.5 ft.
Flow Restrictor Orifice with Square Edge Entry	0.050 inch diameter

Table II (Continued)

THERMAL

Item	Parameter	Symbol	Dimension	NaK Inlet Temp. Schedule	
				Low	High
1	NaK Flow Rate	W_N	lb/hr	57148	57148
2	NaK Inlet Temperature	T_{Nbi}	^oF	1185	1211
3	NaK Temperature Drop	ΔT_N	^oF	170	167
4	NaK Pressure Drop	ΔP_N	Psi	~ 3	~ 3
5	Hg Flow Rate	W_{HG}	lb/hr	13775	13600
6	Hg Exit Pressure	P_{Hbo}	Psia	148	147
7	Hg Exit Temperature	T_{Hbo}	^oF	1165	1190
8	Hg Inlet Temperature	T_{Hbi}	^oF	420	420
9	Hg Vapor Region Press. Drop	ΔP_{HG}	Psi	32	46
10	Hg Flow Restr. Press. Drop	ΔP_R	Psi	143	140
11	Hg Inlet Pressure	ΔP_{Hbi}	Psia	323	333
12	Pinch Point Temp. Diff.	ΔT_{pp}	^oF	38	54
13	Terminal NaK-to-Hg	ΔT_t	^oF	20	22
14	Vapor Superheat	ΔT_{SH}	^oF	197	224
15	Mean Preheat Flux	$q"_{PH}$	$B/hr\text{-}ft^2$	188465	215553
16	Mean MPP Boiling Flux	$q"_{MPP}$	$B/hr\text{-}ft^2$	49237	71292
17	Mean SW Boiling Flux	$q"_{SW}$	$B/hr\text{-}ft^2$	57921	63338
18	Mean Superheat Flux	$q"_{SH}$	$B/hr\text{-}ft^2$	5176	5707
19	Boiling Termination Point	L_{100}	ft	15.4	13.4
20	MPP Vapor Exit Quality	X_{PL}	%	12	18
21	Thermal Power Required	q_t	KW	600	598
22	External Power Loss (Assumed)	q_{HL}	KW	5	5

as the boiler operating thermal and dynamic parameters for the prescribed system state point conditions. The boiler envelope and some of the internal details are shown in Figure 28. The predicted NaK and mercury temperature profiles and the mercury pressure profiles in terms of boiler length at high and low NaK inlet temperature schedules are depicted in Figure 29. To insure a positive pressure drop gradient in the boiler, the mercury tubes were provided with square edge entry restrictors of 0.050 inch diameter. The relationship between the total boiler pressure loss (ΔP_{tot}), net boiler pressure loss (ΔP_{Net}) and the restrictor pressure loss (ΔP_R) in terms of Hg flow is shown in Figure 21. The expected total mercury side pressure drop is 174 psi at 100% mercury flow. The NaK side pressure loss as a function of NaK flow is shown in Figure 30. It was established from water flow tests conducted with a full-scale plastic model. At the design point ($\dot{w}_N$ = 57,000 lb/hr), the predicted NaK side pressure loss is 1.7 psid.

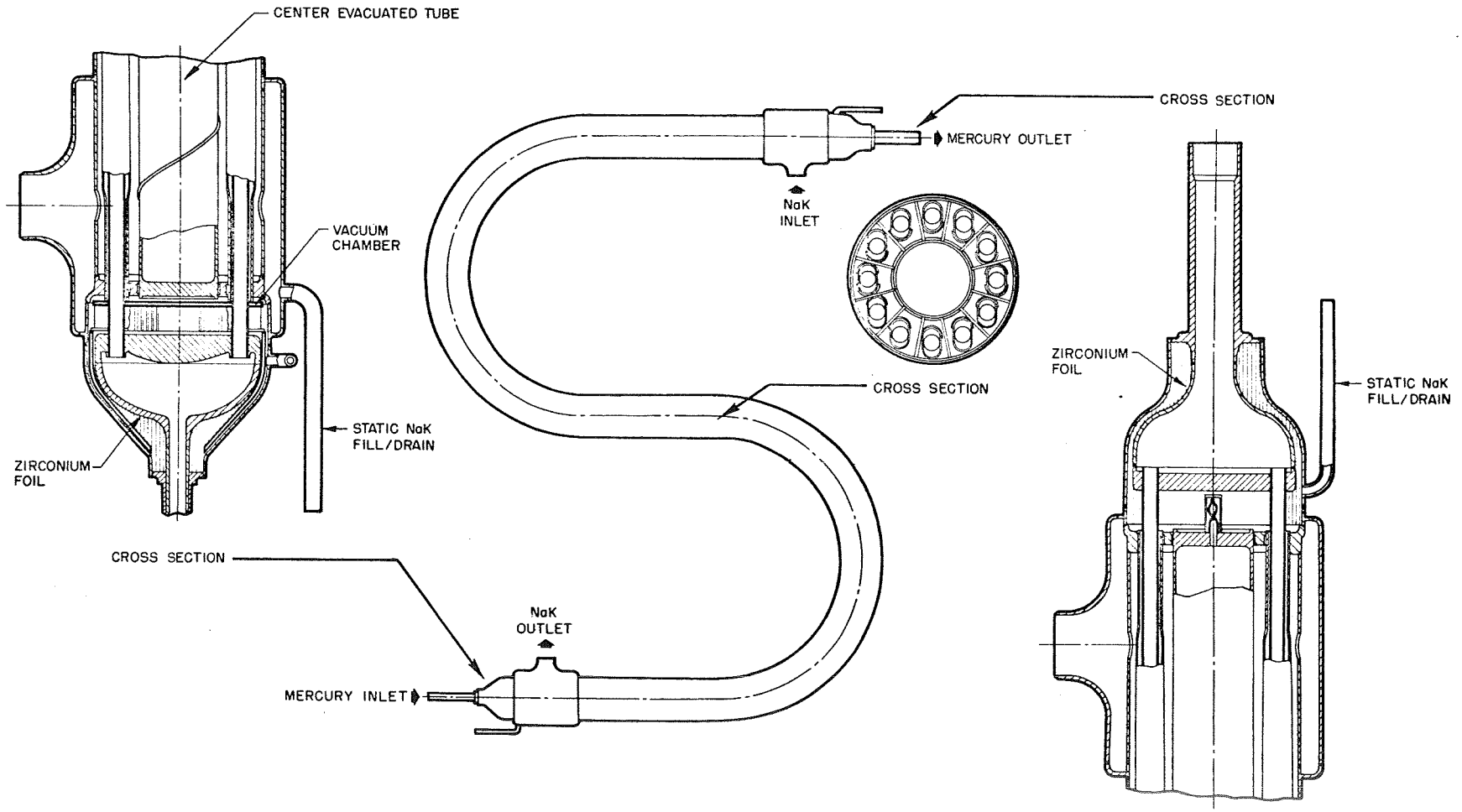

Figure 28.- BRDC Boiler No. 5

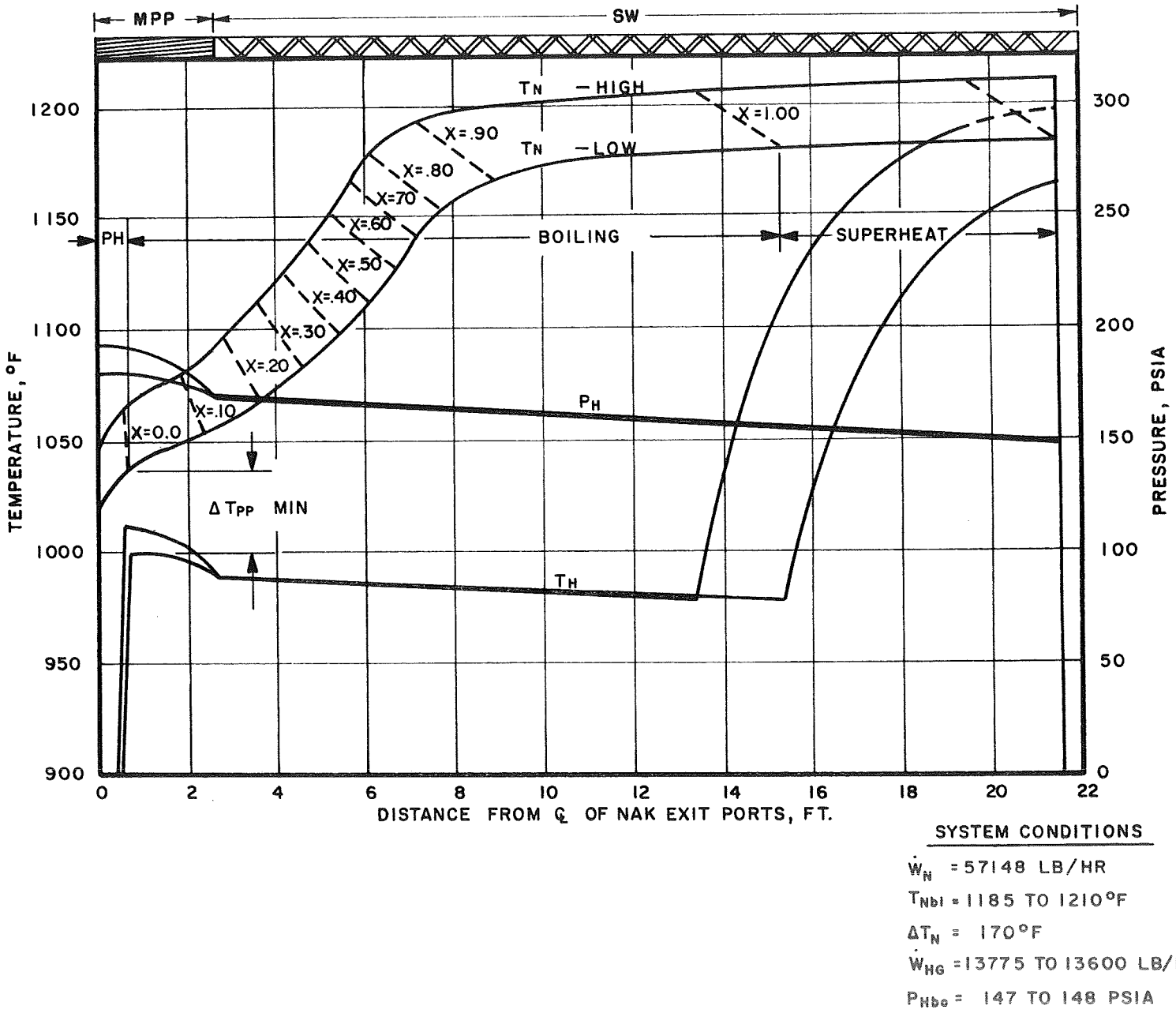

Figure 29.- SNAP-8 BRDC Boiler No. 5 BODEPE Temperature and Pressure Profiles

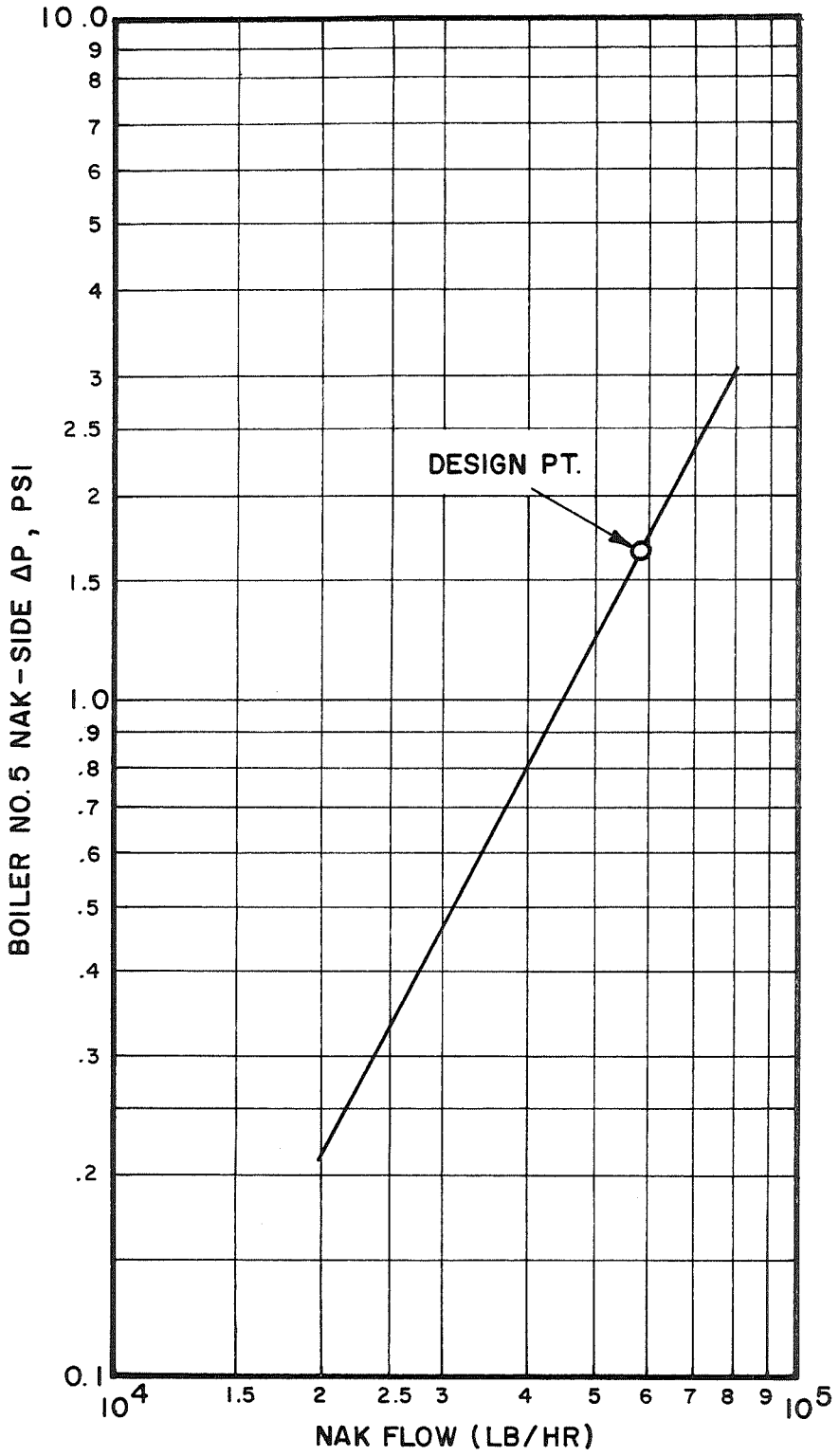

Figure 30.- Predicted BRDC Boiler No. 5 NaK-Side Pressure Drop Versus NaK Flow From H_2O Flow Experiments

9.0 CONCLUSIONS

Heat and momentum transfer in a "once-through" boiler can be based on proposed models of wetting and non-wetting two-phase flow as demonstrated by the agreement between analytical performance predictions and development test results of the tantalum-stainless steel boilers.

Mercury boiling heat transfer effectiveness is dependent on the cleanliness of the mercury-side heat transfer surface. Only clean surfaces wetted by the mercury will develop optimum heat transfer characteristics predicted by the design correlations presented in this report.

Both the bimetal stainless steel tube and the double-containment stainless steel and tantalum tube assembly are suitable for mercury containment and effective vaporization in the boiler.

To meet the safety requirements for a man-rated system, the double-containment concept was adapted for the boiler design.

Helical flow induction devices (such as the multipassage plug insert, swirl wire turbulators, and single-fluted helixes in the mercury flow passages) are mandatory for high acceleration boiling heat transfer independent of external gravity environments.

To secure minimum liquid carryover in the boiler, the single-fluted helix is preferred over swirl wire turbulators. The adoption of the latter was based on simpler boiler fabrication techniques.

To prevent boiler performance degradation, care must be taken not to allow foreign materials such as organic fluids, oxides or air to enter the mercury flow passage. Foreign materials and their decomposition products form a thermal barrier on the mercury-exposed heat transfer surface of the tantalum tube. Chemical cleaning effectively removes the thermal barrier surface films from tantalum which has been exposed to contamination and restores full heat transfer capability of the boiler.

The use of the BODEPE computer code for boiler design and analysis is limited to once-through NaK-to-mercury boilers with a counterflow configuration. The program can be used for other fluid combinations providing their transport properties are made available in the form of function subroutines. Only a helical flow passage geometry can be utilized for the boiling fluid.

SYMBOLS

A_{LIN} - Linear flow cross-section area

C_p - Specific heat

D_1 - Tube ID

De_t - Equivalent diameter, tangential

De_l - Equivalent diameter, linear

d - Channel width in plug insert

g_c - Gravitational constant

h_{fv} - Vaporization heat

h_{forced} - Forced convection heat transfer coefficient

h_{free} - Free convection heat transfer coefficient

h_{Hg} - Mercury side heat transfer coefficient

h_{SH} - Vapor heat transfer coefficient

k_f - Thermal conductivity, liquid mercury

k_v - Thermal conductivity, vapor mercury

N_1 - Number of tubes in boiler

N_2 - Number of flow passages in plug insert

Nu - Nusselt modulus

Nu_l - Nusselt modulus, linear

n_o - Initial droplet population per diameter length

n - Local droplet population per diameter length

p - Pitch, pressure

Pr - Prandtl modulus

q - Heat flow

R - Thermal resistance between bulk NaK and mercury tube ID

r_o - Tube ID radius

r_1 - Liquid-vapor interface radius in divided two-phase flow model

r, r_2 - Radius

T - Temperature

$\bar{u}_1$ - Velocity, mean

u_{TV} - Vapor tangential velocity

V_o - Mean velocity

$\dot{w}_o$ - Liquid phase flow rate

$\dot{w}_1$ - Vapor phase flow rate

$\dot{w}_{TOT}$ - Total flow rate

$\bar{x}$ - Mean vapor quality

x_o - Initial vapor quality

$\bar{y}_1$ - Mean moisture content

α - Helical angle, $\alpha = \tan^{-1}(\pi D/p)$

β - Angle, volumetric expansion

ξ_{int} - Liquid-vapor interface frictional pressure drop coefficient in divided two-phase flow regime

ξ_{tube} - Frictional pressure drop coefficient at tube wall

μ_f, μ_o - Dynamic viscosity, liquid

μ_v, μ - Dynamic viscosity, vapor

$\rho = r_1/r_o$

ρ_f, ρ_o - Density, liquid

ρ_v, ρ_1 - Density, vapor

Φ - Two-phase pressure drop factor

τ - Shear stress

δ - Liquid film thickness

ϵ - Surface roughness

SUBSCRIPTS

PH - Preheat

H - Mercury

PP - Pinch point

N - NaK

REFERENCES

1. "The SNAP-2 Power Conversion System, Topical Report No. 12, Boiler Development," TRW ER-4521, NAA-SR-6304.

2. "The SNAP-2 Power Conversion System, Topical Report No. 17, Mercury Boiling Research," TRW ER-4833, NAA-SR-6309.

3. "SNAP-2 Topical Report, Compact Boiler Development," TRW ER-5411, NAA-SR-6315.

4. Summary Report on High Acceleration Field Heat Transfer for Auxiliary Space Nuclear Power Systems (AEC Contract No. AT(04-3)-409), January 1966, GLR-42, SAN-409-29.

5. H. F. Poppendiek, W. R. Gambill, N. D. Greene, "Helical Forced-Flow Heat Transfer and Fluid Dynamics in Single and Two-Phase Systems," 3rd UN International Conference on Peaceful Uses of Atomic Energy, A/Conf. 28/P/231, USA, May 1964.

6. G. Mouritzen, "Forced Rotation of Flow in Pipes," A Memorandum on High Acceleration Field Heat Transfer for Auxiliary Space Nuclear Power Systems, AEC Contract No. AT(04-3)-409.

7. H. F. Poppendiek, et al, "An Investigation of the Boiler Conditioning and Heat Transfer Characteristics in a Mercury-Tantalum System," NASA CR-72904, (Aerojet Contract OP-119224), GLR-65, July 1968, Geoscience Ltd.

8. H. F. Poppendiek, et al, "Two-Phase Flow Pressure Drop and Heat Transfer in a Multi-Slot Insert in the Entrance of the Boiler Tube (Aerojet Contract OP-119224), GLM-61, November 1967, Geoscience Ltd, NASA CR-72903.

9. H. F. Poppendiek, et al, "Annual Report on Investigation of Fundamental Mechanisms and Parameters that Influence Steady State and Transient Performance of Rankine Cycle Liquid Metal Systems," (AEC Contract No. AT(04-3)-677), GLR-64, SAN-677-29, 1967/68, Geoscience Ltd.

10. H. F. Poppendiek, "SNAP-8 Boiler Performance Degradation and Two-Phase Flow Heat and Momentum Transfer Models," Geoscience Ltd, GLR-84, NASA CR-72759.

11. H. Derow, B. E. Farwell, E. B. Johnson, L. A. Kimura, J. C. Whipple, K. M. Wong, D. Yee, "Evaluation of Tantalum for Mercury Containment in the SNAP-8 Boiler," NASA CR-72651, November 1969.

12. O. E. Dwyer, "Eddy Transport in Liquid-Metal Heat Transfer," BNL-6046, September 1962.

13. O. E. Dwyer, "Recent Developments in Liquid-Metal Heat Transfer," BNL-9597, September 1965.

14. A. J. Sellers, "BODEPE-IBM 360 Computer Code for SNAP-8 Boiler Heat and Momentum Transfer Analysis, Revised June 1971, NASA CR-72907.

15. A. J. Sellers, "SNAP-8 Boiler Development-Evaluation of SB-1 Boiler Test Results and Proposed Design Modifications," NASA CR-72908, 4 October 1968.

16. A. J. Sellers, K. M. Wong, "SNAP-8 Boiler Development-Evaluation of SB-2 Boiler Test Results," NASA CR-72909, 29 September 1969.

17. A. J. Sellers, L. Kimura, K. M. Wong, "SNAP-8 Boiler Development-Test Results of Single Tube Bimetal Tantalum-Stainless Steel Boiler (SF-1A)," NASA CR-72910, 24 July 1969.

APPENDIX - CONTENTS

APPENDIX

10.0 ANALYSIS AND CALCULATIONS USED IN THE SNAP-8 BOILER THERMAL DESIGN

10.1 Calculatition of the Stagnent NaK Thermal Resistance in an Oval-Round Double Containment Tube

A typical oval-round double containment tube cross-section is shown in Figure A-1B & E. It involves varying stagnant NaK thickness distribution around the circular tube. The stagnant NaK thickness distribution is dependent on the tube eccentricity ratio between the round and the oval tube. The eccentricity of the tubes results from the nonuniform thermal expansion coefficients of the two materials, tantalum and stainless-steel, when heated to operating temperature. Such a geometry creates a nonuniform thermal resistance and a nonsymmetric temperature field between the flowing NaK and boiling mercury. The nonsymmetric temperature field also creates a natural circulation heat transfer effect of the stagnant NaK in the heat transfer pass. The description of the oval-round tube heat transfer pass shows that a complicated three-dimensional heat transfer analysis must be employed to determine the true temperature conditions in the mercury flow passage. The complexity of both the heat transfer pass thermal conditions and the two-phase flow heat and momentum transfer correlations result in extreme difficulty in applying a three-dimensional analytical approach. For this reason, a one-dimensional analytical design approach was selected. The heat flow between the primary and secondary fluids was assumed to be strictly radial. An equivalent wall thermal resistance of the oval-round tube assembly was defined to account for the nonsymmetric temperature field around the mercury flow passage.

In the concentric position (Figure A-1F), the stagnant NaK was considered to be of uniform thickness over the entire periphery of the inner tube, such that the stagnant volume in the equivalent wall equals that of the actual wall. The volume of stagnant fluid is:

$$\text{Vol} = (\pi r_3^2 + 2 r_3 \ell) - \pi r_2^2 \qquad \text{(Eq. A10.1-1)}$$

$$= \pi (.38)^2 + (.38)(.27) - \pi (.375)^2$$

$$= .218 \text{ in.}^2$$

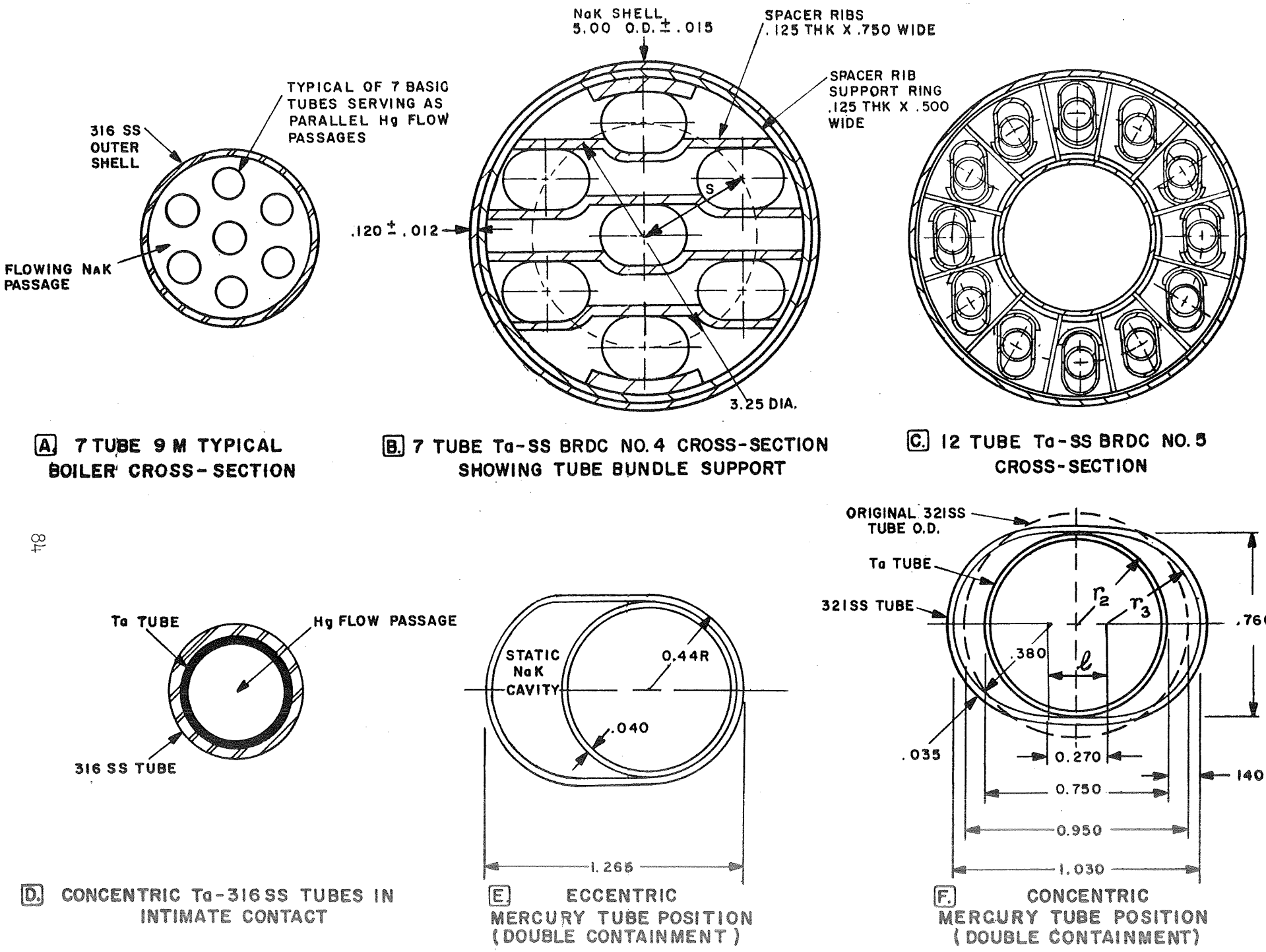

Figure A-1. Typical SNAP-8 Boiler Cross-Section Configurations

The equivalent uniform thickness is then found from:

$$\text{Vol} = 2\pi \left(r_2 + \frac{\Delta r}{2}\right) \Delta r \qquad \text{(Eq. A10.1-2)}$$

and:

$$\Delta r = .0835 \text{ in.} \cong .100 \text{ in.}$$

The thermal resistance of the equivalent stagnant NaK thickness referenced to the mercury tube I.D. is then:

$$R_{\text{concentr}} = \frac{r_1}{\bar{r}} \frac{\Delta r}{12\ K_{st}} = .00044 \frac{\text{hr-ft}^2\text{-}^\circ\text{F}}{\text{Btu}} \qquad \text{(Eq. A10.1-3)}$$

where:
$$\bar{r} = \frac{r_3 - r_2}{\ln\ (r_3/r_2)} \qquad \text{(Eq. A10.1-4)}$$

r_1 = .335 in. Ta tube I.D.

r_2 = .375 in. Ta tube O.D.

r_3 = .395 in. Analytical stagnant NaK containment tube I.D.

k_{st} = 15 Btu/hr-ft-$^\circ$F

The thermal resistance through a maximum eccentrically situated oval-round tube geometry is treated by assuming inner and outer tubes as being concentric over some fraction of the periphery, say 60%, and the remainder (40%) as being comprised of concentric walls separated by stagnant NaK at the maximum eccentricity. For that particular case (Figure A-1E), the stagnant NaK thicknesses and thermal resistance are:

$$\Delta r_1 = r_3 - r_2 = .380 - .375 = .005 \text{ in.} \qquad \text{(Eq. A10.1-5)}$$

$$R_1 = \frac{r_1}{\bar{r}_1} \frac{\Delta r_1}{12\ K_{st}} = \frac{.335}{.3778} \frac{.005}{(12)(15)} = .0000246 \frac{\text{hr-ft}^2\text{-}^\circ\text{F}}{\text{Btu}} \qquad \text{(Eq. A10.1-6)}$$

$$\bar{r} = \frac{\Delta r_1}{\ln (r_3/r_2)} = \frac{.005}{\ln 1.013} = .3778 \text{ in.} \qquad \text{(Eq. A10.1-7)}$$

and:

$$\Delta r_2 = r_3' - r_2 = .895 - .375 = .520 \text{ in.} \qquad \text{(Eq. A10.1-8)}$$

$$R_2 = \frac{r_1}{\bar{r}_2} \frac{\Delta r_2}{12\ K_{st}} = \frac{.335}{.597} \frac{.520}{(12)(15)} = .00162 \frac{\text{hr-ft}^2\text{-}^\circ\text{F}}{\text{Btu}} \qquad \text{(Eq. A10.1-9)}$$

$$\bar{r}_2 = \frac{\Delta r_2}{\ln (r_3'/r_2)} = \frac{.520}{\ln 2.39} = .597 \text{ in.} \qquad \text{(Eq. A10.1-10)}$$

Lumping the two resistances in a parallel resistance network, the overall thermal resistance is calculated as follows:

$$\frac{1}{R_{\text{eccentr.}}} = (.06) \frac{1}{R_1} + (.4) \frac{1}{R_2} \qquad \text{(Eq. A10.1-11)}$$

$$= 24390 + 2469$$

$$= 26859$$

$$R_{\text{eccentr.}} = .000043 \frac{\text{hr-ft}^2\text{-}^\circ\text{F}}{\text{Btu}} \qquad \text{(Eq. A10.1-12)}$$

A comparison of thermal resistance approximations of the oval/round tube concentric ($R_{\text{concentr.}}$) and eccentric ($R_{\text{eccentr.}}$) geometries shows that

$$R_{\text{eccentr.}} = (.1)\ R_{\text{concentr.}} \qquad \text{(Eq. A10.1-13)}$$

Based on this approximation, it seems credible that any tube eccentricity reduces the stagnant NaK thermal resistance from the maximum value when the tubes are in concentric position. For this reason, the utilization of $R_{concentr.} = .00044$ hr-ft^2-$^\circ$F/Btu in local boiling heat transfer analysis throughout the boiler length can be considered as a reasonably conservative value.

10.2 NaK Side Pressure Loss Analysis for BRDC Boiler No. 4

10.2.1 Total NaK Side Pressure Loss

The total boiler NaK side pressure loss ΔP_T, consists of the sum of the following losses that are present in the boiler:

ΔP_{in} = NaK entrance losses

ΔP_{ex} = NaK exit pressure losses

ΔP_f = Frictional flow pressure loss

ΔP_s = Pressure losses incurred by the tube bundle supports

ΔP_c = NaK turbulator coil pressure loss

ΔP_b = Pressure loss incurred by the NaK flow through a curved passage

The total boiler pressure loss is then expressed as:

$$\Delta P_T = \Delta P_{in} + \Delta P_{ex} + \Delta P_f + \Delta P_s + \Delta P_c + \Delta P_b, \text{ psi} \qquad \text{(Eq. A10.2-1)}$$

In the pressure loss analysis, the velocity head method was used for calculating the individual losses at the following NaK side flow conditions:

NaK flow, $\dot{\omega}_N$, = 50,000 lb/hr

Mean NaK temperature = 1250°F

$\rho_{NaK} = 44.75$ lb/ft^3

$\mu_{NaK} = .35$ lb/hr-ft

Figures A-1, 9 and 10 show cross sections of the boiler with their pertinent geometric parameters used in the analysis.

The velocity head coefficients for the tube bundle supports (Figure A-1B) the NaK turbulator coil (Figure 9) and the NaK inlet and exit sections (Figure 10) were determined experimentally on full-scale test sections fabricated and tested at General Electric Co.

The results of these experiments are summarized below (values are based on shell-side velocity head):

K_s = 1.1, for a single spacer

K_c = 2.8, for a 6-foot long turbulator coil

K_{in} = 5.0, NaK inlet section

K_{ex} = 5.0, NaK outlet section

The frictional pressure loss is expressed by the Darcy-Weisbach equation:

$$\Delta P_f = \frac{K_f}{144} \frac{V^2 \rho_L}{2g_c}, \text{ psi} \qquad \text{(Eq. A10.2-2)}$$

where: $K_f = f \frac{L}{D_e}$, dimensionless

Pressure loss due to flow through the coiled boiler is given by:

$$\Delta P_b = \frac{NK_B}{144} \frac{V^2}{2g_c} \rho, \text{ psi} \qquad \text{(Eq. A10.2-3)}$$

where: $K_B = f\left(\frac{R}{d}\right)$ (Ref. 1, pg. 318, Figure 137)

and N = number of 180° bends.

The shell side velocity is:

$$V = (\dot{\omega}_N)\ (\frac{1}{A_f})\ (\frac{1}{\rho_N})\ ,\ \text{fps} \qquad \text{(Eq. A10.2-4)}$$

$$V = (\frac{50{,}000}{3{,}600})\ (\frac{144}{10.78})\ \ (\frac{1}{44.75})\ ,\ \text{fps}$$

$$V = 4.15\ \text{fps}$$

The shell side velocity head is:

$$H_s = \frac{V^2}{2g_c}\ \rho_N = \frac{(4.15)^2\ (44.75)}{(2)\qquad (32.2)}\ ,\ \text{psf} \qquad \text{(Eq. A10.2-5)}$$

$$H_s = 12.0\ \text{psf}$$

$$H_s = .083\ \text{psi}$$

10.2.2 Pressure Losses

The pressure losses are as follows:

(a) Tube bundle support pressure losses:

$$\Delta P_{sp} = n\ K_s\ H_s\ ,\ \text{psi} \qquad \text{(Eq. A10.2-6)}$$

$$n = 10\ \text{supports}$$

$$\Delta P_{sp} = (10)\ (1.1)\ (.083) = .92\ \text{psi}$$

(b) NaK inlet and outlet sections pressure losses:

$$\Delta P_{in} = K_{in}\ H_s = (5.0)\ (.083) = .415\ \text{psi} \qquad \text{(Eq. A10.2-7)}$$

$$\Delta P_{ex} = K_{ex}\ H_s = (5.0)\ (.083) = .415\ \text{psi} \qquad \text{(Eq. A10.2-8)}$$

(c) NaK turbulator coil pressure losses:

$$\Delta P_c = K_c H_s = (2.8)(.083) = .23 \text{ psi} \qquad \text{(Eq. A10.2-9)}$$

(d) Frictional pressure losses:

$$R_e = \frac{(4.15)(44.75)(1.1)(3600)}{(12)(35)} = 175{,}000 \qquad \text{(Eq. A10.2-10)}$$

$$f = .316/R_e^{.25} = .0155 \qquad \text{(Eq. A10.2-11)}$$

$$L = 25 \text{ ft} = 300 \text{ in.}$$

$$D_e = 1.1 \text{ in.}$$

$$K_f = \frac{f\,L}{D_e} = \frac{(.0155)(300)}{1.10} = 4.23 \qquad \text{(Eq. A10.2-12)}$$

$$\Delta P_f = K_f H_s = (4.23)(.083) = .35 \text{ psi} \qquad \text{(Eq. A10.2-13)}$$

(e) Pressure loss due to the boiler coils:

$$K_b = f\left(\frac{R}{d}\right) \qquad \text{(Eq. A10.2-14)}$$

where: $R = 27.125$ in.

$d = 4.72$ in.

$$\frac{R}{d} = 5.76$$

From Ref. A-1, pg. 318; Figure 137 we can obtain the following:

$K_b = .42$ for one 180° bend.

$N = 3$

$$\Delta P_b = (N)(K_b)(H_s) = (3)(.42)(.083) = .10 \text{ psi} \qquad \text{(Eq. A10.2-15)}$$

(f) Total boiler NaK-side pressure loss from Equation A10.2-1 is:

$$\Delta P_T = .92 + 2\,(.415) + .23 + .35 + .10 = 2.43 \text{ psi}$$

10.3 Derivation of the Helical Flow Passage Friction Factor

The following is a derivation of the theoretical friction factor for fluid flow in a helix flow passage. In the derivation no attempt has been made to establish a velocity profile for this type of flow. The end result is used as a means to predict the pressure loss for full-scale mercury flow in the SNAP-8 boiler.

The pressure loss in a single-fluted helix flow passage is given by the Darcy-Weisbach equation as:

$$\Delta P_H = f_H \frac{L_H}{D_H} \frac{U_H^2}{2g_c} \rho \qquad \text{(Eq. A10.3-1)}$$

where:

f_H = Helix friction factor

L_H = Helix flow path length

D_H = Helix equivalent diameter

U_H = Helical flow velocity

ρ = Fluid density

g_c = Gravity constant

Solving Equation A10.3-1 for f_H:

$$f_H = \frac{\Delta P_H}{\rho} \frac{D_H}{L_H} \frac{2g_c}{U_H^2} \qquad \text{(Eq. A10.3-2)}$$

It is postulated that the total pressure loss ΔP_H can be written:

$$\Delta P_H = \Delta P_a + \Delta P_r \qquad \text{(Eq. A10.3-3)}$$

where:

ΔP_a = the axial flow loss

ΔP_r = the rotational flow loss

For the axial component:

$$\Delta P_a = f_a \frac{L_a}{D_a} \frac{U_a^2}{2g_c} \rho \qquad \text{(Eq. A10.3-4)}$$

where: $f_a = .316/Re_a^{.25}$

L_a = Distance between pressure taps

D_a = Axial equivalent diameter

U_a = Axial flow velocity

The axial geometry is obtained from Figure A-2 in the following manner:

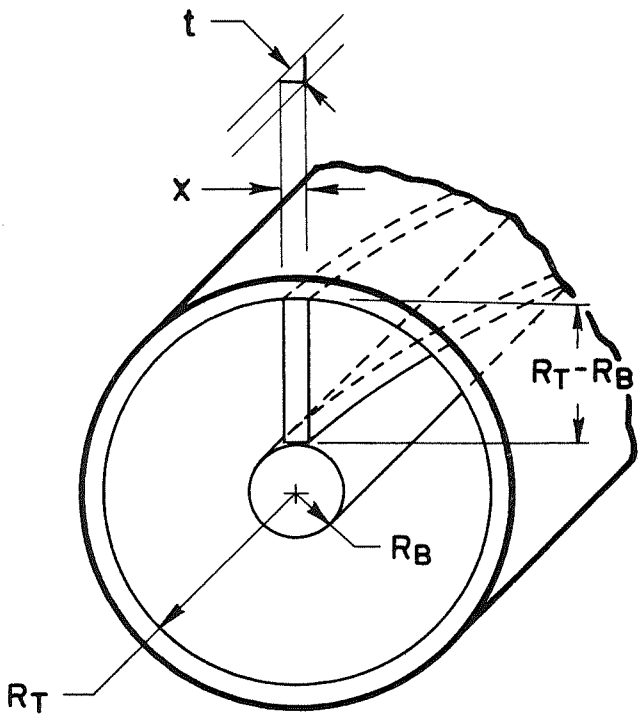

Constant Values:

t = .06 in.

R_B = .094 in.

R_T = .326 in.

Figure A-2. - Plug Section Axial Geometry

then

$$x = t/\cos \alpha_M \qquad \text{(Eq. A10.3-5)}$$

$$A_a = \pi R_T^2 - \pi R_B^2 - x (R_T - R_B) = \text{the free flow axial area} \qquad \text{(Eq. A10.3-6)}$$

The wetted perimeter is given by:

$$P_a = 2 \pi R_T + 2 \pi R_B + 2(R_T - R_B) - 2x \qquad \text{(Eq. A10.3-7)}$$

The equivalent diameter is:

$$D_a = 4.0 (A_a/P_a) \qquad \text{(Eq. A10.3-8)}$$

The rotational pressure loss term ΔP_r is defined by the energy lost in overcoming shear at the tube wall (Reference A-2), such that:

$$\frac{\dot{w}}{\rho} \Delta P_r = \tau_w A_w v_w \qquad \text{(Eq. A10.3-9)}$$

It is assumed that the flow in the radial direction is zero, or:

$$v_r = 0$$

also:

v_w = tangential velocity
= $\tan \alpha_T U_a$

τ_w = shear stress at the tube wall

A_w = area of the tube wall
= $\pi D_T L_a$

$\tan\alpha_T = \frac{\pi D_T}{P}$

$\dot{w} = \rho A_a U_a$

The shear stress at the tube wall for turbulent rotating flows is evaluated in terms of v_w as follows. The velocity at the wall relative to some reference velocity in the flow is given by Kinney (Reference A-3), as

$$\frac{r_w v_w}{r_o v_o} \cong .66 \qquad \text{(Eq. A10.3-10)}$$

and $$r_o v_o = \frac{r_w v_X}{2K_4} \qquad \text{(Eq. A10.3-11)}$$

where:

r_o = reference radial position

v_o = reference tangential velocity

r_w = radius of the wall

v_w = tangential wall velocity

v_X = tangential wall velocity

$$= \sqrt{\frac{\tau_w g_c}{\rho}} \qquad \text{(Eq. A10.3-12)}$$

$$K_4 = \text{constant} = .028 \qquad \text{(Eq. A10.2-13)}$$

By substituting Equation A10.3-13, 12, and 11 into 10 and solving for the shear stress results in the following expression for τ_w

$$\tau_w = .0073\ \rho\ \frac{v_w^2}{g_c} \qquad \text{(Eq. A10.3-14)}$$

Substituting the expressions for v_w, $\tan\alpha_T$, $\dot{w}$, A_w and Equation A10.3-14 into -9 gives:

$$\Delta P_r = .0073\ \left(\frac{\pi D_T^3}{p}\right)\left(\frac{\pi D_T}{A_a}\right) L_a \frac{U_a^2}{g_c}\ \rho \qquad \text{(Eq. A10.3-15)}$$

The term, $\pi D_T/A_a$, in Equation A10.3-15 can be represented by:

$$\pi D_T/A_a = \frac{4.0}{D_a}\left(\frac{D_T - t}{D_T + D_B}\right)$$

then:

$$\Delta P_r = .0292\ \left(\frac{\pi D_T}{p}\right)^3 \left(\frac{D_T - t}{D_T + D_B}\right) \frac{L_a}{D_a} \frac{U_a^2}{g_c}\ \rho \qquad \text{(Eq. A10.3-16)}$$

Substituting (16) and (4) into (3), the helix flow pressure drop is:

$$\Delta P_H = f_a \frac{L_a}{D_a} \frac{U_a^2}{2g_c} \rho + .0292 \left(\frac{\pi D_T}{p}\right)^3 \left(\frac{D_T - t}{D_T + D_B}\right) \frac{L_a}{D_a} \frac{U_a^2}{g_c} \rho \qquad \text{(Eq. A10.3-17)}$$

Placing the above expression for ΔP_H in Equation A10.3-2 gives:

$$f_H = f_a \frac{D_H}{D_a} \frac{L_a}{L_H} \left(\frac{U_a}{U_H}\right)^2 + .0292 \left(\frac{\pi D_T}{p}\right)^3 \left(\frac{D_T - t}{D_T + D_B}\right) \frac{D_H}{D_a} \frac{L_a}{L_H} \left(\frac{U_a}{U_H}\right)^2 2.0$$

(Eq. A10.3-18)

However:

$$\frac{L_a}{L_H} = \cos\alpha_M \qquad \text{(Eq. A10.3-19)}$$

and since: $\dot{w}_a = \rho\ A_a\ U_a = \dot{w}_H = \rho\ A_H\ U_N$

then: $$\frac{U_a}{U_H} = \frac{A_H}{A_a} \qquad \text{(Eq. A10.3-20)}$$

and $$RE_a = RE_H \frac{A_H}{A_a} \frac{D_a}{D_H}$$

then:

$$f_a = \frac{.316}{RE_a^{.25}} = \left(\frac{.316}{RE_H^{.25}}\right) \left(\frac{A_H}{A_a}\right)^{-.25} \left(\frac{D_a}{D_H}\right)^{-.25} \qquad \text{(Eq. A10.3-21)}$$

Substituting Equation A10.3-19, 20 and 21 into Equation A10.3-18 we get f_H as follows:

$$f_{H_{(theo.)}} = \left(\frac{.316}{RE_H^{.25}}\right) \left(\frac{A_H}{A_a}\right)^{1.75} \left(\frac{D_H}{D_a}\right)^{1.25} \cos\alpha_M + .0584 \left(\frac{\pi D_T}{p}\right)^3 \left(\frac{D_T - t}{D_T + D_B}\right) \left(\frac{A_H}{A_a}\right)^2 \left(\frac{D_H}{D_a}\right) \cos\alpha_M$$

(Eq. A10.3-22)

APPENDIX REFERENCES

Reference A-1: Vennard, John K., Elementary Fluid Mechanics, 4th Edition, John Wiley & Sons, Inc., February 1963.

Reference A-2: Smithberg, E., Landis, F., "Friction and Forced Convection Heat Transfer Characteristics in Tubes with Twisted Tape Swirl Generators," Trans. ASME Series C Journal of Heat Transfer, February 1964, pp. 39-49.

Reference A-3: Kinney, R. B., "Universal Velocity Similarity in Fully Turbulent Rotating Flows," Trans. ASME Series E, Vol. 34, Journal of Applied Mechanics, June 1967, pp. 437-442.